DELFT UNIVERSITY OF TECHNOLOGY

MASTER OF SCIENCE THESIS

UNDERSTANDING THE MORPHOLOGICAL DEVELOPMENT OF THE WALSOORDEN SEDIMENT DISPOSALS

GEERT WILLEMSEN

JUNE 2016

TU Delft

Delft University of Technology

Deltares

Enabling Delta Life

Front cover: Aerial view of the tidal flat of Walsoorden on 15 February 2015
Source: Rijkswaterstaat/Edwin Paree 2015 ©

DELFT UNIVERSITY OF TECHNOLOGY

MASTER OF SCIENCE THESIS

UNDERSTANDING THE MORPHOLOGICAL DEVELOPMENT OF THE WALSOORDEN SEDIMENT DISPOSALS

by

G. (Geert) Willemsen

in partial fulfilment of the
requirements for the degree of

Master of Science
in Civil Engineering

at

Delft University of Technology

May 2016, Delft, The Netherlands

Graduation Committee:

Prof. Dr. Ir. Z.B. Wang	Delft University of Technology and Deltares
Dr. Ir. B.C. van Prooijen	Delft University of Technology
Ir. P.L.M. de Vet	Delft University of Technology and Deltares
Dr. Ir. J.J. van der Werf	Deltares
R.A. Schrijvershof, MSc	Deltares

PREFACE

This master thesis finalizes the Master of Science programme Hydraulic Engineering at Delft University of Technology. The research was conducted in cooperation with Deltares in the context of the project meso-scale morphology in the Western Scheldt. I would like to thank Deltares for giving me the opportunity to work in an environment with a lot of people with great expertise.

I would like to thank all members of my committee for their help and feedback on my work. I really appreciate the time that you all invested in me. Especially the advice and guidance of my daily supervisor Reinier was a great support during the course of my thesis. You were always thinking along and willing to help me. Besides, I would like to thank Meinard, Michal and Johan for their availability, help and support regarding to questions about Dflow FM and numerical modelling.

Furthermore, I want to say that I really enjoyed the coffee breaks and walks around the Deltares campus with my fellow students. Thanks therefore.

Last but not least I want to thanks my family and friends for their unconditional support, patience tolerance during the last months of my study.

Geert Willemsen
Delft, June 2016

SUMMARY

The objective of this study is to identify the mechanisms that drive the morphodynamic behaviour of the sediment disposals in the subtidal zone north of the intertidal shoal Walsoorden. The morphological development of the sediment in the subtidal zone near this shoal has been monitored and measured. The gathered bathymetric data show that one year after the sediment disposals had stopped, the sediment was spread out mainly in the flood direction. Little lateral spreading was found. After one year, 1.45 million m^3 of the 3.72 million m^3 sediment had disappeared from the control polygon. Sixty percent of this sediment disappeared during the execution of the disposals and 40 % can be assigned to the morphological development between September 2010 and October 2011.

The new Delft3D Flexible Mesh (DFM) software was used to simulate the hydrodynamics and sediment transport around the disposed sediment. During the course of this study, the Delft3D Flexible Mesh software is still under development and not all functions are available yet. This is the reason why no simulations with a varying bed were performed and why a different model grid is used for the hydrodynamic calculations than for the sediment transport calculations.

To include the seasonal variations in the water level, the hydrodynamic model simulates a full spring-neap tide cycle. The results are used to find the impact of the disposed sediment on the local water levels and flow conditions. Three model simulations with different bathymetries but the same initial and boundary conditions were produced. The first simulation is the reference situation and contains the bathymetry prior to the sediment disposals. The second contains the bathymetry just after the first sediment disposals. And the third contains the bathymetry just before new sediment disposals are executed.

Because it was not possible to run a DFM model with sediment transport in parallel model during this study, a reduction of the grid was necessary to calculate the sediment transport with the used model. The simulations of the model that calculate sediment transport investigate a period of one tidal cycle. Similarly, as in the hydrodynamic simulations, the model that calculates the sediment transport was performed with three different bathymetries. For all three bathymetries this was executed for a spring tide and a neap tide.

A discrepancy between the measured data and the modelled sediment transport was found. The model calculated a residual sediment transport into the balance polygon around the disposed sediment for all the sediment transport model simulations. This implies that the sediment volume within the balance polygon increases while a decrease of the sediment volume is obtained from the data. A conclusive reason for this has not been found.

The migration of the sediment in the flood direction can be explained by the gradient of the residual sediment transport that is introduced by the disposed sediment. An increase of the flow velocity at the location of the disposed sediment and a decrease of the velocity at the downstream end of the disposed sediment during flood are responsible for this gradient. The impact of the disposed sediment turns out to be the largest on the peak flood velocities. During flood, the increased peak velocities at the location of the disposed sediment transport more sediment towards the shoal. In the downstream area of the disposed sediment the flow velocity decreases again and part of the transported sediment is deposited. The strongest gradient, and thus changes in bed level, occur during spring tide conditions.

Deltares

TABLE OF CONTENT

1 Introduction

1.1 Background

The Scheldt Estuary is a tide-dominated estuary that is of major importance for both the Netherlands and Belgium. It includes the entire gradient from fresh to salt water creating various environments for animals and plants. In addition to the ecological value, the estuary is of great economic significance as it provides access to the ports of Antwerp, Gent, Terneuzen and Vlissingen (Jeuken & Wang, 2010). A third aspect of major importance is the role it plays in the safety against flooding.

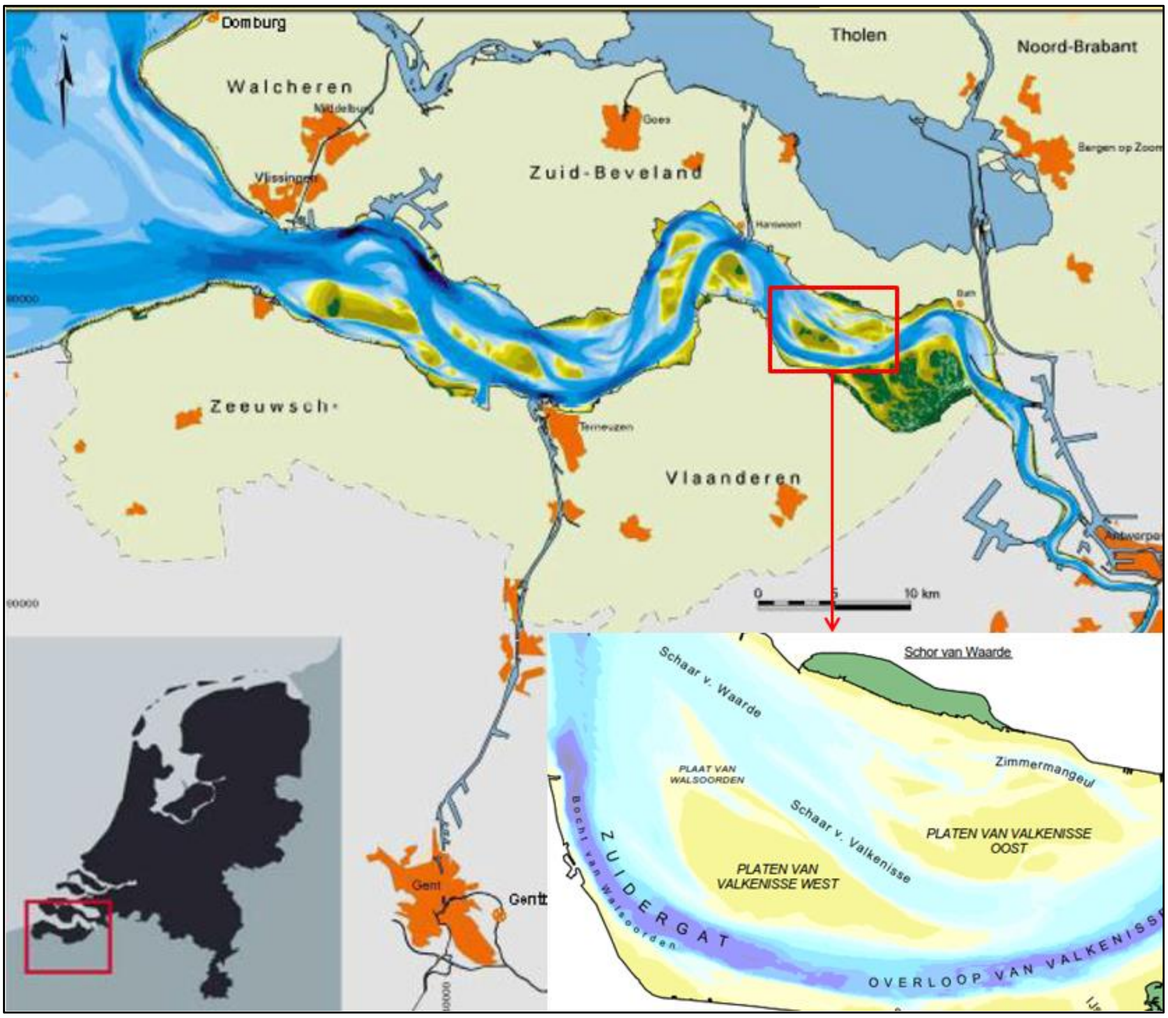

Figure 1-1 Overview of the Scheldt Estuary (Van der Werf & Briere, 2013) and magnified figure of intertidal shoal *Walsoorden*

To accommodate tide independent navigation for large ships, the navigational channels are held at depth by dredging activities. The dredged sand is redistributed along the estuary. During the latest expansion of the navigational channel in 2010, a new disposal strategy was introduced to mitigate the negative side effects of expansion (VNSC, 2015). The intertidal shoal Walsoorden became one of the new disposal locations. Sand was deposited in the shallow waters at the seaward end of the intertidal shoal to prevent further erosion and to create new ecologically valuable areas (Plancke, et al., 2009a). Simultaneously, a monitoring programme to assess the hydrodynamic and morphodynamic impact, called MONEOS was set up.

A vision on the preferred functions of the system was approved by a joint Belgian-Dutch agreement (LTV2030) in 2001. It was pointed out that the present dynamic state of the estuary is strongly impacted by a range of historic and recent human interventions such as land reclamation, defence and training works, channel expansions and sand mining (Berlamont, et al., 2003). Therefore, it was emphasized that any further human interventions should not endanger the ‘multi-channel system’ (MCS) of the Scheldt Estuary.

Wang and Winterwerp (2001) emphasized that there is a limit to the disposal rate in order to preserve the multiple channel system. If the disposal rate exceeds this limit the system will ultimately develop into a single channel system (Jeuken & Wang, 2010), resulting in a loss of ecologically valuable. The newly introduced disposal strategy aimed to reduce the uncertainties of the system by monitoring morphological and ecological developments (Plancke, et al., 2008). It was proposed to make beneficial use of the dredged material by disposing it near (eroding) tidal flats to create valuable intertidal areas (De Vriend, et al., 2011). In this way, a more effective ebb-flood current distribution could be created so that the multiple channel system would be maintained and the dredging efforts minimized for the long term (De Vriend, et al., 2011).

1.2 Problem Analysis

The bathymetry near the intertidal shoal of Walsoorden was measured two times per month to investigate the morphological developments. Flow velocities were monitored at observation points in the neighbouring shallow waters. The bathymetric data set showed that the disposed sediment migrated towards the shoal. Furthermore, a sediment balance of the introduced control polygon showed that the added sediment volume within the polygon reduced. Despite the intensive measuring campaign, specific knowledge about the relevant mechanisms that drive the morphodynamic development is still lacking.

In order to create a more sustainable disposal strategy, it is vital to have better predictions of the morphodynamic impact of disposed sediment. Better predictions will help to anticipate instead of respond to undesired morphological developments. It is especially needed to better understand the interactions on the scale of intertidal flats and channels (meso scale) in order to improve the effectiveness of dredging and disposal activities. To achieve this, local hydrodynamics and sediment transports must be described and modelled in as much detail as possible. A detailed model can point out why sediment is transported in a certain direction or how sediment disposals can influence the local morphodynamics.

1.3 Objective and Research Questions

The objective of this study is to identify the mechanisms that drive the morphodynamic behaviour of the subtidal sediment disposals near intertidal shoal of Walsoorden over a period of thirteen months. Sediment has been disposed at this location since the flexible disposal strategy was introduced in 2010. This study will answer the following research questions:

Q1. *What is the morphological development of the subtidal sediment disposals near the intertidal shoal of Walsoorden?*

Q2 *What is the impact of the sediment disposals on the flow velocities and sediment transport, and how can this impact be explained?*

Q3 *What processes drive the morphological development and impact of the sediment disposals?*

1.4 Research Methodology and Thesis Outline

Due to the highly dynamic character of the estuary, it is difficult to distinguish which specific processes cause which response. This is why the research questions will be answered using the available measurements and a Delft3D Flexible Mesh numerical model. This model software is chosen because it is relatively easy to locally increase the level of detail without a significant increase of the computational time. However, at the time of writing part of this software is still being developed, and not all functions of its predecessor (Delft3D Flow) are available (yet). Meso-scale developments will be modelled with the numerical modelling software. The outcomes of the model simulations will be used to get better insights into which mechanisms cause which response. The provided data set will be used to describe the morphological development of the disposed sediment. Knowledge gained in this study can contribute to a sustainable disposal strategy for the Scheldt Estuary, minimizing the dredging costs.

First, a literature review is presented in Chapter 2. The most important characteristics of the Scheldt Estuary, intertidal flat morphodynamics, the flexible disposal strategy and previous model studies will be addressed. In Chapter 3, an analysis of the available bathymetric data will be carried out. A more detailed analysis of the local displacement of the sediment will be executed in order to get more insight in the morphological development of disposed sediment. Here a distinction is made between the difference contour lines that trace the disposed sediment and the larger control polygon that was introduced by the MONEOS measuring campaign. In particular, the bathymetric development of the sediment disposal after the third expansion of the navigational channel in 2010 will be investigated.

The next step is the model setup and validation (Chapter 4). A Delft3D Flexible Mesh numerical model will be used to gain better insight in the spatial and temporal variability. To do so, an existing numerical model of the Scheldt estuary with a locally refined grid will be used. The model is hydrodynamically validated for the year 2013. In the region of interest the grid resolution is approximately 50 to 75 m. This model will be used to compare the hydrodynamic response and sediment transport of the system with three different bathymetries to the same hydrodynamic forcing. The local bathymetry is adjusted with the available bathymetric data set.

The model results will be analysed in Chapter 5 and 6. Chapter 7 presents the discussion, and Chapter 8 finalizes the report with the conclusions and recommendations.

2 LITERATURE REVIEW

2.1 Estuarine interactions

Throughout time the Scheldt Estuary has been subject to various natural processes and human interventions. The combination of these two has led to a dynamic system that is constantly changing in time due to the interaction between hydrodynamics and morphology. The interaction between morphology and tidal asymmetry in estuaries can be described by Figure 2-1.

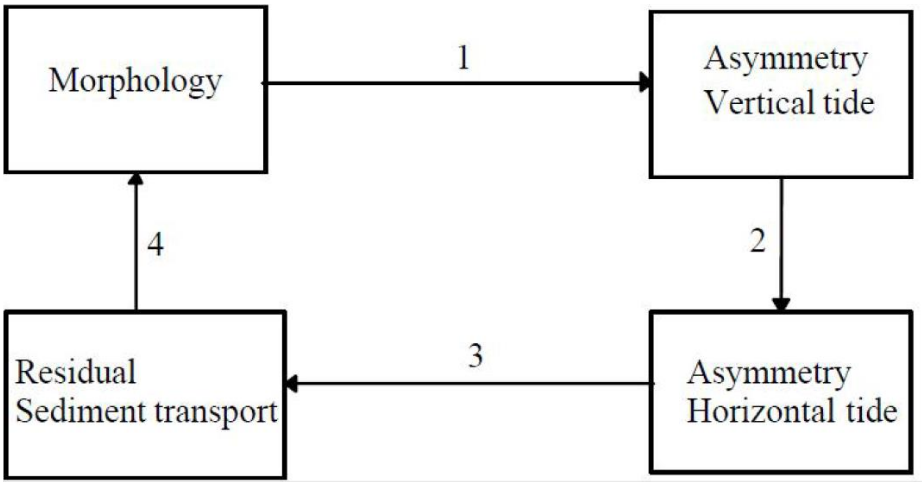

Figure 2-1 Schematic representation of the interaction between morphology and tidal asymmetry within an estuary (Van der Werf & Briere, 2013)

The vertical tide (water level) is influenced by the geometry of the tidal basin. According to Taal et al. (2015) the tidal intrusion can be changed by the channel cross-section, the funnel shape of the estuary, the intertidal area and the bed friction. When the geometry of the tidal basin is changed, the vertical tide can become asymmetric. As a result, the horizontal tide (discharges and velocities) will become asymmetric as well. Due to a non-linear relation between velocities and sediment transport, this will lead to a residual sediment transport. The sediment transport gradients will then lead to a change in the morphology (bed level).

2.2 Scheldt Estuary

2.2.1 Multiple-Channel-System and Cell Concept

The behaviour of the Scheldt Estuary is generally well known. The upstream river discharge is negligible compared to the tidal prism, and fluvial sediment input is virtually nil (De Vriend, et al., 2011). This holds for sand and mud fractions as well (Cleveringa, 2013a). The morphology of the Scheldt Estuary consists of a repetitive pattern of mutually evasive meandering ebb channels and relatively straight flood channels, also referred to as multiple-channel system (MCS) (Van der Werf & Briere, 2013). The main channels are separated by highly dynamic intertidal areas: the intertidal shoals. Along the fully embanked shores intertidal mudflats and salt marshes are found.

Winterwerp et al. (2001) schematised this system into a chain of macro- and meso-cells on the basis of morphology. Figure 2-2 gives a schematisation of the Western Scheldt estuary into macro cells on the basis of this concept. The more detailed meso-cells can be found in the LTV reports (Cleveringa, 2013b). Each macro cell consists of two main channels divided by intertidal shoals. In the deeper ebb channels more water and sediment is transported during ebb while the opposite applies to the shallower flood channels. The ebb and flood channels meet at highly dynamic shallow areas that form sills in the navigation channel (Van der Werf & Briere, 2013). These sills form the boundaries between the neighbouring macro cells. On a smaller scale, connecting channels form linkages between the main channels.

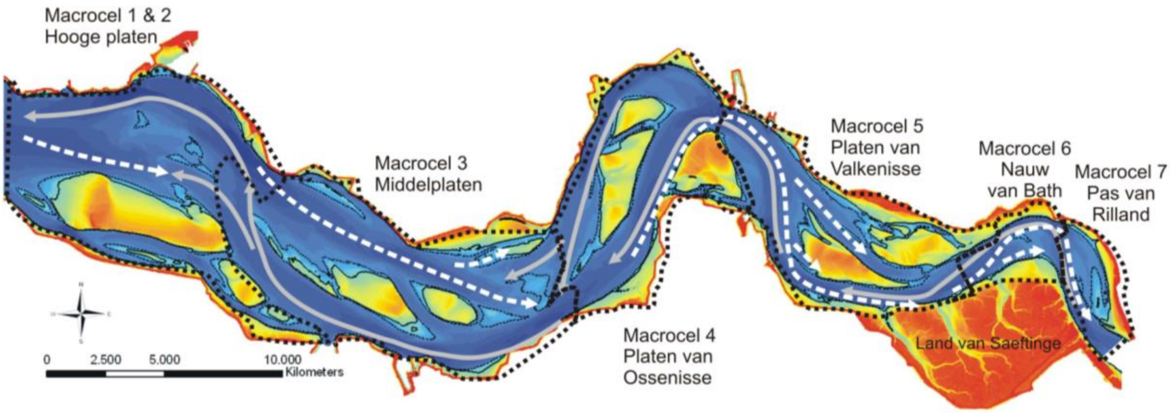

Figure 2-2 Schematisation of the Western Scheldt in morphological cells divided by the dotted black lines. The main ebb direction is indicated by the dashed white lines, while the main flood direction is indicated by the solid grey lines (Taal, et al., 2013).

2.2.2 Morphodynamic Development

The influence of human interference on the morphology and hydrodynamics of the Scheldt Estuary has been present for centuries. From the 10th century onward, human interferences mainly consisted of dikes and land reclamations. During the last century, the focus shifted towards dredging the shallow parts in the navigation route to the port of Antwerp. Currently, the main interferences are dredging and disposal to deepen and maintain the access channel to the port of Antwerp (Coen, 2008). The geometry of the estuary determines the propagation of the tidal wave into the estuary, while the hydrodynamics determine the geometry of the basin on a timescale of years to decades due to morphology.

The impact of a changing bathymetry on hydrodynamics depends on local conditions. Direct – and indirect (via morphology) effects can be distinguished. Indirect effects are difficult to identify because they develop gradually. The timescales of morphological development is variable because it depends on many changing factors (e.g. flow velocity, sediment composition and bed shear stress). Furthermore, the effect of changing geometry can also affect foreign regions due to the above-mentioned interaction between geometry and tidal propagation. It is difficult to point out which change results in which effect because of the feedback between morphology and hydrodynamics, and the system which is constantly in motion.

Both gradual changes and instantaneous changes have been observed in the water levels (Depreiter, et al., 2013). The most profound morphological development of the past century is the increase of the (main) channel volume (Depreiter, et al., 2013). The increased channel volume is a result of human interferences in the sediment balance. As a direct result of the large sand extractions during the first expansion of the navigational channel, the water volume in the system increased. These interferences have led to large changes in the propagation of the tide into the estuary over the last century (Pieters, 2002). The increased water volume has led to:

1) an increase in tidal range with higher high water levels and lower low water levels;

2) an increase in propagation speed of the tidal wave;
3) larger tidal intrusion with a landward shift of the location of maximum tidal range (Coen, 2008).

Due to the funnel shape of the estuary, shoaling, reflection, and bottom friction the tidal wave deforms as it propagates through the estuary. The tidal distortion creates an amplifying tidal range upwards into the estuary. Embankments and land reclamation led to reduced available space. This has resulted in higher water levels, larger gradients, higher flow velocities and thus larger sediment transport (Jeuken, et al., 2007). The increased (tidal) flow has led to erosion of the channels and again to larger tidal intrusion. This feedback has been enhanced by human interferences.

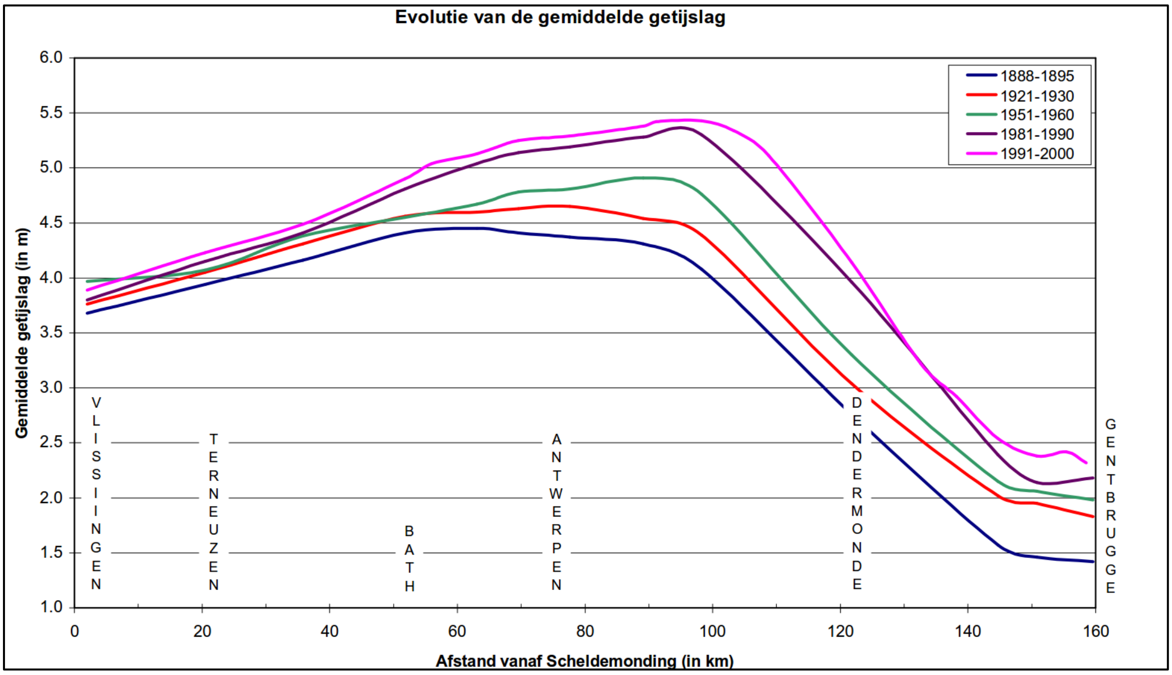

Figure 2-3 Evolution of the average tidal range in the Scheldt estuary over the last century (Jeuken, et al., 2007)

Today, the average tidal range increases from 3.8 m at Vlissingen to a maximum of 5.3 m at Rupelmonde, which is located just upstream of Antwerp (Pieters, 2002). Figure 2-3 shows the evolution of the average tidal range in the Scheldt Estuary over the past century. The increased tidal intrusion can be explained by the decreased friction and deepening of the channels.

2.2.3 Hydrodynamics

In the Scheldt estuary the tide is dominant over the river influences and wind waves. Waves do not fully propagate into the estuary while the river discharge is negligible compared to the tidal flow. The average river outflow of 5 million m^3 per semi-diurnal tide corresponds to less than 1% of the tidal prism (Wang, et al., 2002). It can thus be concluded that at present the tide is clearly the driving force of the water motions in the Western Scheldt.

Tide

The tide is composed of different tidal constituents that are caused by gravitational forces exerted by the moon and the sun, and the tilting and rotation of the earth. In the North Sea these constituents form a semi-diurnal tide with two nearly equal high and low waters every day. The tidal range varies with a two-week cycle due to the interaction between the moon and the sun. When the sun and the moon are in line the exerted forces reinforce each other and the tidal amplitude is the largest (spring tide). When the sun and the moon are 90 degrees out of phase the tidal range is the smallest (neap tide). Typical tidal ranges at the mouth of the estuary vary between 2.5 m and 4.5 m.

The flow velocities within the estuary are closely related to the water level gradients. Conventional maximum flow velocities in the channel are in the order of 1.5-2 m/s. As mentioned before, the geometry of the basin causes a distortion of the tidal wave. The difference in propagation speed of the tidal constituents causes a phase difference. A phase difference between the tidal constituents is a measure for tidal asymmetry, which leads to net sediment transports. Large phase differences lead to large tidal asymmetry and an increase in net sediment transport. Shorter flood (ebb) periods with higher flow velocities generally lead to net sediment import (export). A changing friction term can lead to tidal asymmetry. In the Western Scheldt the flood period generally is shorter than the ebb period, indicating flood dominance (Kuijper, 2013). This is most profound in the eastern part of the Western Scheldt. As a result of the morphological development in the estuary over the last decades, tidal asymmetry has reduced, resulting in a smaller net sediment transport (Kuijper, 2013).

<u>Tide induced circulation residual currents</u>
Tidal asymmetry is generated by a tidal wave that deforms during its propagation. The deformation occurs if the wave crests (HW) and wave trough (LW) travel at a different speed. During high water the propagation speed of the wave is larger than during low water. This in combination with lower bottom friction during high water, results in a higher propagation velocity of the wave crest than the wave trough. As a result of the orbital motion of the fluid particles in the tidal wave, a net discharge in the propagation direction of the wave, called Stokes drift, is introduced. The Stokes drift is compensated for by return flow driven by a water level gradient. The return current is in the order of 0.05 m/s in the ebb direction (Van der Werf & Briere, 2013). Locally a residual discharge or depth-averaged velocity can be introduced or enhanced by geometry and bathymetry. In the Scheldt Estuary, the bathymetry-induced circulation is ebb-directed in the relatively deep parts and flood directed in the relatively shallow parts. With the bimodal cross-sections as in the Western Scheldt, the residual flow is ebb-directed (flood-directed) in the deeper (shallower) channels. The ebb or flood dominance can be determined based on three physical quantities: the vertical tide (water level), the horizontal tide (discharge & velocity) and the net sediment transport (Bolle et al, 2010). An analysis based on either one of these quantities can result in a different dominance.

<u>Wind</u>
Because the North Sea is relatively shallow, strong winds can cause high floods and storm surges. The wind set up can then cause a secondary flow as a result of a water level gradient. When the direction of this current is similar to the tidal current high flow velocities can occur (Schroevers, 2013). Since the 1950s the number of storm surges has increased considerably compared to the period before that (1880-1950). However, the average height of the high floods and storm surges has not increased (Kuijper, 2013). Moreover, persistent wind can induce currents via wind shear stress. The transfer of momentum decreases with increasing depth. These wind driven currents can be important in shallow water.

<u>Waves</u>
Locally, wind can generate waves that induce orbital velocities that are largest near the surface and decrease with increasing water depth. These orbital velocities can have a significant influence on the near surface shear stress (Henderson & Mullarney, 2013). In shallow water this shear stress can exceed the bed shear stress and hence have substantial influence on the sediment transport, especially also due to wave-current interaction. Wind wave orbital velocities are indicated to be an

important process for the stirring of sediment. These velocities themselves have only a small impact on the net transports due to net the orbital velocity. However, the velocities are capable of suspending sediment that can be transported by mean tidal currents to less hydrodynamically active regions (Hunt, et al., 2015).

The length of the fetch is an important parameter for the generation of waves. Within an estuary the largest fetches occur during high water. However, the potential of wave growth is larger in shallow water. Besides, the wave induced bed shear stress is not necessarily largest during high water because the orbital velocity decreases with increasing depth. Therefore, sediment transport due to waves is not necessarily the largest during high water either. The maximum impact of the wave generated shear stress will occur when a balance between the available fetch and sufficiently shallow water that allows the orbital velocity to reach the bed exists (Hunt, et al., 2015). In the deeper channels the waves are unlikely to have a large effect on bed sediment transports. Therefore channel morphology is often dominated by tidal currents only. In shallower areas the influence of waves is larger.

2.2.4 *Sediment Transport*

The magnitude and direction of the net transport in the Western Scheldt has been determined by dredging and disposal activities (Cleveringa, 2013a). Especially during the first expansion of the navigational channel (mid 1970s) a lot of dredged sediment was extracted from the system (Santermans, 2013). In the east of the Western Scheldt there has been a decrease of sediment volumes due to an export of sediment towards the *Land van Saeftinghe* and the upstream river. To avoid further decrease of the sediment volumes, it has been decided to stop commercial sand extraction within the Western Scheldt in 2010 (van Leeuwen, 2013). Furthermore, the material that is dredged from the navigational channel for maintenance is now all disposed back into the estuary.

Despite of these interventions and multiple disposal strategies, the deficit of sediment eastern part of the Western Scheldt persisted. The persisting deficit of sediment in the eastern part led to decrease of sediment volumes and an increase of the area of flow. This trend extended from east to west but has not appeared in the cells west of macrocel 4 (Taal, et al., 2013). Dredging and disposal operations at least enhanced decreasing sediment volumes in the eastern part of the Western Scheldt.

Furthermore, partial disappearance of the connecting channels and the raise of intertidal shoals led to the loss of valuable low dynamic shallow water areas (Swinkels, et al., 2009). A link between the presence of connecting channels and the raise of intertidal shoals has been suspected after observations. The intertidal shoals became higher while the connecting channels and spits decreased in number and size. However, recent observations have questioned this link because the heights of some intertidal shoals have stabilized, while the decrease in number and size of the connecting channels and spits has continued (Cleveringa, 2013c).

2.3 *Estuarine morphodynamics*

According to Friedrichs (2011) the shape of tidal flats is the result of the interplay between a variety of factors including tidal currents, wind waves, sediment supply, fluvial inflow and biological and anthropogenic activities.

Sediment dynamics, which includes both sediment deposition and erosion, are important to understand whether tidal flats will accrete or erode. A key parameter in sediment dynamics is the bed shear stress, τ_b, which controls deposition and erosion of the bottom top layer. The bed shear stress acts as a friction force in the direction of the flow and is mainly determined by the flow velocity and bottom friction. In a turbulent open channel flow the bed shear stress can be estimated with:

$$\overrightarrow{\tau_b} = \rho g \left(\frac{\vec{u}}{C}\right)^2 \qquad \text{Equation 2-1}$$

With:

$\overrightarrow{\tau_b}(x, y, t)$	bed shear stress in flow direction [N/m^2]
$\vec{u}\ (x, y, t)$	depth averaged flow velocity [m/s]
$C\ (x, y, t)$	Chezy roughness coefficient
ρ	density of the water [kg/m^3]
g	gravitational constant [m/s^2]

The majority of sediment that settles on the flats is supplied by the channels. Both during ebb and flood, water can flow over the intertidal areas leading to accretion (or erosion). The intertidal flats have highly dynamic surface areas where the direction of the flow can be indicated by the mega ripples. The ripples give an indication of the flow velocity and the flow direction (Consortium ARCADIS - Technum, 2007b). Another relevant process that leads to erosion of tidal flats is local flow from the flat during low water conditions. The water left on the tidal flat flows off through gullies.

2.3.1 Morphological Development and Dynamic Equilibrium

A difference in incoming and outgoing sediment leads to deposition or erosion of the local bed. If more sediment comes in (goes out) than goes out (comes in), the local bed level will increase (decrease). In other words: a gradient in sediment transport will lead to a change of local bed level. A positive gradient (an increase in sediment transport in the transport direction) leads to erosion. The opposite can be said about a negative gradient. Changes in morphology depend on spatial and temporal fluctuations of sediment transport rates. If no gradients are present the system is in an equilibrium state and no net transports can be seen. In terms of continuity or mass balance (Bosboom & Stive, 2015):

$$\frac{\partial z_b}{\partial t} + \frac{\partial S_x}{\partial x} + \frac{\partial S_y}{\partial y} = V \qquad \text{Equation 2-2}$$

Where:

$z_b\,(x,y,t)$	Bed level above a certain horizontal datum [m]
$S_x\,(x,y,t)$, $S_y\,(x,y,t)$	Sediment transport rates per m width of flow in the horizontal x-and y-direction [m^3/m/s including the effect of porosity]
$V\,(x,y,t)$	Sink or source term per unit area representing local sediment gains and losses (zero in case of equilibrium) [m^3/m/s]

Waves, tidal induced velocities and sediment availability determine the local sedimentation or erosion of tidal flats. Because most forcing is periodic, Friedrichs (2011) used a concept called dynamic equilibrium to describe the equilibrium of intertidal flats. This means that the sink or source term of Equation 2-2 is zero over some characteristic period of natural forcing. However, instantaneous sediment transports can be present over the same time span. Examples of periods of natural forcing are a tidal cycle, a neap-spring tidal cycle, or storm plus recovery cycle.

This means that sediment can be transported landward (seaward) during flood (ebb); while no net transport is present over a full tidal cycle. Interferences in hydrodynamics or sediment availability can disturb a dynamic equilibrium and lead to residual transports.

2.3.2 Tidal Influences on Sediment Transport

Tidal Asymmetry

Changing hydrodynamic conditions over time can lead to net sediment transport. This can be due to tidal asymmetry; residual (river) currents; asymmetric bed shear stress; turbulence due to tidally varying stratification and bed slope effects (Friedrichs, 2011). The geometry and composition of the bed can lead to different properties that can influence the before mentioned mechanisms.

Tidal distortion can occur when the tidal wave propagates on the coastal shelf (Dronkers, 1986). A distortion of tidal rise and fall within the basin itself leads to asymmetries in tidal velocities due to dependence of velocity on the water level; independent of the tidal flats profile. The difference in magnitude and duration of the ebb and flood currents results in different sediment transport during ebb than during flood. The difference in maximum current velocity during ebb and flood is an important feature that is responsible for residual sediment transport. A reason for this is that the proportionality between the sediment transport and flow velocity is to a higher power (3-5) than one (Soulsby, 1997). Dronkers (1986) emphasizes that local dominance of ebb or flood mainly influences the suspended load. This can be explained by the fact that suspended sediment transport is proportional with a higher power of the sediment transport than bedload transport. This effect is the largest on the coarser fraction of the suspended sediment. For finer sediment the difference in the slack water period before ebb and flood is an important parameter as well.

Larger local ebb (flood) velocities lead to export (import) of coarser sediment because flow velocity and sediment transports have a non-linear relation. Friedrichs (2011) explains this with the assumption that sediment suspension and transport rate increase with the order of magnitude of the bed shear stress, $\tau \sim u^2$, and is only present above a certain threshold, τ_c . Note that this is a simplification because the relationship between flow velocity and sediment transport rate is to a higher power. High flood velocities result in larger bed shear stress during flood and thus more sediment transport (Figure 2-4). Oppositely, larger ebb velocities result in larger sediment transport during ebb. This assumption is most valid if the sediment transports react instantaneous to the increase in bed shear stress.

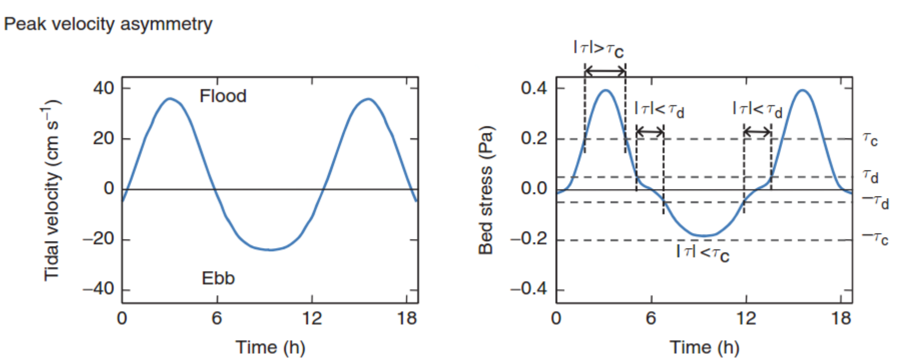

Figure 2-4 Idealized flood dominant current with no residual transport (left) and resulting asymmetry in peak stress (right) favouring landward sediment transport.

Longer (shorter) high water slack results in a landward (seaward) transport of fine sediments because the sediment has more time to settle after flood (ebb). According to Friedrichs (2011) this can be explained with the assumption that deposition is favoured if the bed shear stress drops below a certain value, τ_d. A longer high water slack will result in a longer period of low bed shear stress around high water and thus more sediment deposition (Figure 2-5). In the same way, longer low water slack results in more sediment deposition during low water. Tidal flats usually have longer high water slacks because they are dry during low water. This effect increases the transport of fine sediments towards shallower regions. In the shallower regions smaller sediments can be expected than in the channels.

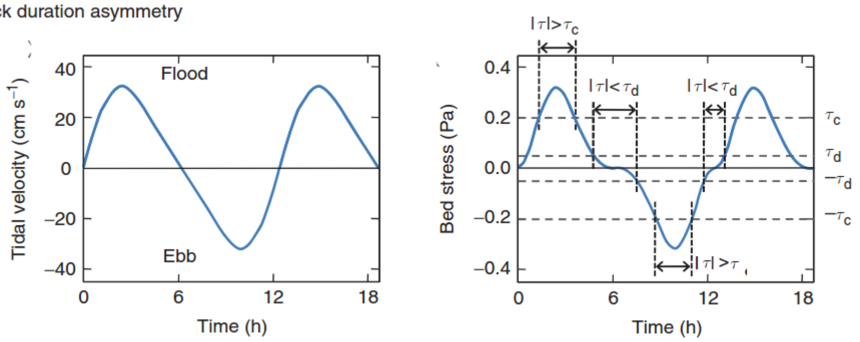

Figure 2-5 Longer slack duration after flood with no residual transport on the left hand side and resulting asymmetry in periods of low stress magnitude on the right hand side (Friedrichs, 2011).

A combination of initially distorted tide and profile shape can lead to rather complex tidal velocity patterns. Distortion within the estuary itself can be influenced by the basin geometry of tidal flats and channels. According to Friedrichs & Aubrey (1988), non-linear distortion of the tide in tidal basins is a composite of two principal effects:

1) Frictional interaction between the tide and channel bottom causes relatively shorter flood periods, reflected in the ratio of the tidal amplitude and the channel depth (R/h). Flood dominance thus increases with R/h
2) Intertidal storage causes relatively longer flood periods as the flow over the intertidal flats slows down the high tide propagation, measured by the ratio of the intertidal flat volume storage and the channel volume below mean sea level (V_s/V_c). Flood dominance thus increases with increasing V_s/V_c.

<u>Spatial variations</u>

Variations in spatial sediment transport are often the result of variations in hydrodynamic energy in combination with time lag effects. Locally the sediment concentration is determined by multiple factors (e.g. tidal flow, waves, wind). If a horizontal gradient in energy is present, net sediment transport is introduced. More sediment is entrained in the more energetic area. As the tide moves from an area with high energy into an area with lower energy, it takes the sediment time to settle to the bed. Thus, temporarily there is a surplus of the suspended sediment concentration compared to the equilibrium sediment concentration. When the tide moves from low energetic areas to high energetic areas, the sediment takes time to get into suspension and the sediment concentration lags behind. The sediment movement across tidal flats is determined by the tide in combination with energy driven concentration gradients (Friedrichs, 2011).

Spatial variations in water depth can affect the period of slack water. Shorter period of slack water will result in less time for the sediment to settle. This effect is largest in deeper water because it takes more time for the sediment to settle in the deeper parts. If the settling velocities are the same but the depth is not, the particles will travel further during high water slack than during low water slack. The direction of the sediment transport during high water slack is landward. Additionally the sediment will also have more time to settle in the shallower areas. This will favour the deposition of sediment on intertidal areas (De Swart & Zimmerman, 2009).

Postma (1954) and van Straaten & Kuenen (1957) showed that spatial settling lag effects result in net transport in the direction of the decreasing tidal current and/or decreasing depth. Pritchard and Hogg (2003) emphasized this concept. In Figure 2-6 the movement of a particle over one tidal cycle is schematized. Figure 2-6 (a) displays a situation with a spatially uniform velocity distribution. A particle is entrained at location A when the flood velocity exceeds the threshold velocity and is carried with the flow until the velocity drops below the threshold again. When the velocity has dropped below the threshold the particle gradually settles to the bed again at B. At ebb the particle is entrained again into the water at location B. The ebb current caries the particle in the ebb direction until the ebb velocity drops below the threshold value again. The particle gradually settles again to come to the bed at location C. This is the same location as the start location A, i.e. there is no net sediment transport occurs.

If the tidal velocity profiles are similar but the water depths differ the particle will travel further during high water slack (after flood) than during low water slack (after ebb). This is displayed in Figure 2-6 (b). This will lead to net sediment transport in the direction of the largest water depths. Conversely, if the water depths are the same but the tidal velocities differ, the particle will travel further on the tide with the highest velocities (with similar settling distance). This process is schematically displayed in Figure 2-6 (c) and leads to net sediment transport towards locations with lower velocities.

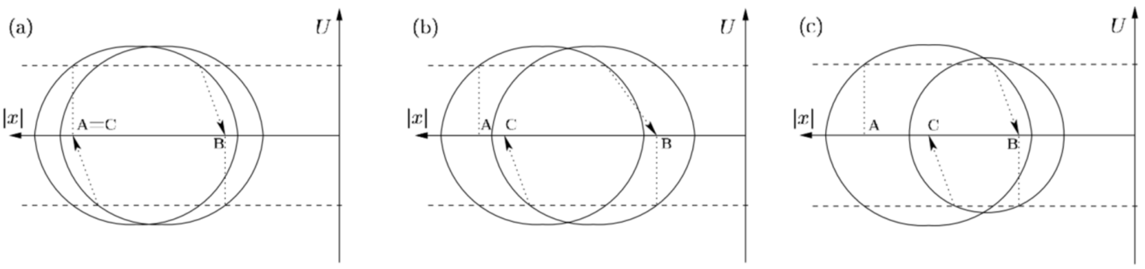

Figure 2-6 Schematic illustration of settling lag mechanism. The solid lines indicate trajectories of the fluid elements forced by the tide. A positive flow velocity indicates flood and a negative velocity indicates ebb. The fluid elements travel in the clockwise direction. The dashed lines indicate the threshold velocity above which transport is expected. The dotted lines indicate the entrainment and settling of the sediment. If the velocity exceeds the threshold value the sediment is carried along the fluid elements. The horizontal axes is positive in the positive in the ebb direction (Pritchard & Hogg, 2003).

2.3.3 Wave-Tide Interaction

Both the time that the shear stress exceeds the critical shear stress and the duration of the exceedance change if waves are present. Friedrichs & Aubrey (1996) used a simplified one dimensional model on a linearly sloping bed to consider the spatial distribution of tide and wave induced velocties and access likely trends in hydrodynamic energy across tidal flats. The model neglects friction, wave shoaling and wave breaking; assumes a sinusoidal tidal elevation that is uniform in space and approaches the depth average flow velocity and wave orbital velocity as follows:

$$\overrightarrow{u_T(x,t)} = \frac{x_f(t)-x}{h(x,t)}\frac{d\eta(t)}{dt} \qquad \text{Equation 2-3}$$

$$\overrightarrow{u_W(x,t)} = \frac{1}{2}\frac{H}{h(x,t)}\sqrt{gh(x,t)} \qquad \text{Equation 2-4}$$

With:

$\overrightarrow{u_T(x,t)}$	tidal current velocity [m/s]
$\overrightarrow{u_W(x,t)}$	wave orbital velocity [m/s]
$x_f(t)$	boundary between the wetted and exposed portions of the flat [m]
η(t)	local tidal elevation [m]
H	wave height (spatially uniform and constant in time) [m]
h(x,t)	water depth [m]
Z(x)	local elevation of the bed [m]
L	length of the lineairly sloping flat [m]
R	tidal range [m]
ω	tidal radian frequency [-]

Figure 2-7 shows the situation as described by Friedrichs & Aubrey (1996) and schematically displays the above mentioned parameters.

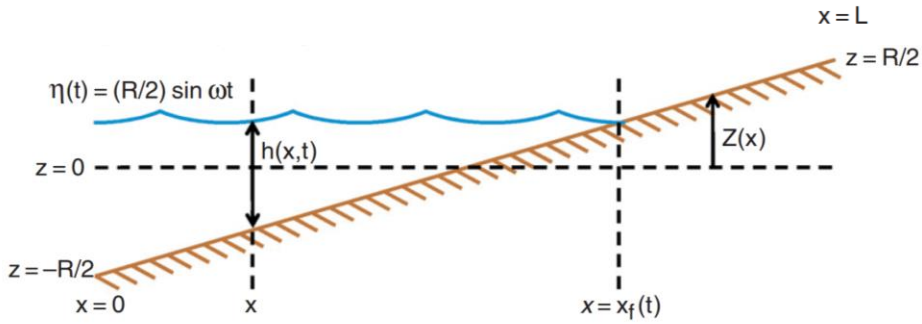

Figure 2-7 Schematic side view of a linearly sloping flat along a straight shoreline which is dominated by tidal currents (Friedrichs, 2011).

Based on Equation 2-2 and 2-3, the spatial distribution of the tidal current and wave orbital velocity can be determined. Figure 2-8 shows the spatial variation of the 90th percentile of the tidal current velocity (left) and the wave orbital velocity (right) based on these equations. The use of the 90th percentile has been found to be a useful scale for evaluating coastal morphology because it accounts for both the characteristic magnitude of energetic velocities as well as the fraction of the time that velocities are large (Friedrichs, 2011).

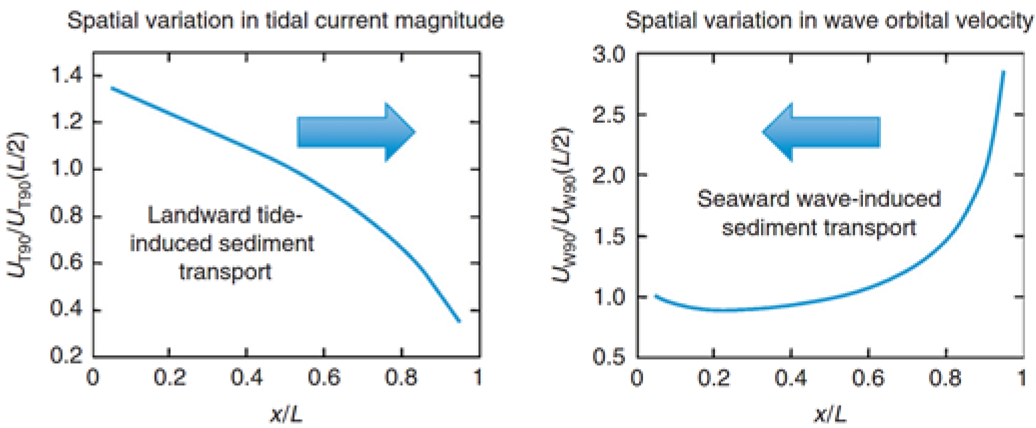

Figure 2-8 Cross flat spatial variation in the 90th percentile of the tidal current velocity (left) and 90th percentile of the wave orbital velocity (right)

From this simplified approach it follows that the tidal current magnitude of a sinusoidal tide decreases landward, while the non-dissipative wave orbital velocity increase. This means that the tidal energy decreases in landward direction, favouring landward deposition of sediment. The wave energy of non-dissipative waves increases in landward direction, favouring sediment transport in the seaward direction. The spatial distribution of tidal and wave energy across tidal flats as displayed in Figure 2-8 is supported by observations on tidal flats of 1) spatial gradients in suspended sediment concentration, 2) the direction of net sediment flux and 3) bed change as a function of tidal versus wave energy (Ridderinkhof, et al., 2000; Janssen-Stelder, 2000; Allen & Duffy, 1998).

2.3.4 Tidal Flat Hypsometry

The shape of the tidal flat can locally influence the tidal asymmetry and durations of slack water. If a flat is convex-up, the tidal flow velocities will locally increase as the tide rises. Equation 2-3 helps to explain the relationship between the shape of the profile and the local duration of slack water. If a flat profile is covex-up, $(x_f - x)/h$ will locally increase in magnitude as the tide rises. As a result, the duration of high water slack reduces, potentially reducing the time for fine sediment to settle. Figure 2-9 shows the how a symmetric tidal forcing is influenced by a convex-up tidal flat profile. This potentially reduces the deposition of fine sediments (Friedrichs, 2011). Conversely a concave upward shape would result in lower flow velocities of rising tide and thus a longer slack and potential deposition of fine sediment.

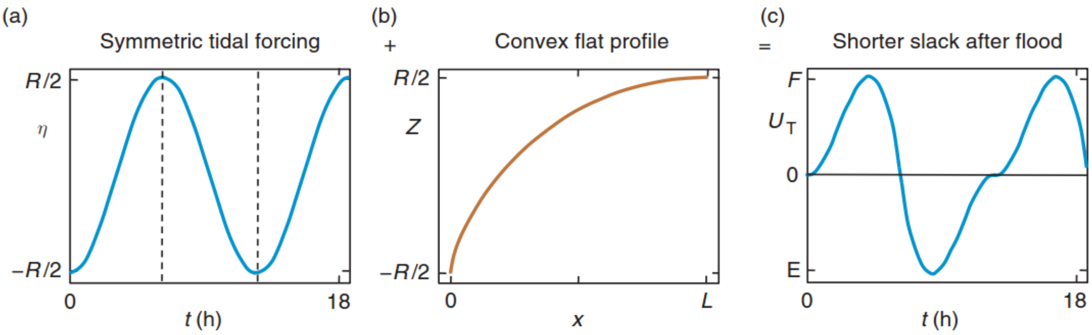

Figure 2-9 Tidal currents with a shorter slack after flood (c) due to a sinusoidal tidal forcing (a) and a convex-up tidal flat profile (b). The velocity profile at x=0 is displayed (Friedrichs, 2011).

2.4 Flexible Disposal Strategy

To maintain the accessibility of the port of Antwerp permanent dredging of the navigational channel is needed. Because of a limited exchange of sand between the estuary and the sea, the dredged sediment is disposed again within the estuary. Until the second expansion of the navigational channel in 1997-1998 the maintenance dredging was mainly disposed back into the secondary channels in the eastern part of the estuary (WLB, 2006). Because this disposal strategy might endanger the ‘multiple channel system’ in this part of the estuary, the sediment has been distributed more evenly over the estuary ever since. In advance of the third expansion of the navigational channel it was suggested to investigate the impact of an even greater sediment disposal due to increasing (construction) dredging. An independent team of experts (Peters, et al., 2001) came up with the idea to use the dredged sand in to create or redistribute natural habitats. This disposal strategy could contribute to establish a sustainable Scheldt Estuary.

After the feasibility study and two in situ disposal tests, this disposal strategy was introduced parallel to the third expansion of the navigational channel in 2010. This disposal strategy is now used to create as much ecologically valuable areas as possible by disposing dredged sediment on shallow areas near intertidal shoals (VNSC, 2015). The locations of the disposal can be changed at any time within the permitted disposal area (Figure 2-10). In this way it is possible to anticipate to the impact of the disposals itself, as well as to the natural morphological developments. When the shallow water area disposal sites do not have sufficient capacity, disposal locations in the main or secondary channels can be used.

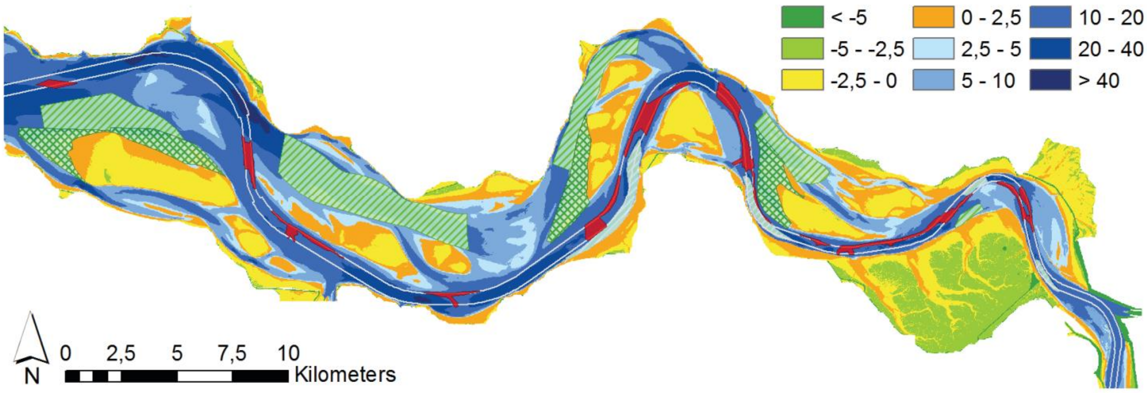

Figure 2-10 Dredging - (red) and permitted disposal locations (near intertidal shoals: dark green, secondary channels: light green, main channels: white) of the flexible disposal strategy (Plancke, et al., 2011)

Adjusting the disposal strategy and monitoring campaign is done on the basis of three main criteria: 1) maintaining the multiple channel system, 2) creating new ecologically valuable areas and 3) preserving the present ecologically valuable areas. Sediment is disposed on the side of intertidal shoals in order to create more static intertidal -or shallow water areas. The stability of the disposed sand and the total area of low dynamic intertidal area are monitored. The quality of the (created) intertidal areas is judged by their elevation, the maximum and average flow velocities and their sediment composition. Intertidal areas with flow velocities lower than 0.8 m/s are desired (Plancke, et al., 2009b).

During the third expansion of the navigational channel, 3.72 million m^3 dredged sediment was disposed at the seaward tip of intertidal shoal *Walsoorden* between February and October 2010. This location was chosen because it has been eroding for several decades (Plancke, et al., 2009a). It was hypothesized that the disposed sediment would be transported towards the shoal by the flood current. The transported sediment would create valuable ecological areas with low flow velocities in the sheltered area behind the disposed sediment. Due to these low flow velocities smaller grain sediment would be able to settle. Besides the creation of ecologically valuable area, a more efficient distribution of ebb and flood currents over the channels was also a goal. Flow velocities in the adjacent channels, and thereby the self-erosive capacity, would increase in order to reduce the dredging activities (Vos, et al., 2009).

2.5 Previous Model Studies

2.5.1 Delft3D and Delft3D Flexible Mesh

<u>NEVLA model</u>

Several hydrodynamic and morphological models of the Western Scheldt have been set up in the past. A widely-used model is the NEVLA model designed with SIMONA software. This hydrodynamic model includes a large part of the Belgian continental shelf, and all its tributaries which are tidal dependent, Durme, Rupel, Nete, Dijle, Zenne (Figure 2-11). Upstream time series of measured discharge are imposed. Downstream the offshore boundaries are based on nesting in the larger ZUNO North Sea model. The 2D depth averaged NEVLA model is continuously subject to further improvements and maintenance (Vanlede, et al., 2015).

Figure 2-11 Delft3D NEVLA grid (Vanlede, et al., 2015)

Meso Morphological Modelling Studies

Tiessen, et al. (2016) converted and validated the Delft3D NEVLA model to a Delft3D Flexible Mesh model in order to use this model to simulate the flow velocities on meso-scale in the Western Scheldt. The main advantages of Delft3D Flexible Mesh are the possibility to locally increase the level of detail without a large increase in grid size and its faster computations. Due to these advantages, the Delft3D Flexible Mesh software is promising software to simulate the developments on a meso-scale. Developments on a meso-scale are smaller than the developments that the NEVLA model is used for in the past.

Besides, Tiessen, et al. (2016) compared simulated velocities close to the intertidal shoal *Walsoorden* with measurements. The flow velocities at the shallow sub tidal areas were reproduced very well, while the flow velocities at the intertidal areas were reproduced reasonably well. Larger errors were found for very small water depths. However no unambiguous relationship was found between the mean absolute error and the water depth. For locations with a maximum flow velocity between 0.5 m/s and 1.5 m/s, the average mean absolute error of the flow velocities was 0.14 m/s. A sensitivity analysis pointed out that small improvement could be obtained by an adjustment of the bed level and a changed Manning roughness coefficient. Still an averaged absolute error of 0.12 m/s was approximately twice as big as the uncertainties in the measurements. An increase in roster resolution gave only limited improvements in the results. The bathymetry of the intertidal shoal was already represented well by the coarser grid size. However, this does not mean that this is the case for all shallow water locations.

Palaiogianni (2015) modelled the hydrodynamic response of large scale sediment disposal in the Western Scheldt using the new Delft3D Flexible Mesh software. Because the used software was under development at the time of this study, sediment transports were calculated with an offline approach and compared to Delft3D results. The initial response of the system was estimated by predicting residual transports using hydrodynamic model results. She concluded that the influence of several processes that were not included in her model, such as waves, might affect morphology on intertidal flats. A comparison with measurements instead of another numerical model would give a better reliability of the results. Finally she recommended running a similar model including morphology to get better insight in how morphological developments and residual transports are related.

2.5.2 *Finel2D*

Dam (2013) used a Finel2D model of the Scheldt Estuary to calculate the long term morphological development. The results of this model were compared with measurements and the Delft3D NEVLA model. Areas above NAP -2 m were imposed with higher roughness in order to reduce the erosion. The found results were very similar to the results found by the Delft3D NEVLA model.

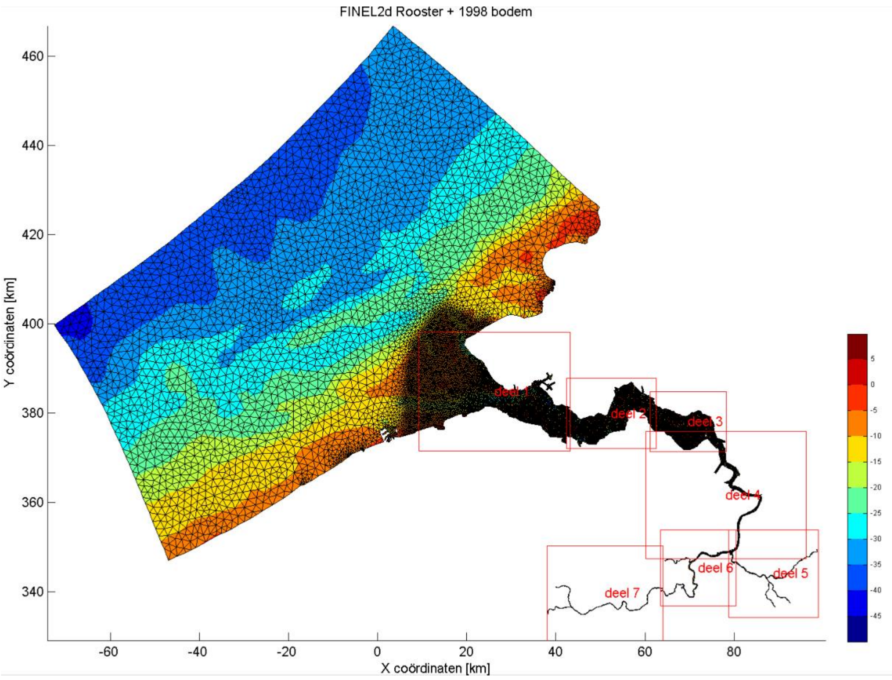

Figure 2-12 Finel2D Scheldt Estuary grid (Dam, 2013)

Due to a too large grid size, the model was not able to reproduce detailed developments on intertidal shoals. In order to evaluate the sedimentation erosion patterns a short term run of the sediment disposal on intertidal flat *Walsoorden* with a locally refined grid was made. A full neap spring tidal cycle with a morphfac of 24.75 was simulated. The results were compared with measured bathymetric data. From this it was concluded that the spatial patterns of erosion and sedimentation were reproduced reasonably well. The locations north of the shoal with the largest magnitudes of sedimentation and erosion were reproduced. The actual magnitude of these sedimentation and erosion were underestimated by the model. The flood dominated sediment transport in this area is clearly reproduced by the model. South of the shoal the model reproduces the bathymetric developments less good.

Dam recommended including multiple grain sizes and running a 3D model to gain better results for short term morphological development of intertidal areas.

3 Analysis of Intertidal Shoal *Walsoorden* Data and Development

The morphological cell that will be looked into in more detail is macro cell 5 (see Figure 2-2).This macro cell contains the area around the intertidal shoal *Valkenisse* and intertidal shoal *Walsoorden* (Figure 3-1). First, the natural developments over the last decades will be summarized. Later on, the developments after the (test) nourishments will be looked into in more detail.

3.1 Situating

The main channel changes name within the cell. The channel west and south of intertidal shoal Walsoorden is ebb dominated and is called Zuidergat, Bocht van Walsoorden and Overloop van Valkenisse from west to east. The channel above intertidal shoal of Walsoorden is flood dominated and contains the Schaar van Waarde and Schaar van Valkenisse. This channel divides the intertidal shoal Valkenisse and the intertidal shoa of Walsoorden. Several key morphodynamic developments of the area will be addressed in the following chapters.

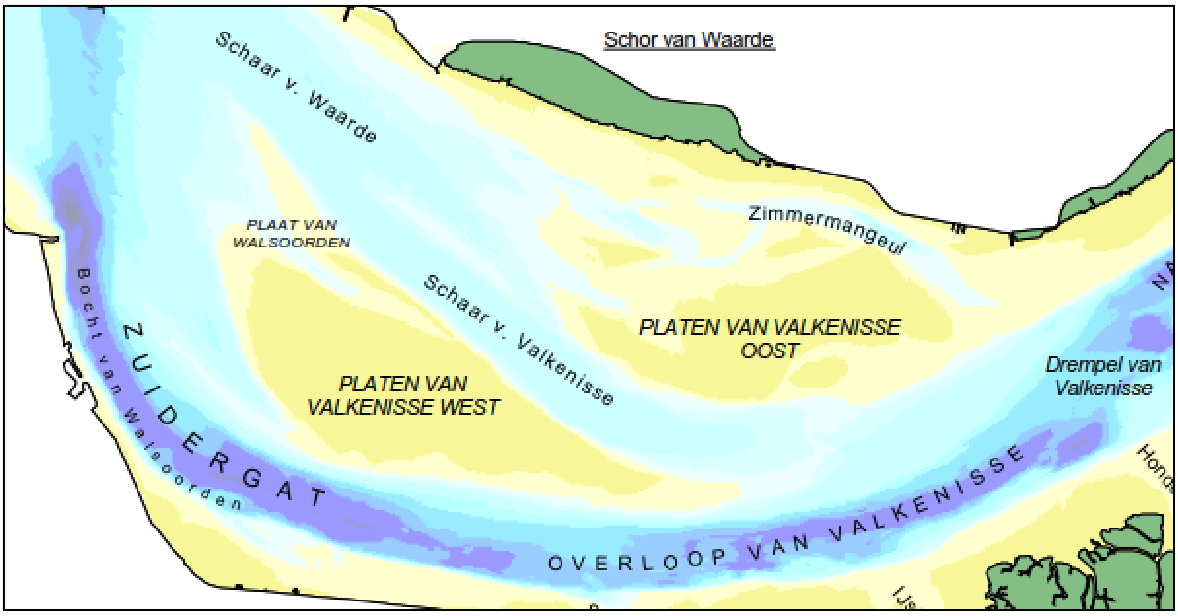

Figure 3-1 Macro-cell 5

3.1.1 Channels

The expansion of the navigational channel is clearly visible in the area around the intertidal shoal of Walsoorden. Since 1970 the sediment volume of the main ebb channel below NAP -2 m has decreased by 65 million m^3 and the average depth has increased by 3 m since 1955 (Cleveringa, 2013b). This is the result of multiple dredging activities corresponding with the deepening of the navigational channel. The most profound changes due to dredging activities can be found at the natural sills. Maintenance dredging is used to keep these sills sufficiently deep for navigation.

Besides the ongoing deepening of the channel, the channel migrated southward. The outer bend of the main channel eroded while the northern channel bank migrated to the south. Because the southern bank migrated faster than the northern bank, the width of the channel increased. The widening of the main channel continued until into the 1990s and stabilized later. The erosion of the main channel has continued until the outer bend of the main channel was fixed with an embankment (Cleveringa, 2013b).

Figure 3-2 shows that the flood-dominant secondary channel Schaar van Valkenisse varied in both location and size resulting in different geometries of the basin (Consortium ARCADIS - Technum, 2007b). During the 1980's the channel almost disappeared, but it has been recovered in the 1990's. In the last few years, the channel migrated south west and eroded the southern part of intertidal shoal Walsoorden. The northern flood channel Zimmermangeul is degenerating (Consortium ARCADIS - Technum, 2007a).

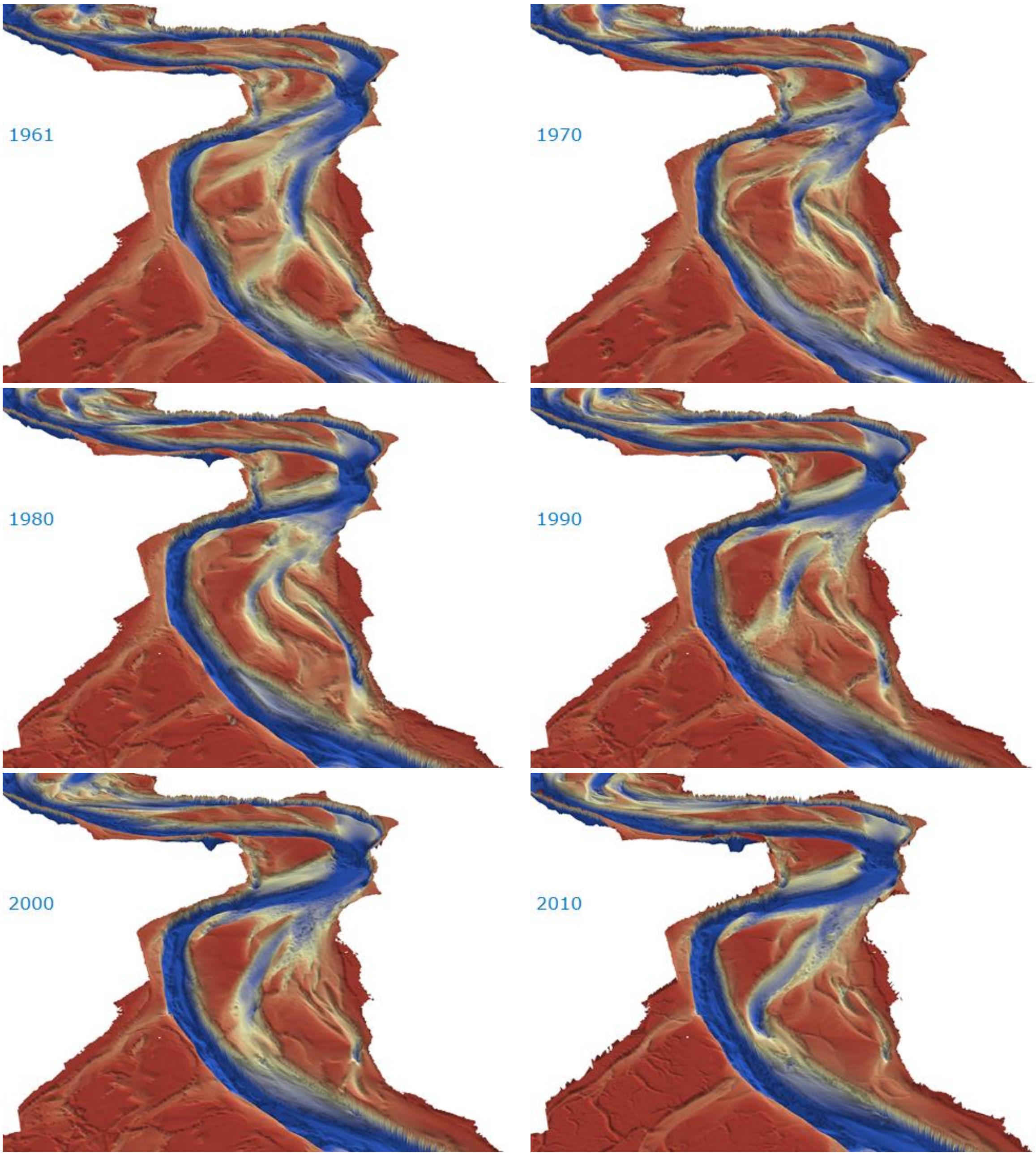

Figure 3-2 Bathymetric data of macro-cell 5 for the years 1961, 1970, 1980, 1980, 1990, 2000 and 2010. The direction of the view is towards the west (North Sea) (Rijkswaterstaat, 2012).

3.1.2 Intertidal Shoals

Despite the decrease of sediment in the macro cell, the sediment volume of the intertidal shoals has increased over the last decades. The number of shoals decreased while the total surface area and average height of the shoals increased. The increase of surface area and decrease in numbers of shoals can be explained by the sedimentation of the connecting channels. As a result of the decreasing number of connecting channels the dynamics decreased and more sediment was deposited on the shoals. Deepening the channel caused the disappearance of connecting channels over the shoal area in macro-cell 5 (Consortium ARCADIS - Technum, 2007a). Connecting channels originate from water level differences between two main channels. The key parameter that plays a role in temporal variations in water level differences is the difference in depth between the main channels (Swinkels, et al., 2009). Deepening of the one of the main channels for navigational purposes attributed to a decrease in the water level difference between the main channels. The smaller difference in water level led to a loss of connecting channels and thus the number of intertidal shoals.

The increase in height of intertidal shoals has led to more permanent dry areas. On these dry areas vegetation is more likely to be present. The presence of vegetation influences the flow conditions. Sedimentation has increased due to the capture of sediment by the vegetation on intertidal shoal Walsoorden. Especially the sedimentation of finer sediments has increased. The already high parts of the shoals increase even further (Cleveringa, 2013c). Due to the migration of Schaar van Valkenisse the whole intertidal shoal Walsoorden migrated eastward over the last decades.

Since 2005 several flow slides have been observed at the south side of intertidal shoal Walsoorden (Mastbergen en Schrijvershof, 2015). This is the result of sedimentation of the intertidal zones that lead to steeper slopes. Due to the dynamics in morphology, the sensitivity of flow slides has changed over the last few years as well (Mastbergen en Schrijvershof, 2015).

3.2 Test Disposals

3.2.1 Monitored Sediment Disposals

Within the framework of "*the Walsoorden pilot project*", two in situ disposal tests were executed between November 2004 and March 2007. Detailed measurements of both hydrodynamics and morphology have been taken since November 2004. At the first disposal, 500.000 m^3 of sand was disposed using a diffuser spray nozzle. This way, the sediment could be placed very precisely. Between January 2006 and March 2007 two additional disposals, of 500.000 m^3 and 900.000 m^3 respectively, were executed using the traditional "clapping" technique.

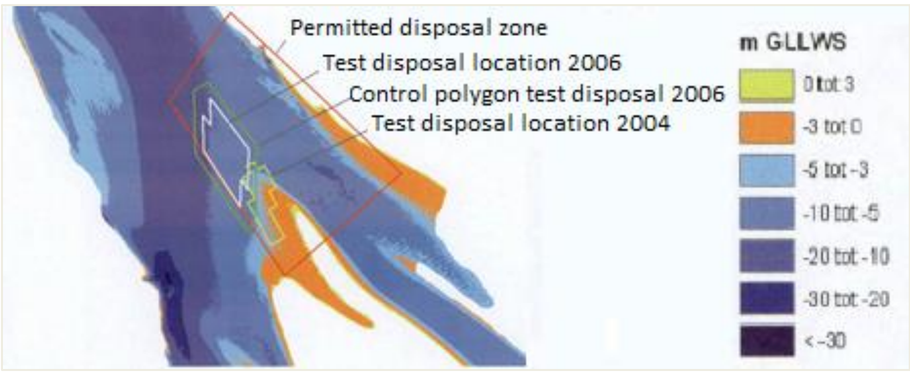

Figure 3-3 Locations of the test sediment disposals and the permitted disposal site (WLB, 2008)

The location of the test disposals is displayed in Figure 3-3. WLB (2006, 2008) evaluated the measurements and concluded that the tests were a success from a morphological point of view. Both disposals led to a transport of the sediment towards the shoal. From an ecological point of view neither positive - nor negative changes in trends were identified as a result of the tests.

Besides the analyses of the bathymetric data, an analysis of the local sediment grain size distribution was also made (WLB, 2008). Samples were taken at of the intertidal zones near the shoal and of the locations were the sediment was disposed. Median grain sizes in the intertidal zone varied between 131 µm at the higher parts of the shoal and 214 µm at the spit north of the shoal. At the location of the sediment disposals the median grain size was between 200 and 250 µm. Only at the centre of the shoal a significant amount of fine sediments (<63 µm) were found (10-15%). In the intertidal and subtidal areas at the location of the disposals the found mud fractions were smaller than 2%. It was concluded that the executed test disposals did not result in an evident change of the local sediment distribution.

3.2.2 Currents

Both measurements (Plancke, et al., 2010; IWA, 2003; WBL, 2007) and numerical models (Plancke, et al., 2009b) have been used to determine the size and direction of the flow around the intertidal shoal *Walsoorden*. A validated numerical model was used to asses average and maximum flow velocities around intertidal shoal *Walsoorden* during neap, average and spring tide conditions (Plancke, et al., 2009b). For all conditions both average and maximum flood velocities exceeded the corresponding ebb velocities. Figure 3-3 shows the spatial variations of the maximum tidal current for average and spring tidal conditions. It shows that the spatial variation is similar for both tidal conditions. Plancke, et al. (2009b) conclude that this holds for both average and maximum velocities

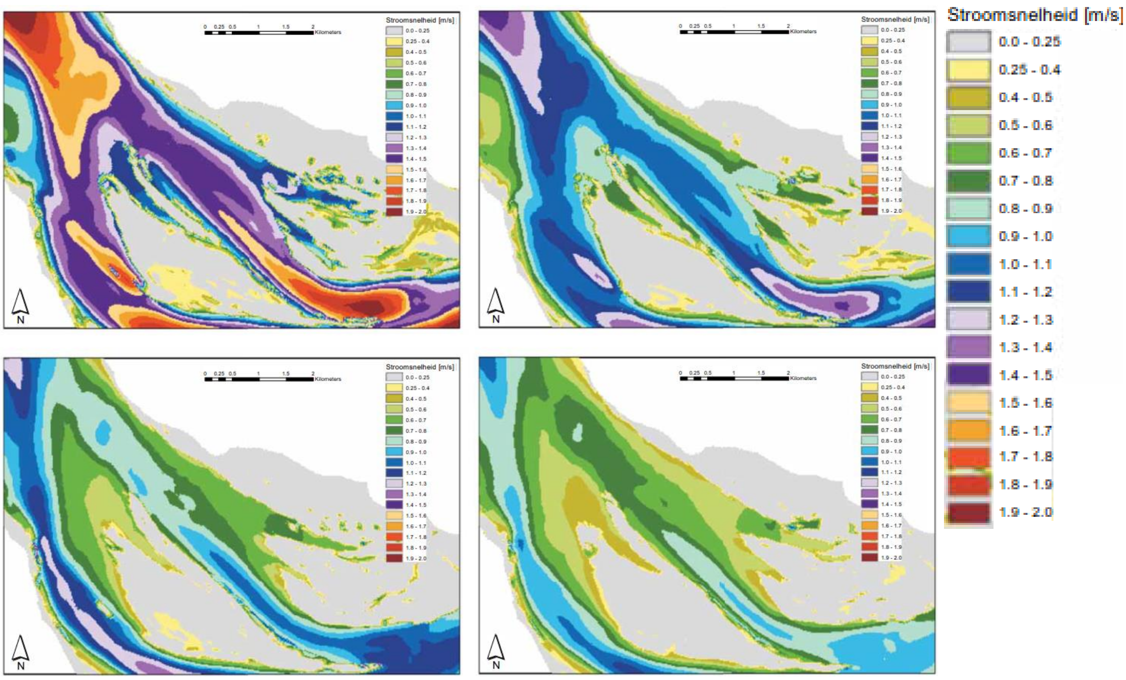

Figure 3-4 Maximum tidal flow velocities near intertidal shoal of Walsoorden for spring (left) and average (right) tidal conditions for flood (upper figures) and ebb (lower figures) simulated by Plancke, et al. (2009b).

During neap tide conditions, average flow velocities do not exceed 0.5 m/s. During average tidal conditions, the average ebb flow velocities, at the tip of intertidal shoal of Walsoorden are smaller than 0.5 m/s, while the average flood velocities differ between 0.6 and 0.8 m/s. Similar average velocities are found in the channel Schaar van Waarde.

Local ebb- or flood-dominance was determined by the asymmetry of present bed forms and the ratio between the average flood and ebb velocities (Plancke, et al., 2009b). If the seaward (landward) slope of the bed forms is longer than the land ward (seaward) slope (ebb) flood dominance is indicated. If the current velocities during rising (falling) tide are higher than during falling (rising) tide, flood (ebb) dominance is indicated. From both analyses a clear distinction could be made between the channels and the leeward zones of the intertidal flats. While the main channels are neutral or slightly ebb dominated, the sheltered zone north of the intertidal shoal of Walsoorden where the test disposals were carried out show flood dominated behaviour.

3.2.3 Sediment Transport

Vandenbruwaene, et al. (2012) analysed local measurements of flow and bathymetric data to estimate sediment transports at the tip of intertidal shoal *Walsoorden*. The flow velocities of a hydrodynamically validated model data were used to set up the boundary conditions for a computational grid which calculates the sediment transport at the disposal site prior to the sediment disposal. The simulated period was from November 2009 to February 2010. The found sediment transport varied between 1.5 m^3/m/tide in the flood direction and 2.0 m^3/m/tide in the ebb direction.

Near the subtidal area north of intertidal shoal *Walsoorden,* the residual transport is directed in the flood direction towards the shoal. As the distance to the flat increases, so does the transport. Near the southern flood chute there is a large scatter in residual transport. The chute itself is flood dominated while the sandbar south of it, next to the *Zuidergat,* is ebb dominated. Figure 3-5 gives an indication of the sediment transports near intertidal shoal *Walsoorden.*

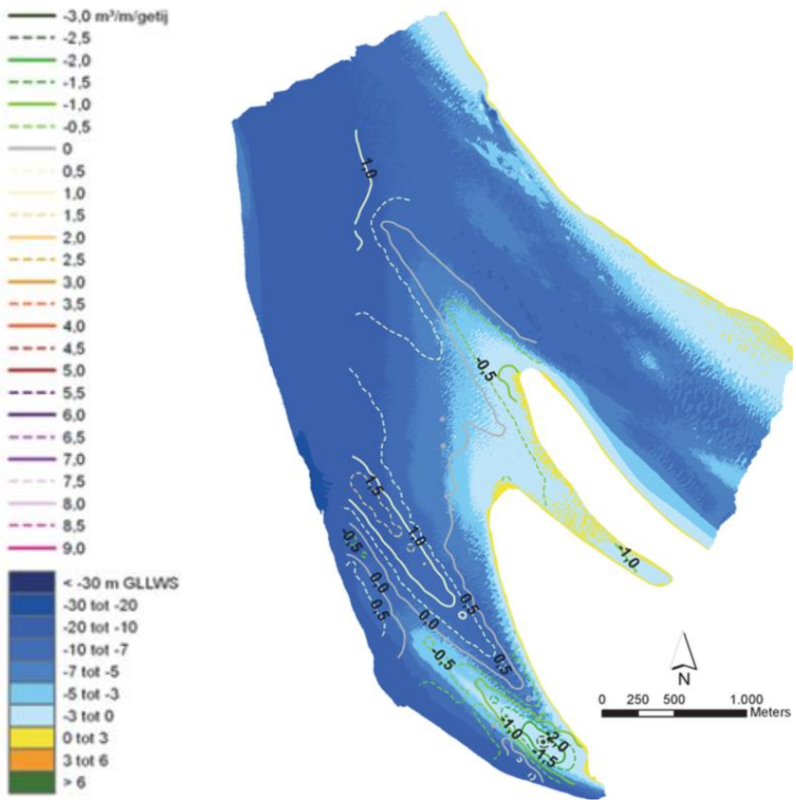

Figure 3-5 Contour plot of the natural transport between 17/11/2009 and 16/02/2010 near intertidal shoal *Walsoorden. Positive values indicate flood dominant transport; negative values indicate ebb dominant transport* (Vandenbruwaene, et al., 2012).

3.3 Sediment Disposals

After the test disposals and measuring campaign, 3.72 million m^3 sand was disposed at the tip of intertidal shoal *Walsoorden* between February and September 2010. This sand was dredged from the *Zuidergat* related to the third expansion of the navigational channel. A control polygon was introduced in which topo-bathymetric surveys were executed twice a month with a multi-beam echo sounder, producing very high resolution bathymetric charts (1x1m). Figure 3-6 shows the bathymetry before and after the disposal including the location of the control polygon.

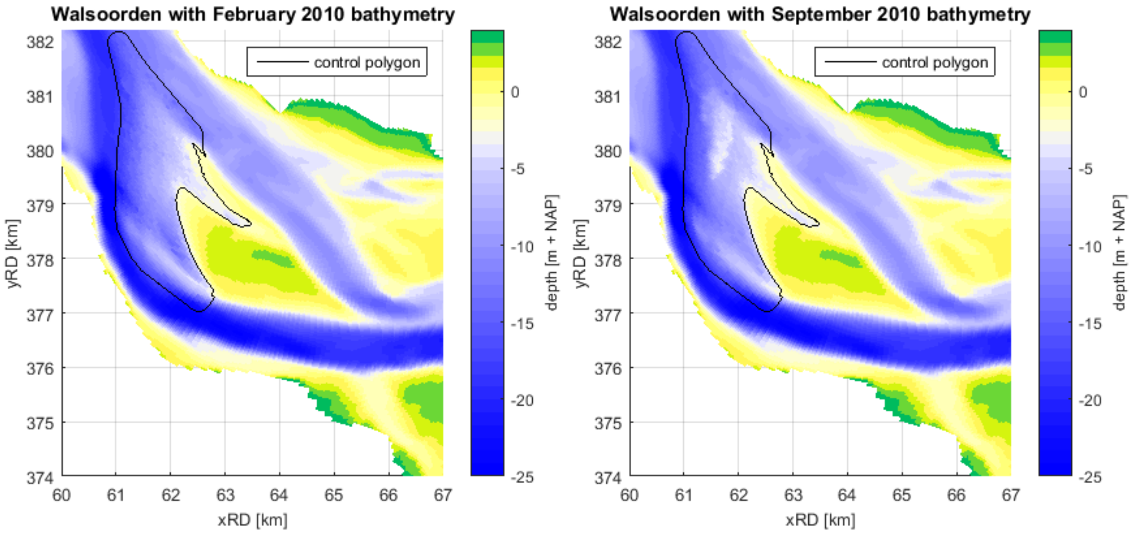

Figure 3-6 Intertidal shoal *Walsoorden* with February 2010 - and September 2010 Bathymetry including control polygon

The figure on the left in Figure 3-7 shows the difference between these two bathymetries within the control polygon. The volumes in the control polygon for all measurements were compared with the volume in the control polygon in February 2010 before the disposals had started (IMDC, 2012). Differences between the measurements were used to quantify the erosion or sedimentation of the control polygon. The found differences in volume were used as a parameter to describe the stability of the disposed sediment. In October 2011, the sediment volume of within the control polygon had decreased with approximately 40 % of the volume of the disposed sediment (IMDC, 2012).

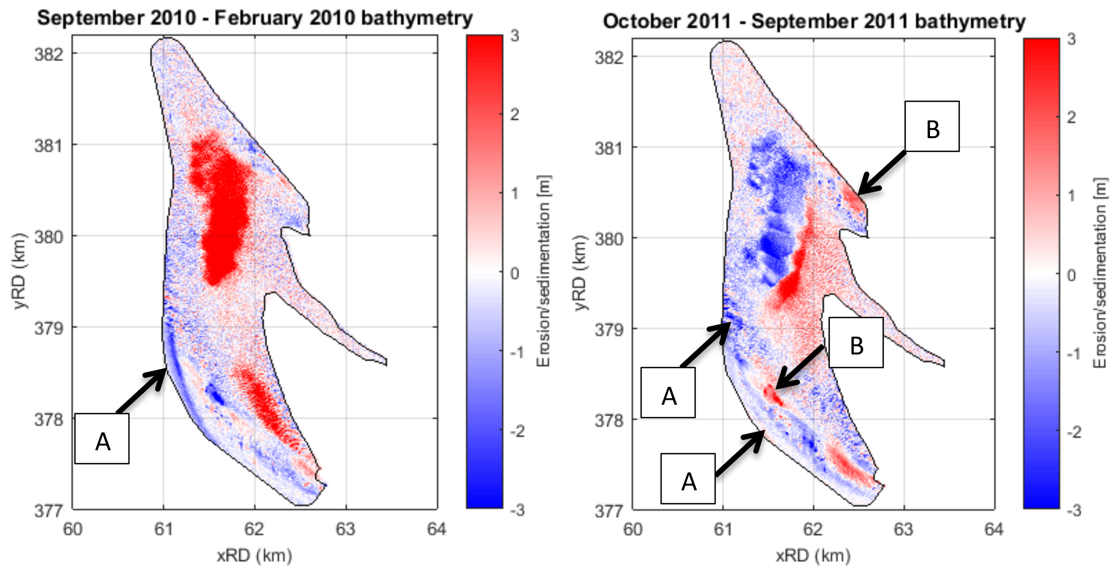

Figure 3-7 Difference in bathymetry between September 2010 and February 2010 (left) and October 2011 and September 2010 (right)

A large part of the sediment was lost during the execution of the works at the north side of nourishment (IMDC, 2012). An overview of the measured and disposed sediment at intertidal shoal *Walsoorden* between the start of the disposal and October 2011 is given by Figure 3-8. Just after the execution works stopped in September 2010, the difference between the disposed sediment and the measured volumes was 0.88 million m^3. Between September 2010 and October 2011 the difference in sediment volumes within the control polygon increased to almost 1.45 million m^3. The right side in Figure 3-7 shows the difference between the September 2010 and October 2011 bathymetry. From this Figure it can be obtained that part of the disposed sediment had moved in the flood direction towards the shoal. Locally large sedimentations and erosions have occurred between September 2010 and October 2011. Except for small regions near the northern and southern flood spits (See B in Figure 3-7), the deeper parts of the subtidal area around the shoal near the navigational channel have increased in depth (see A in Figure 3-7) (IMDC, 2012).

It needs to be taken into account that the developments in sediment volumes in the control polygon are not solely the result of the sediment disposals. The natural developments that were present before the sediment disposals occur simultaneously with the development of the disposed sediment.

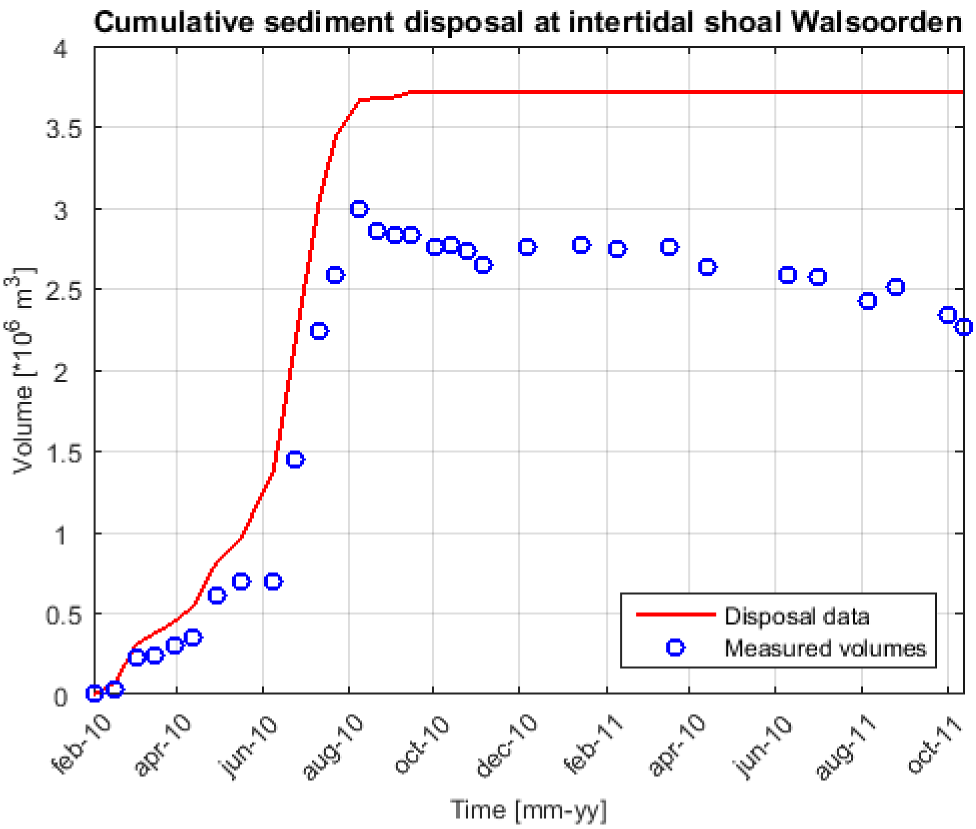

Figure 3-8 Overview of the sediment disposals at intertidal shoal *Walsoorden*. The data of the disposed hopper volumes is displayed with the red line. The blue dots display the volumes calculated on the basis of bathymetry measurements. (IMDC, 2012)

Because the largest loss of sediment occurred during the execution works, and no significant losses occurred between September 2010 and February 2011, the consultation group Flexible Disposal decided to carry out more sediment disposals in the subtidal region north of intertidal shoal Walsoorden from October 2011 onward (IMDC, 2013). Between October 2011 and November 2011 another 0.82 million m^3 of sediment was disposed of at the subtidal zone north of intertidal shoal Walsoorden.

The rest of this chapter will focus on the development of the sediment that is disposed during the first execution works between February and September 2010. Figure A- 1 shows areas within the control polygon where the sedimentation or erosion exceeds certain threshold values between September 2010 and October 2011. Note that the Figure is the same as the right side in Figure 3-7 and that the used bathymetry is of 12 October 2011 just before the new sediment disposals were carried out. This analysis gives an indication of the spatial variation and magnitudes of the sedimentation and erosion of the disposed sediment. Table 3-1 shows the areas and volumes of zones as displayed in Figure A-1 where the sedimentation or erosion is larger than the specified threshold value. Overall it can be concluded that the areas and eroded volumes in the erosion zones are larger than the areas and accreted volumes in the sedimentation zones.

Table 3-1 Areas and volumes eroded and accreted sediment in the different polygons displayed in figure A -3

Threshold value	Area of the erosion zone [$*10^6$ m^2]	Area of the sedimentation zone [$*10^6$ m^2]	Volume of the erosion zone [$*10^6$ m^3]	Volume of the sedimentation zone [$*10^6$ m^3]
0.50 m	1.09	0.70	1.32	0.82
0.75 m	0.69	0.48	1.03	0.70
1.00 m	0.56	0.24	0.92	0.47
1.25 m	0.33	0.18	0.63	0.39

The contour lines in Figure 3-9 indicate the spreading and migration of the disposed sediment. Similar Figures for the 1.5 and 2.0 m difference contour lines can be found in Appendix A. It can clearly be seen that the sand is transported towards the flat and that the sediment is spreading out. The spreading of the contour lines is predominantly in the flood direction; the spreading in the lateral direction is limited.

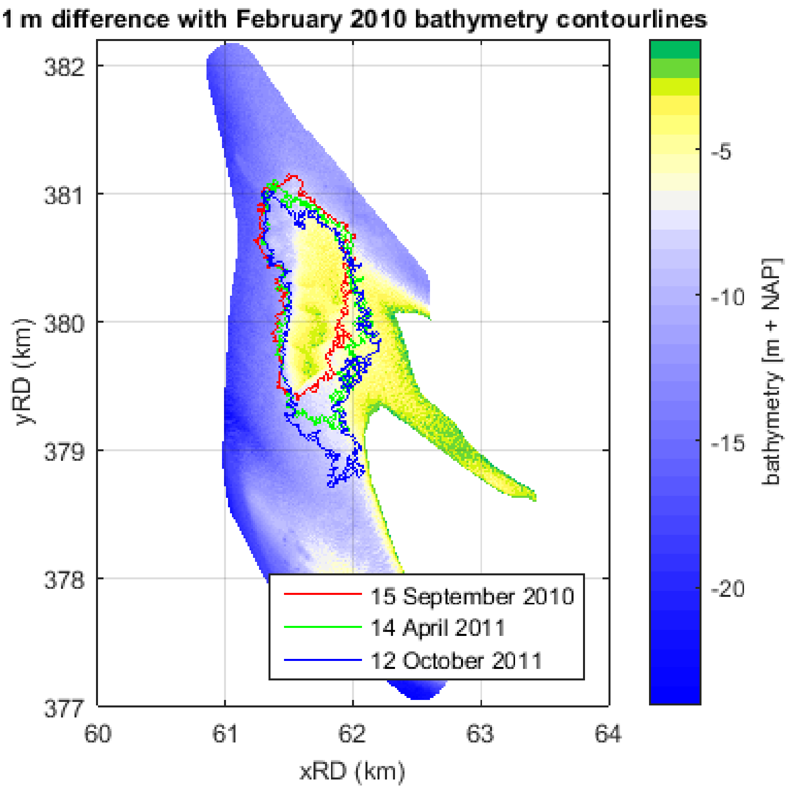

Figure 3-9 Contour lines that indicate a difference in bathymetry that is larger than 1.0 m compared to the February 2010 bathymetry displayed on a September 2010 bathymetry.

The areas and corresponding differences in sediment volumes of the difference polygons of Figures 3-9, A-2 and A-3 are displayed in Table 3-2. The calculated volumes can be used to explore how much the sediment that is disposed at the subtidal zone north of the intertidal shoal of Walsoorden contributes to the total sediment that is lost from the control polygon in this period. The surface of the 1.0 m difference polygon increases while the sediment volume decreases. This is a consequence of the smoothening of the sediment. The regions with a larger initial difference decrease in volume and surface. However, the decrease in volume is larger than the decrease in area. This can also be seen as an indication for the smoothening of the sediment because the average difference in depth with the initial situation decreases. Figures 3-10 supports this observation.

Table 3-2 Areas and corresponding differences in sediment volumes of the difference polygons of Figures 3-9, A-2 and A-3

	1.0 m difference contour line	**1.5 m difference contour line**	**2.0 m difference contour line**
Area within the September 2010 polygon [ha]	80.3	70.3	63.6
Area within the April 2011 polygon [ha]	92.8	66.0	50.7
Area within the October 2011 polygon [ha]	100.6	61.4	44.9
*Difference in sediment volume between September 2010 and February 2010 within the polygon [*10^6 m^3]*	2.55	2.42	2.31
*Difference in sediment volume between April 2011 and February 2010 within the polygon [*10^6 m^3]*	2.33	1.97	1.69
*Difference in sediment volume between October 2011 and [*10^6 m^3]*	2.29	1.79	1.48

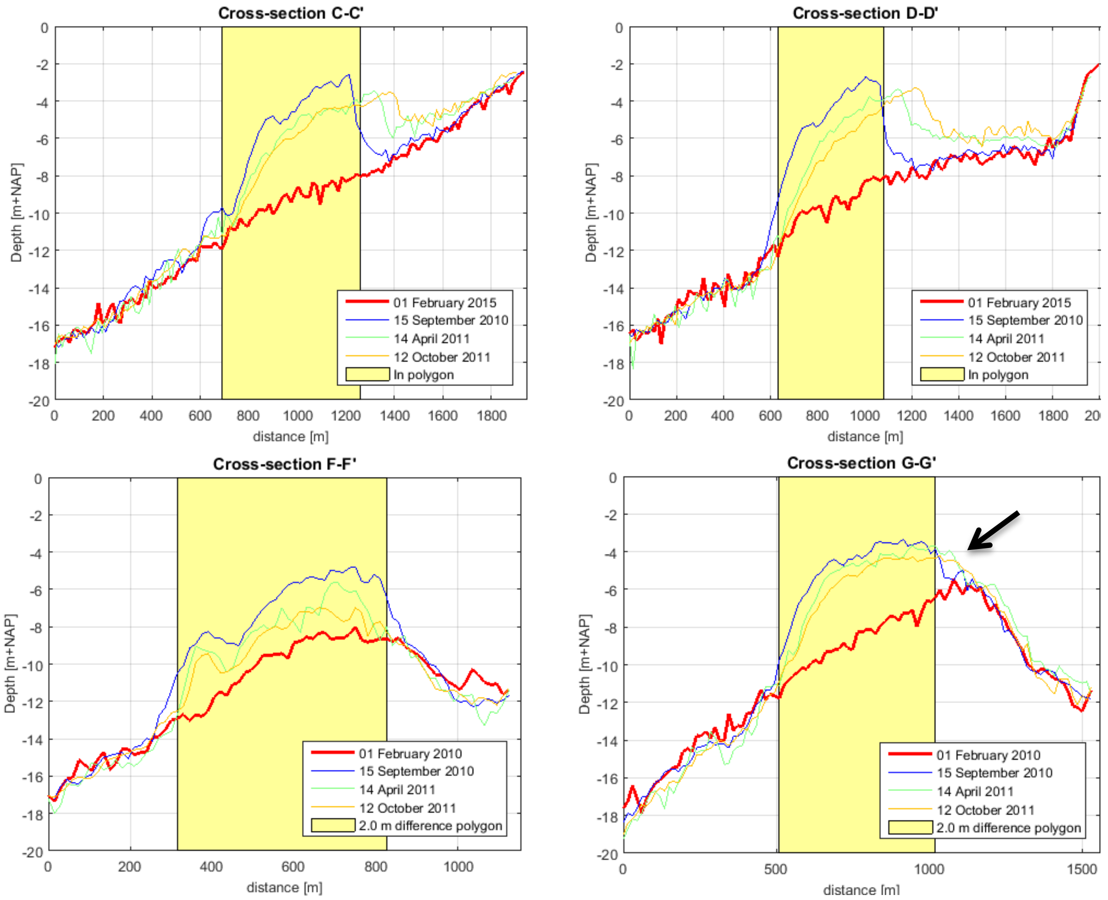

Figure 3-10 Developments of the longitudinal (C-C' & D-D') and transverse (F-F' & G-G') cross-sections of the disposed sediment at the subtidal zone north of intertidal shoal *Walsoorden.*

The profile of two longitudinal and two transverse cross-sections is displayed in Figure 3-10. The directions have been adopted from the monthly reports of the consultation group Flexible Disposal and are parallel and perpendicular to the dominant flood and ebb direction. The location of these and the other cross-sections can be found in Figure A-4 in Appendix A. The longitudinal cross-sections show that the disposed sediment has moved in only one direction (flood direction). Furthermore, the top of the disposed sediment is decreasing in magnitude and is transported towards the shoal. The landward slope of sediment disposal (on the right side in the figures) is steeper than the slope of the seaward end. Plancke, et al. (2009b) used this asymmetry to indicate the local dominance. The steeper landward slope indicates flood dominance. This is also what is expected from the shift of the disposed sediment towards the shoal.

The transverse cross-sections (F-F' and G-G') show that the spreading in transverse direction is indeed very little. Except for the location that is indicated by the arrow in Figure 3-10, the green and yellow lines that represent the bathymetry of April and October 2011 are below the blue line that represents the situation in September 2010. This means that the height of the bed decreases and that very little sediment in transported in the direction of these cross-sections.

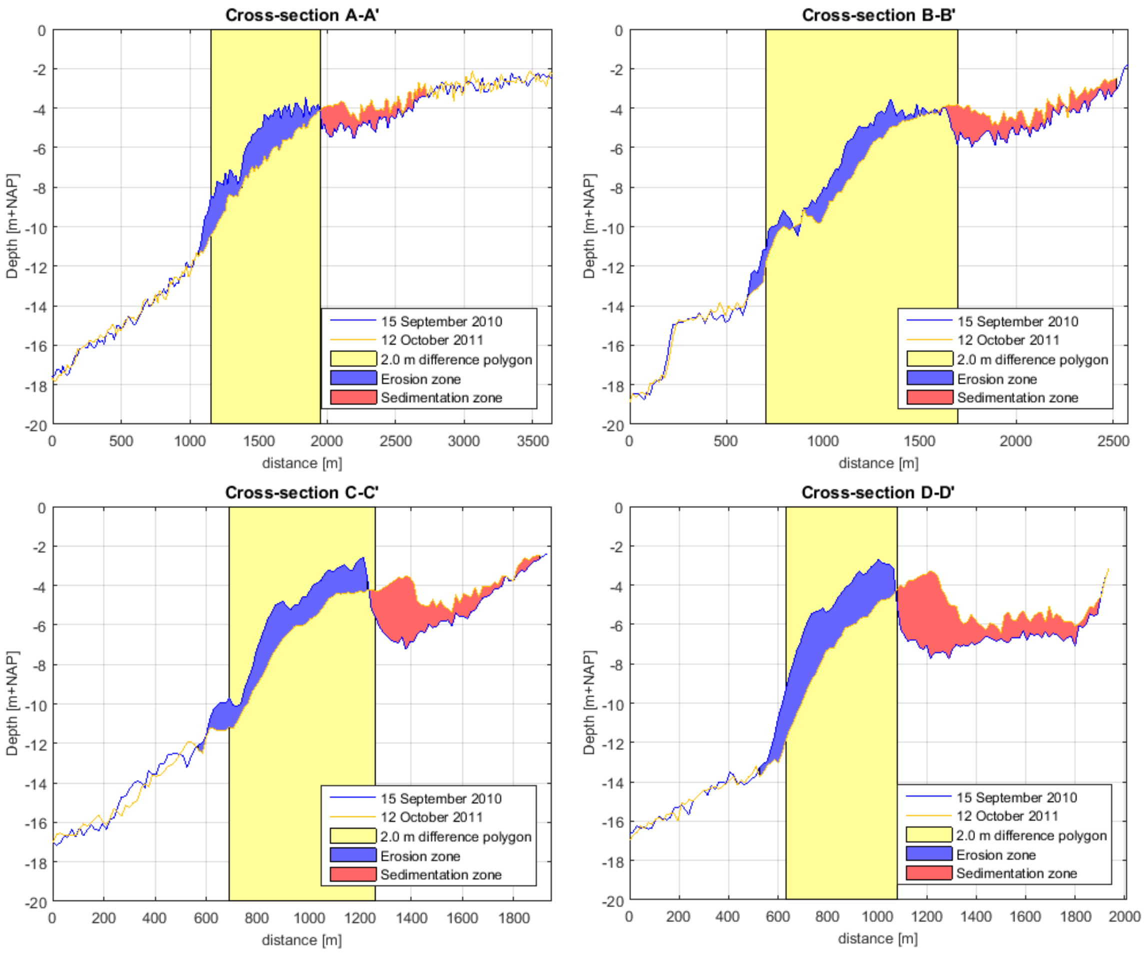

Figure 3-11 Sedimentation (red) and erosion (blue) zones of cross-sections A-A', B-B', C-C' and D-D' between September 2010 and October 2011

For the longitudinal cross-sections (A-A', B-B', C-C' and D-D') the sedimentation and erosion zones between September 2010 and October 2011 have been identified in Figure 3-11. The volumes of these zones have been calculated and compared. This gives an indication of the displacement and the stability of the disposed sediment. The ratio between the eroded and accreted volumes is added to get an idea about the proportionality between the two. The results are displayed in

Table 3-3.

Table 3-3 Sedimentation and erosion volumes between September 2010 and October 2011 of the longitudinal cross-sections.

Cross-section	Volume of the Erosion zone [m^3/m]	Volume of the Sedimentation zone [m^3/m]	Difference between sedimentation and erosion zone [m^3/m]	Ratio of the accreted and eroded volumes
A-A’	1204	666	-538	0.553
B-B’	848	726	-122	0.856
C-C’	901	792	-108	0.880
D-D’	1202	1269	67	1.056

For cross-sections A-A’, B-B’ and C-C’ the volume that has been eroded from the erosion zone is larger than the volume that has accumulated in the sedimentation zone. This means that sediment has been transported out of the cross-section. Because the spreading of the sediment in transverse direction is very limited, it is likely that this sediment has been transported in the longitudinal direction. However, Figure 3-11 shows that the difference between the yellow and the blue line decreases into the landward direction. At the seaward and landward ends of the figures the yellow line and the blue line almost overlay each other. This implies that the changes in volume on the higher parts of the shoal are very small and do not compensate for the deficit of sediment in the evaluated cross-sections.

The ratio between the accreted and eroded volume increases from northwest (cross-section A-A’) to southeast (cross-section D-D’). In cross-section D-D’ the sedimentation is larger than the erosion. The increase of the ratio between the accreted and the eroded volumes might be explained by the fact that some of the sediment is transported from the cross-sections in the north towards the south. Another explanation might be that the hydrodynamic conditions at cross-section A-A’ are more dynamic than at cross-section D-D’.

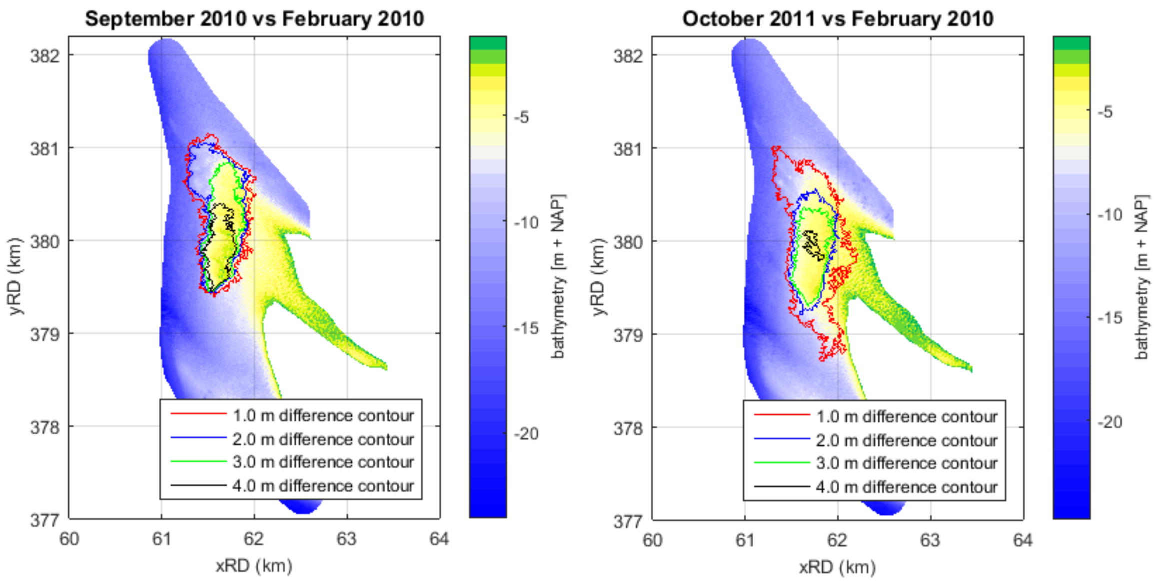

Figure 3-12 Contour lines that indicate the difference in bathymetry between 15 September 2010 and 1 February 2010 (left) and the difference in bathymetry between 12 October 2011 and February 2010 (right)

Figure 3-12 shows how contour lines that indicate a difference with the February 2010 bathymetry develop over time. The contour lines represent discrete differences between the considered bathymetry and the February 2010 bathymetry. The development shows how the sediment is spreading out over time. As can be seen from this figure, the areas that are enclosed by the 2.0, 3.0 and 4.0 m polygon decrease. This means that on these locations more sediment is eroded than accreted. The space between difference contours increases. This indicates that the slopes become more gradual. Due to the two above mentioned reasons it can be conlcuded that the sediment is spreading out over time.

3.4 Observations and Findings

In this subchapter a twofold is made between the observations of the development of the shoal that was present prior to the sediment disposal and the development of the disposed sediment itself. Firstly, the observations of the natural development will be summarized. Next, the observations and findings of the morphological development of the disposal will be addressed.

Morphological Developments Prior to the Sediment Disposals

The trend of an increasing volume of the main channel that has been enhanced by human interventions led to a decrease of the dynamics in intertidal areas. Slopes between the channel and the intertidal shoal became steeper and valuable intertidal areas were lost to the channel or became the shoal. The average height of the shoal increased and sediment was brought from intertidal areas up to the shoal. Degeneration and loss of interconnecting channels contributed to this trend.

Morphological Development of the Disposed Sediment

During the seven months that the sediment was disposed, 0.88 million m^3 of sediment disappeared from the control polygon. Between September 2010 and October 2011, 0.57 million m^3 sediment was lost from the control polygon. The difference in volumes and areas of the zones that are enclosed by the 1.0 m difference polygons in Figure 3-9 (Table 3-2) can explain part of this loss. While the area of this zone has increased, the sediment volume has decreased with 0.26 million m^3. Furthermore, the cross-sections show that the surfaces of the erosion zones are larger the surfaces of the sedimentation zones. The rest of the sediment that has disappeared from the control polygon is most likely to be due to the natural development of the shoal that was already present prior to the sediment disposals.

Figures 3-7 and 3-9 to 3-12 show that the sediment that was disposed in the subtidal zone north of the intertidal shoal of Walsoorden smoothens out, and that it is mainly transported in the flood direction. Figure 3-10 shows that the top of the sediment decreases in magnitude, the slopes of the disposal decrease and the displacements are towards the shoal. From the difference contour lines it can be concluded that the sediment spreads out. The transverse cross-sections show that only very limited spreading has occurred in the lateral direction. Finally, the ratio between the accreted and the eroded volumes of the longitudinal cross-sections increase from northwest to southeast. A conclusive reason for this has not been found by looking at the bathymetric data.

4 MODEL SETUP AND VALIDATION

In this chapter the set-up of the hydrodynamic model and model that includes sediment transport is explained. The modelling system that was used to simulate the hydrodynamics and morphology is Delft3D D-flow Flexible Mesh. The starting point from this study is the validated DFM NeVla model (Tiessen, et al., 2016). This model is a derivative from the original Delft3D NeVla model that has been used in the LTV V&T report A27 (Grasmeijer, 2013) and has been validated for the years 2013 and 2014 validated by Vroom et al. (2015) (see also Figure 2-11). The model is a hydrodynamic model that describes the depth average flow velocities forced by the wind, the tide, river discharges and the influences of salinity. The effect of wind waves is not included in this model.

4.1 *Delft3D Flexible Mesh (DFM)*

Delft3D Flexible Mesh (DFM) is the latest hydrodynamical simulation program by Deltares. It is part of Deltares its unique, fully integrated computer software suited for a multi-disciplinary approach and 1D, 2D and 3D computations for coastal, river and estuarine areas. At the moment of writing, the software is still in development and many features such as waves, sediment transport and morphology are not yet fully operational.

The most noticeable differences with its predecessor, Delft3D-flow, are the use of unstructured (flexible) grids and its faster computations. Large regions with curvilinear grids can be coupled with more freedom than before, using triangles, pentagons and hexagons. Grid refinement (and coarsening) is possible without domain decompositions in one model grid. This means that a larger level of accuracy can be obtained without a large increase of the computational time or splitting up the model domain.

Delft3D Flexible Mesh uses the depth-averaged, homogeneous shallow water equations for the calculation of the hydrodynamics. In contrary to Delft3D-flow, the time-step is variable and is calculated by the model based on local flow velocities. Relatively small cells with high flow velocities limit the calculation time. The possible performance penalty that may result from this approach can often be remedied by coarsening the computational grid at the right locations (Deltares, 2016).

4.2 *Baseline Model*

4.2.1 *Computational Grid and Time Step*

Due to the before mentioned advantages of an unstructured grid difficult geometries like bifurcations, confluences or local grid refinements are easier to construct. These advantages resulted in a reduction of the number of grid cells from 230.000 cells in the original Delft3D model to 170.000 cells in the DFM model without a significant loss of the grid resolution. Only some cells in the upstream part of the river were coarsened in order to reduce the computational times. Decreasing the resolution of these grid cells resulted in an increase of average time step, and thus a decrease in computations and computation time. In the reference DFM model the computational time is approximately 15 hours for one month. The average time step is 9.5 seconds. The grid resolution varies from ~400 meters, at the North Sea, to ~10 meters in the river branches. In the region of interest a local refinement increases the level of detail. Locally the grid cells are approximately 50 – 75 m. The original Delft3D NeVla model has a computational time of approximately 105 hours per month. The computational grid of the DFM model is displayed on the left side of figure 4-1.

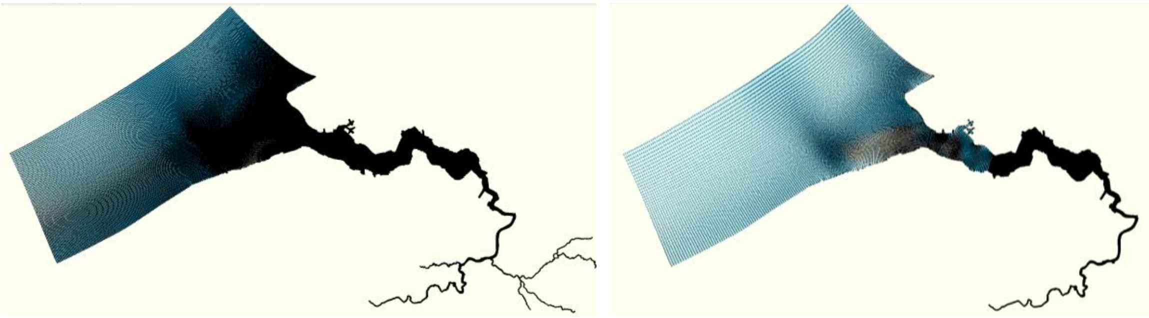

Figure 4-1 DFM NEVLA model (left) and reduced DFM NEVLA model (right) for the purpose of the sediment transport calculations

4.2.2 Bathymetry

The bathymetry of the model that was provided was composited of measurements executed by Rijkswaterstaat and is composited from bathymetries of different years. At the North Sea and in the Western Scheldt the bathymetric data is obtained in 2011. This means that the used bathymetry is the bathymetry after the third deepening of the navigational channel. Further upstream, data is used from bathymetric surveys in 2006.

4.2.3 Initial Conditions

The initial conditions of the used model are set-up for 1 January 2013. The initial salinity is adopted from the restart file of the simulation after one year. In this way, the initial salinity is representative for the month January. However, it is not exactly similar to the salinity that was present at 1 January 2013. This means that there is a spin-up time before the hydrodynamics can be compared with the measurement data.

4.2.4 Boundary Conditions

The boundary conditions at the North Sea are generated by the ZUNO SIMONA model. This model describes the water motions for the north-western part of the European continental shelf. At the northern and southern boundary flow velocities are imposed. At the western offshore boundary, a water level boundary is implemented. At the upstream river boundaries the river discharge measurements are used. The salinity boundary conditions are based on MWTL measurements off the coast of Walcheren. These measurements are limited in time, but give a very good representation of the seasonal variation, which is larger than the tidal variation.

4.2.5 Physical Parameters

The roughness in this model is described with a spatially varying Manning coefficient. The value of this Manning coefficient is based on the comparison between the simulated and measured water levels and has values between 0.017 and 0.028. Around the intertidal shoal of Walsoorden the Manning roughness coefficient is 0.023. Both the horizontal eddy viscosity and the horizontal eddy diffusivity were given a uniform value of 1.0 m^2/s. The wind conditions that were used are a spatially uniform wind field based on measurements of the Dutch meteorological institute, KNMI, at Vlissingen in 2013.

4.2.6 Validation

The water level of the model was validated and calibrated by Tiessen, et al. (2016) with data from 23 measurement stations along the estuary (Figure D-1). To indicate the quality of the model the systematic error (BIAS) and root mean squared error (RMSE) are calculated. A positive (negative) BIAS means that the average water level in the model is larger (smaller) than the measurements. A positive (negative) RMSE means that the variation of the water level in the model is larger (smaller) than in the measurements. The model shows a RMSE that increases from 0.10 m at the mouth, to 0.17 m at Antwerp, up to 0.39 m at Melle. The astronomical water level has smaller errors. The BIAS also increases further upstream into the estuary. Near Walsoorden the BIAS is 0.06 m and the RMSE is 0.09 m. These errors are very comparable with the errors of the original Delft3D model.

The flow velocities are validated with the measurements of 6 stations along the Western Scheldt that are indicated in red in Figure D-1 in the months July and August 2013. An analysis is made for both the magnitude and the direction of the flow. At the station Hansweert, which is closest to the region of interest, the BIAS and RMSE of the flow velocity are 0.04 m/s and -0.14 m/s. The BIAS and RMSE of the flow direction are 1.7 ° and 27.4 °. As mentioned in Section 2.5.1, a more detailed check around the intertidal shoal of Walsoorden was also done. This resulted in a very good agreement of the model results with the measurements. Only the peak flood velocities during spring tide were slightly underestimated by the model. However, the peak flood velocities are an important parameter in determining the magnitudes of the sediment transport. Figures 4-2 and 4-3 show the results for two of the observation points as presented by Tiessen, et al. (2016). The location of these observation points can be found in Figure D-1.

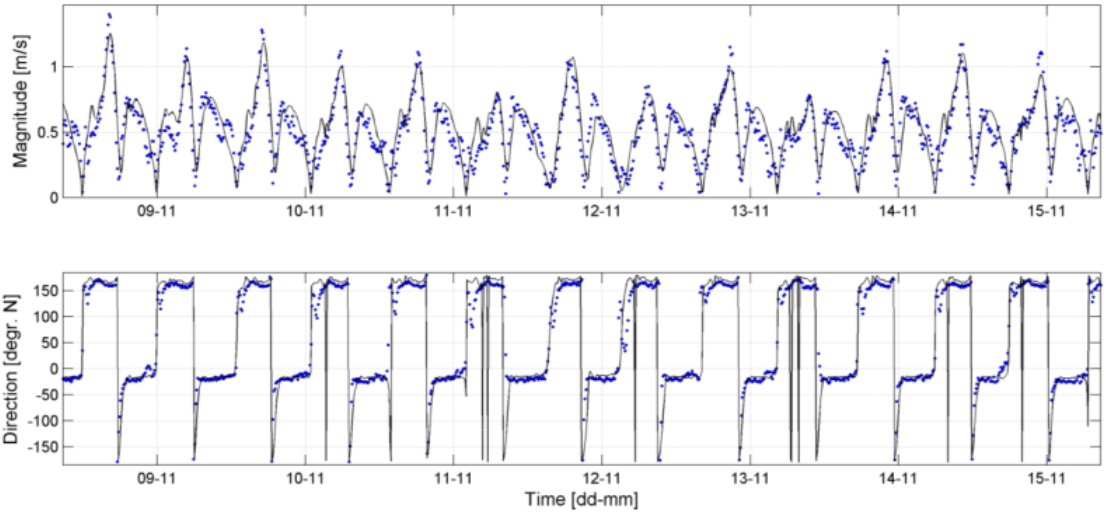

Figure 4-2 Measured (dots) and modelled (black line) flow velocity and direction for observation point MP101 in the subtidal area. (Tiessen, et al., 2016)

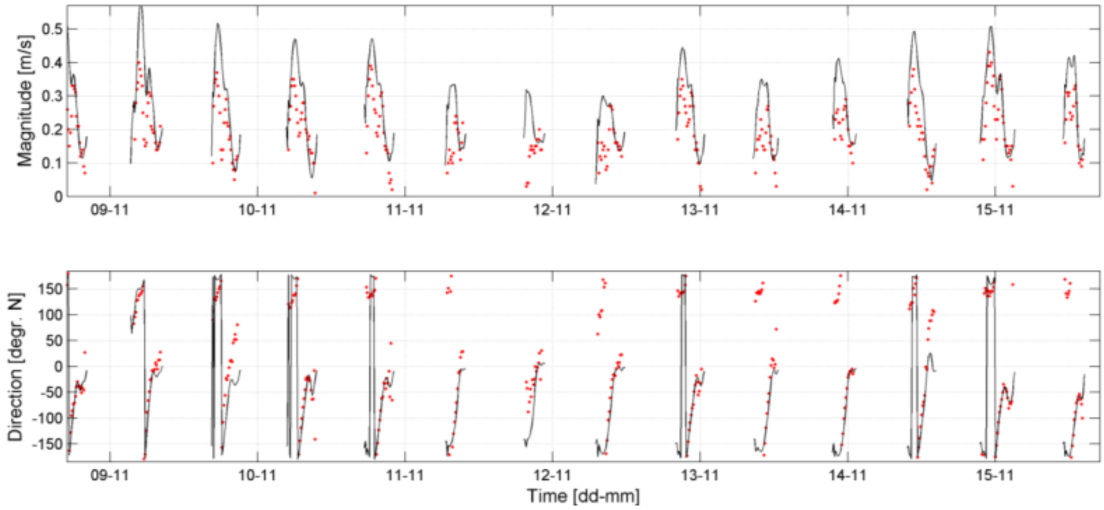

Figure 4-3 Measured (dots) and modelled (black line) flow velocity and direction for observation point MP520 on the intertidal area of intertidal shoal *Walsoorden.* (Tiessen, et al., 2016)

The salinity is validated using three measuring locations along the estuary. A comparison between the measured and calculated values shows good results for the mouth of the estuary. Further upstream in the estuary near Baalhoek, the calculated salinity is 5 to 10 PSU higher than the measured salinity.

4.3 Model Settings

Two different models are used in this study. The first model is used to do strictly hydrodynamic simulations. The second model is used to calculate the sediment transport.

4.3.1 Hydrodynamic Model

The hydrodynamic model uses the grid with a local refinement around *Walsoorden* that is also used by Tiessen, et al. (2016) to investigate the effect of the grid resolution on the hydrodynamic on the local flow velocities. Different bathymetries around the intertidal shoal *Walsoorden* are used. The bathymetry measurements around the intertidal shoal *Walsoorden* are used to have a detailed and representative bathymetry in the area of interest before and after the sediment disposals. In this way the initial hydrodynamic response to the sediment disposal can be studied. The used bathymetric data is measured at the following dates:

1) 1 February 2010: just before the sediment disposals at intertidal shoal *Walsoorden;*
2) 15 September 2010: just after the first execution works ended;
3) 12 October 2011: just before the second execution works started.

Because the baseline model has been calibrated and validated for the initial and boundary conditions of 2013, these values have also been used in this study. Salinity and wind driven transport are included in the calculation. Wind waves are not taken into account because this feature was still not fully developed during this study. The simulation period is one full spring neap tide cycle to include the effects of differences between spring - and neap tide. The used hydrodynamic input starts at 7 January 2013 06:20:00 and stops at 21 January 2013 19:20:00. This period lasts 14 days and 13 hours and it coincides with 29 full tidal cycles. In advance of the simulation a spin up time of two 24 hours is included.

4.3.2 Sediment Transport Model

Because the morphological branch of the Delft3D Flexible Mesh software is still under development at the time of writing, the grid of the model that includes the sediment transport had to be reduced in order to get a working model. Parallelization of the model was not possible for the morphological model. This is why the model had to be run sequentially on one computer. The grid of the reference model gave a simulation that was too large to run sequentially.

In order to reduce the size of the model, the grid resolutions of the seaward and upstream parts of the model were reduced. Additionally, the upstream branches of the Scheldt River were deleted. This reduction led to a decrease in the number of flow cells from 195648 to 107914. The right side in Figure 4-1 shows the reduced model grid that is used for the sediment transport calculations. The upstream discharge of the river branches that are cut of are imposed at the locations where the branches are cut.

<u>Simulation Period and Model Validation</u>

Because the sediment transport model could not be simulated parallel, the calculation times for the sediment transport model are much longer than for the hydrodynamic model. For this reason, the simulations that include sediment transport are made for two individual tidal cycles instead of a full spring neap tidal cycle. The two tides that are simulated are one neap and one spring tidal cycle. Due to the faster calculations of the hydrodynamic model, it was decided that the hydrodynamics were produced with the model without the reduced grid. Figure 4-4 compares the water levels and flow velocities for the neap and spring tidal cycle from the reduced model with the reference model in the *Zuidergat*. To give an indication about the quality of the model, the sediment transport model is quantitatively compared with the hydrodynamic model in terms of the RMSE and BIAS. The BIAS and RMSE of the water level are 0.4 cm and 6.3 cm respectively. This shows that the water level of the reduced and the validated reference model are very similar. The BIAS and RMSE of the flow velocities are -2.9 cm/s and 4.6 cm/s.

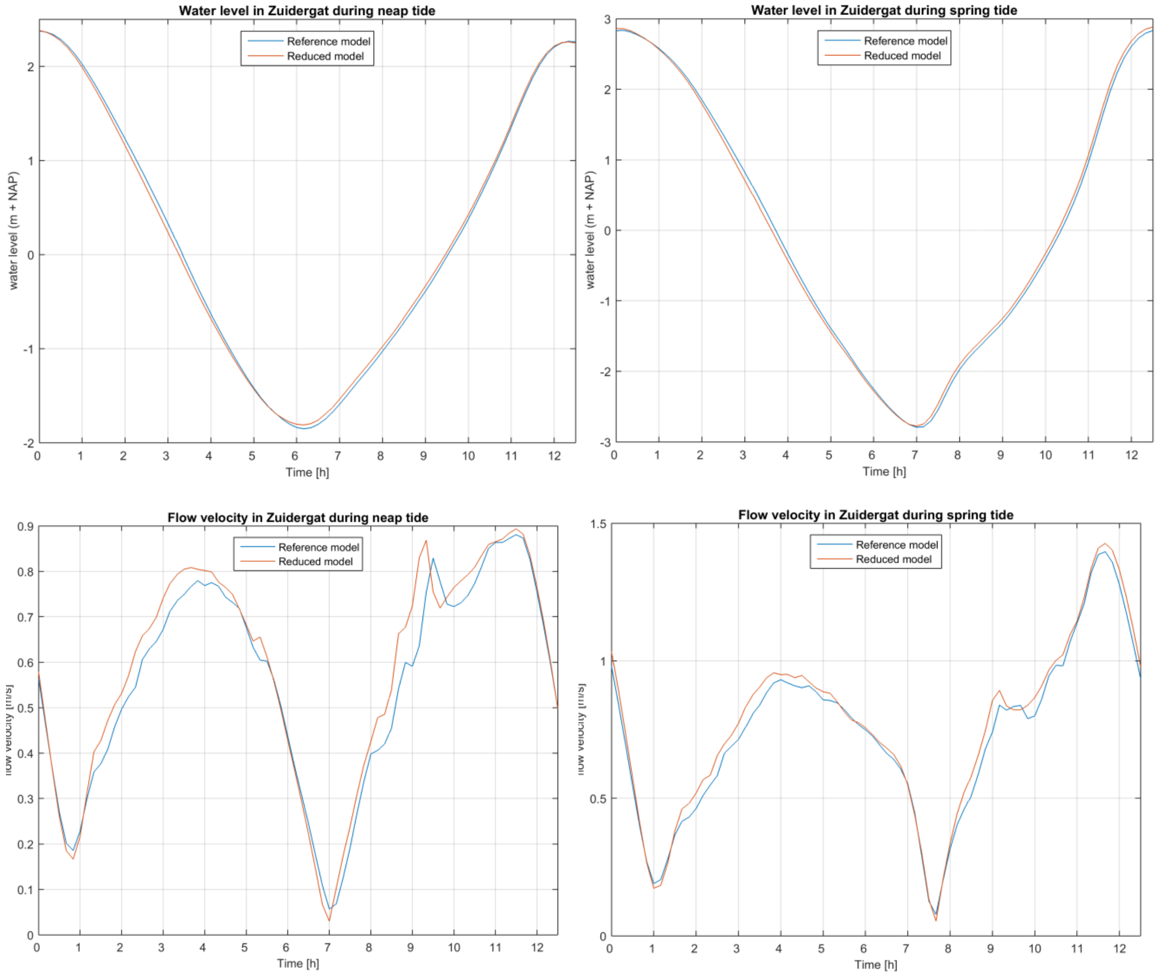

Figure 4-4 The top two figures show the water levels of a neap (left) and spring tide (right) in *Zuidergat* for the reference and the reduced model. The lower two figures show the corresponding flow velocities.

Morphological Input Parameters

The calculation of the sediment transport by Delft3D Flexible Mesh is done with the default sediment transport formula of Van Rijn (1993). For the calculations, sediment with a median sediment diameter of 200 µm and a specific density of 2650 kg/m^3 is used. The used dry bed density is 1600 kg/m^3 and the initial available sediment layer thickness at the bed is set on 30 m. At the inflow boundaries the equilibrium sand concentration profile is opposed. All the scaling and multiplication factors are kept at the default values. This means that multiplication factors for the bed-load transport vector magnitude and the suspended sediment reference concentration and the stream wise bed gradient factor for bed-load are kept at 1.0. The transverse bed gradient factor for bed-load transport is kept on 5.0. The used current related roughness height is 0.01 m.

4.3.3 Overview

An overview of the simulated model runs is given by Table 4-1.

Table 4-1 Overview of the used model simulations

Scenario	Type of simulation	Used bathymetry	Simulation period
H1	Hydrodynamic model	February 2010	Spring neap tidal cycle
H2	Hydrodynamic model	September 2010	Spring neap tidal cycle
H3	Hydrodynamic model	October 2011	Spring neap tidal cycle
M1.1	Sediment transport model	February 2010	Neap tide
M1.2	Sediment transport model	February 2010	Spring tide
M2.1	Sediment transport model	September 2010	Neap tide
M2.2	Sediment transport model	September 2010	Spring tide
M3.1	Sediment transport model	October 2011	Neap tide
M3.2	Sediment transport model	October 2011	Spring tide

5 HYDRODYNAMIC MODEL RESULTS

The model uses an output frequency of once every ten mintues. This holds for the map and the history files. Because the direction and the magnitudes of the flow are different during ebb than during flood, in the following sections a distinction between the ebb and flood period is made. The distinction between ebb and flood is made on the basis of the water level per grid cell. If the water level in the concerned grid cell is larger (smaller) than it was in the previous time step, the grid cell is considered to be in flood (ebb) period. For the analysis of the flood (ebb) flow velocities and bed shear stresses, the values that fall into the ebb (flood) period are not included in the calculations.

5.1 Flow velocities

The model shows significant variations in flow velocities over the edges of the intertidal flat can be found over one tidal cycle. The water surface is forced by the tide and creates a water level gradient. The changing water level gradient causes a variation in flow velocities. In the next section the impact of the disposal on the local flow will be discussed.

5.1.1 Flow Patterns and Velocities

To get an indication about the variability of the flow velocities and directions around the tip of intertidal shoal *Walsoorden*, the mean and peak velocities of both ebb and flood are distinguished. If the flow velocities are higher, larger sediment transports can be expected. The peak velocities are an important indicator to determine the sediment transport.

Figure 5-1 shows the simulated averaged flood peak velocities (top) and the differences between the three model simulations (bottom). The the average peak velocities are found by averaging the peak velocities of all the individual flood (or ebb) periods. The maximum flow velocities of each individual tide are obtained with the Matlab function findpeaks. The mean flood (ebb) velocities are found by averaging all the flow velocities that fall into the flood (ebb) period. From this figures it can be seen that the peak velocities are the highest in the channels, reaching magnitudes up to 1.8 m/s to 2.0 m/s. At subtidal zone north of intertidal shoal *Walsoorden* the peak velocities vary around 1.3 m/s. Further towards the shoal the velocities gradually decrease. On the shoal itself the velocities do not exceed 0.5 m/s. The flow is directed around the shoal through the main channels and flood chutes on the north and south of the shoal.

Figure 5-2 shows the simulated mean flood velocities (top) and the differences between the three model simulations (bottom). What can be seen is that the spatial patterns of the mean flood velocities are similar to the patterns of the flood peak velocities. The mean flow velocities in the channels are 0.7 m/s to 0.9 m/s. The mean flow velocities in the subtidal zone where the sediment is disposed are in the order of 0.6 m/s to 0.7 m/s.

The lower figures in Figure 5-1 and 5-2 show that the impact of the sediment disposal on the local flow is similar for the mean and peak velocities. The largest difference in flow velocity between the models is obtained downstream of the location of the sediment disposal. Flow velocities in this zone have decreased in comparison with the reference situation. Furthermore, the increase in flow velocity at the location of the disposal suggests that the disposal acts as an artificial spillway. The increase of the flow velocities in the neighbouring channels however suggest that part of the water flows around the disposed sediment. The changes in the direction of the flow (Figure B-5) are very small and indicate that some water is directed around the 2.0 m difference contour line.

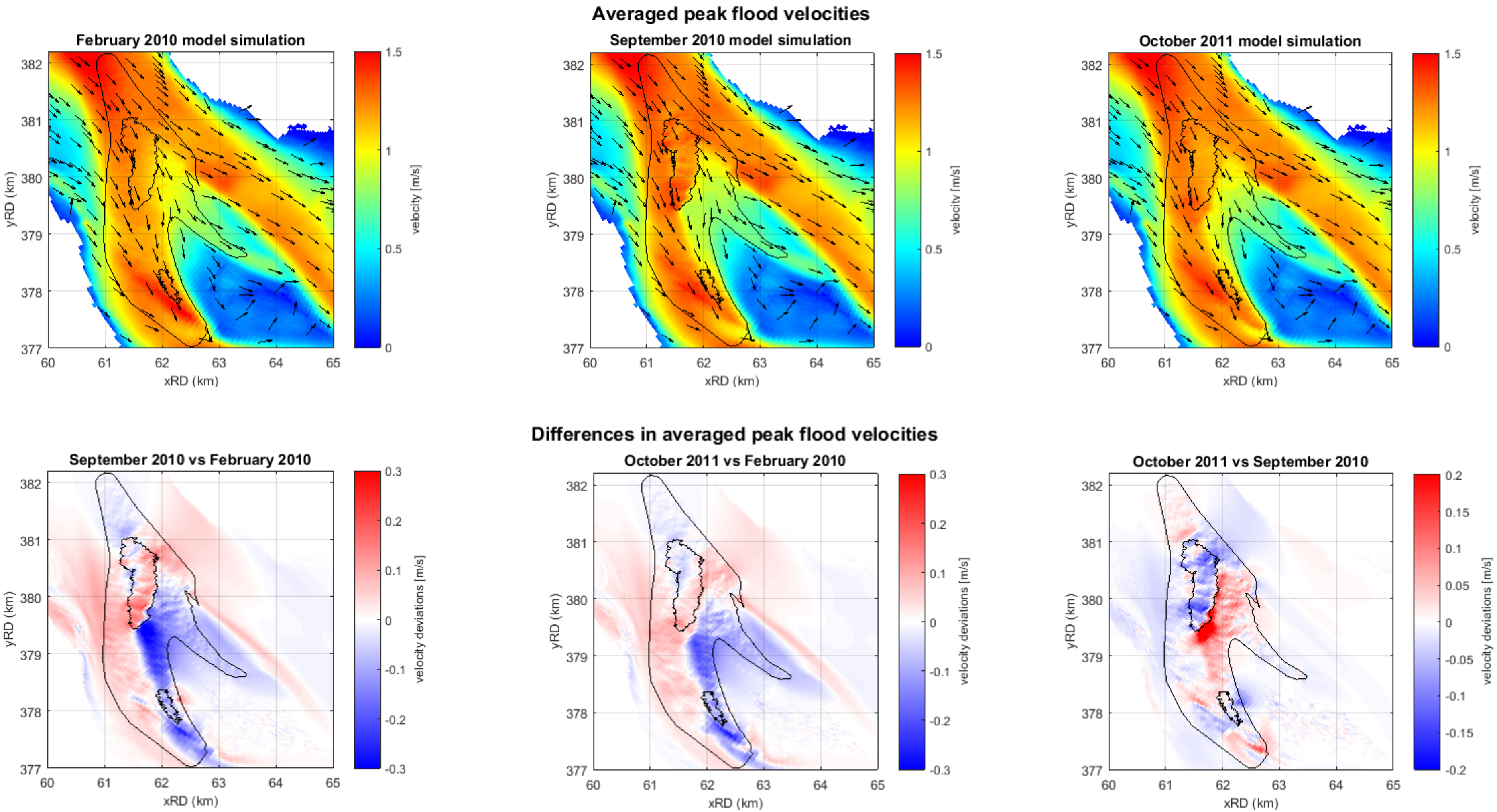

Figure 5-1 Averaged flood peak velocities of the three model simulations (top) and the differences between the three model simulations (bottom). The black lines indicate the control polygon and the 2.0 m difference contour line between the bathymetry of February 2010 and September 2010 model. Note that the arrows in the figures do only indicate the direction and not the magnitude of the flow. The magnitude of the flow is indicated by the colour.

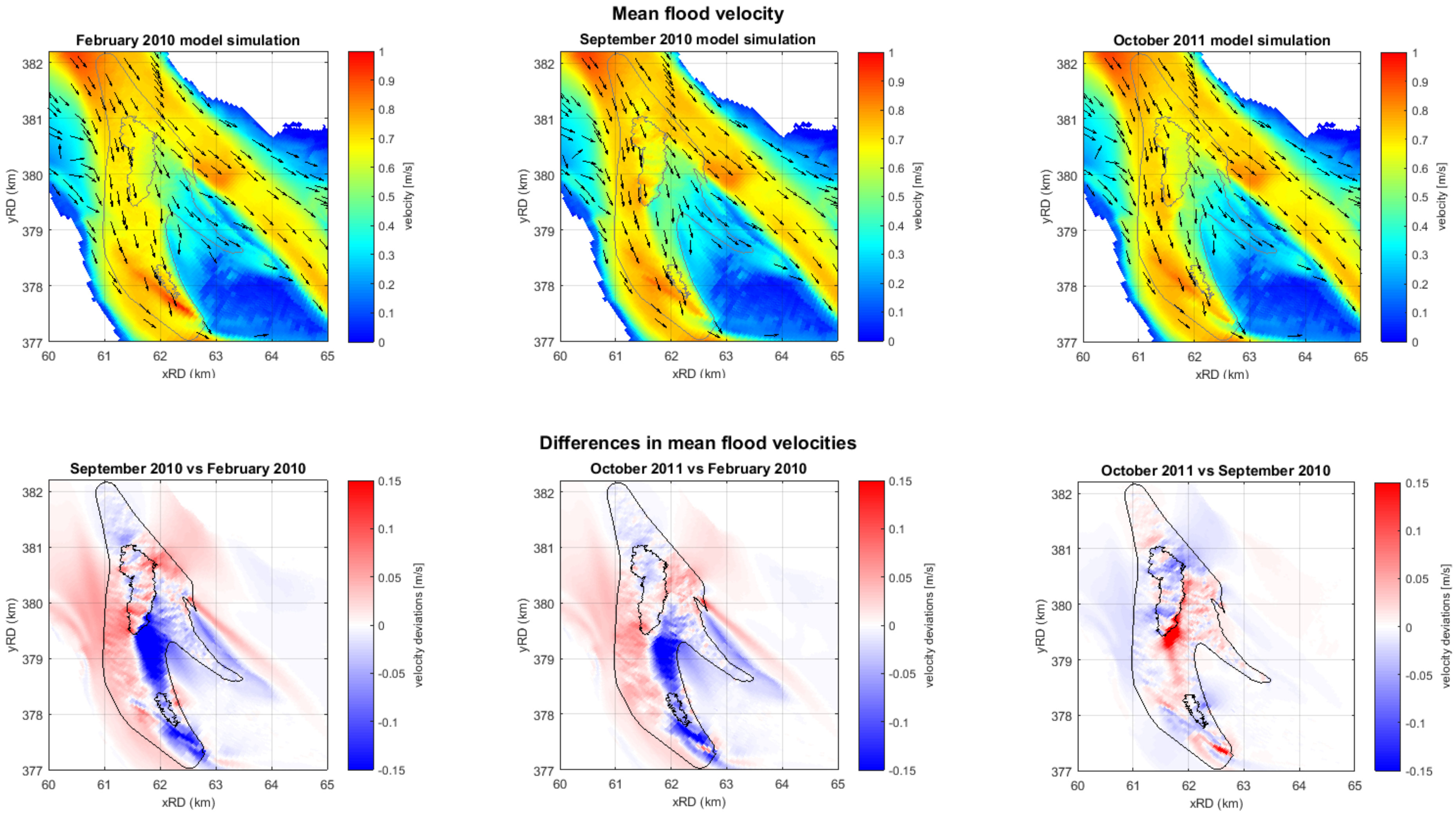

Figure 5-2 Mean flood velocities of the three model simulations (top) and the differences between the simulations (bottom). The black lines indicate the control polygon and the 2.0 m difference contour line between the bathymetry of February 2010 and September 2010.model.Note that the arrows in the figures do only indicate the direction and not the magnitude of the flow. The magnitude of the flow is indicated by the colour.

Similarly as in Figures 5-1 and 5-2, Figures 5-3 and 5-4 show the averaged peak and mean velocities for the ebb period for the different model simulations and the differences between these simulations. From the colours of the plot it can clearly be noticed that the peak ebb velocities are smaller than the peak flood velocities in this region. The peak ebb velocities in the channels reach a maximum magnitude of 1.5 m/s. At the tip of the shoal the ebb peak velocities are in the order of 0.6 m/s. These velocities are much smaller than the peak flood velocities of 1.3 m/s in this region. At the shoal itself, the peak velocities do not exceed 0.5 m/s. The mean flow velocities in the channels are of the same magnitude as during flood (0.7 m/s to 0.9 m/s). At the subtidal zone north of the shoal were the sediment is disposed, the mean ebb flow velocities are clearly lower than the mean flood velocities.

The absolute changes in the flow velocity due to the disposed sediment are smaller during ebb than during flood. This can be explained by the fact that the direction of the incoming flood current is straight towards the location of the sediment disposal, while this is less clearly the case for the incoming ebb current. Besides, the flow velocities during ebb are smaller than during flood. However, the difference plots in Figure 5-3 and 5-4 show that there is a small decrease of the flow velocity just before and just after the disposal site. In the 2.0 m difference contour a small increase of the ebb peak velocity can be observed. This again indicates that the disposed sediment acts as a spillway and makes the local flow velocities increase and that it does not force the flow to go around the disposal site. Another indication for this is that the ebb flow is directed in the direction of the sill (Figures 5-3, 5-4 and B-1).

What can be observed from the difference plots is that the locations where the velocities initially increase or decrease in the situation in September 2010 are still present in Ocotber 2011. The plots that show the differences between the situation in October 2011 and February 2010 (plots in the middle of the Figures) emphasize this. If these figures are compared with the figures that indicate the differnces between the September 2010 and February 2010 (plots on the left side in Figures) situation, it can be seen that the locations of the blue and red zones that indicate a difference in flow velocity are in the same locations. The magnitude of the differences has decreased. The difference plots between the model runs with the October 2011 bathymetry and September 2010 bathymetry (plots on the right side in Figures) show that the morphological development derects the system back to its original situation. Locations where flow velocities initially increased show a decrease of flow velocity; whilst the opposite can be said about locations where the velocities initially decreased. This holds for both the ebb and the flood velocities.

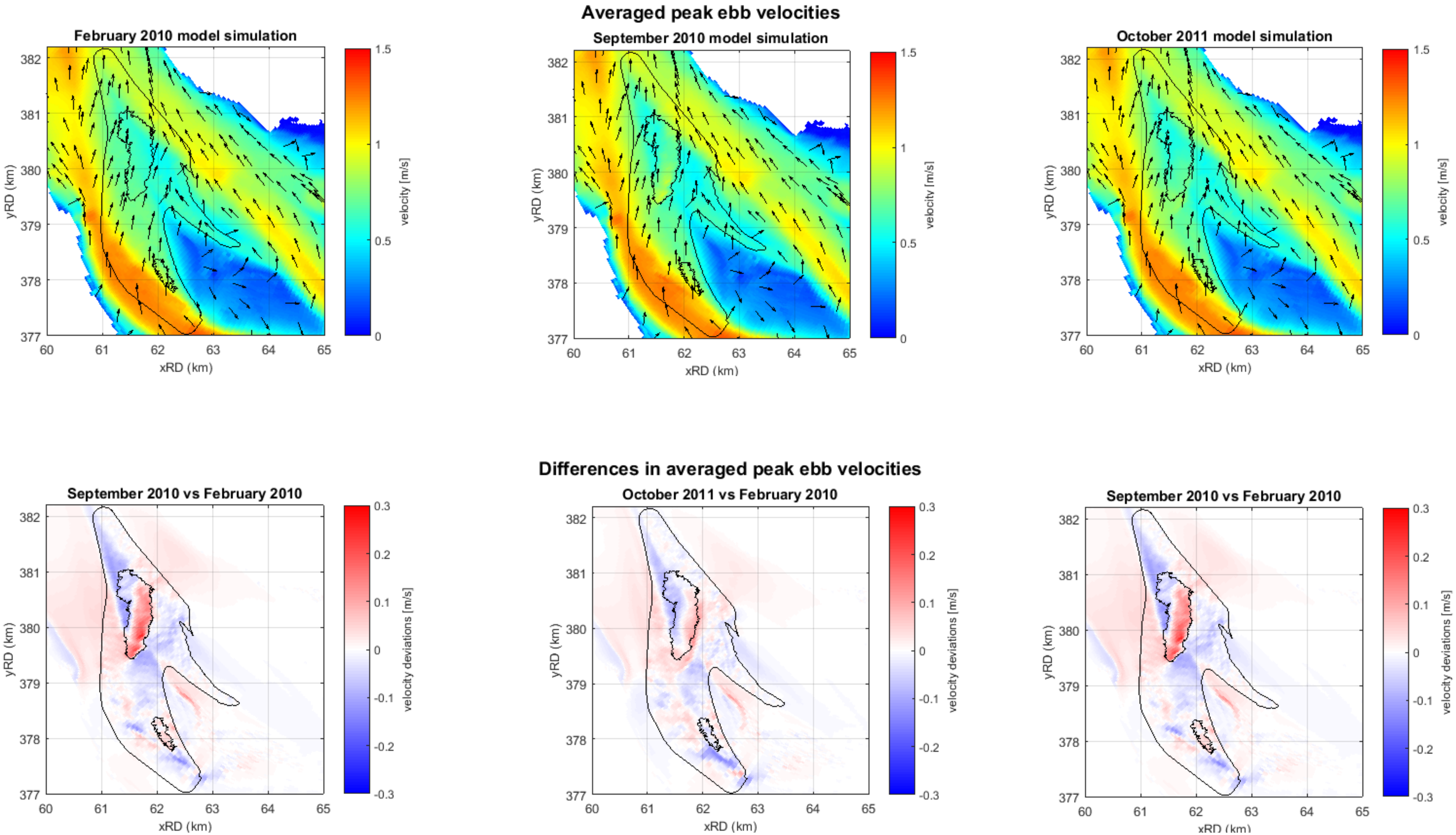

Figure 5-3 Averaged ebb peak velocities of the three model simulations (top) and the differences between the three model simulations (bottom). The black lines indicate the control polygon and the 2.0 m difference contour line between the bathymetry of February 2010 and September 2010 model. Note that the arrows in the figures do only indicate the direction and not the magnitude of the flow. The magnitude of the flow is indicated by the colour.

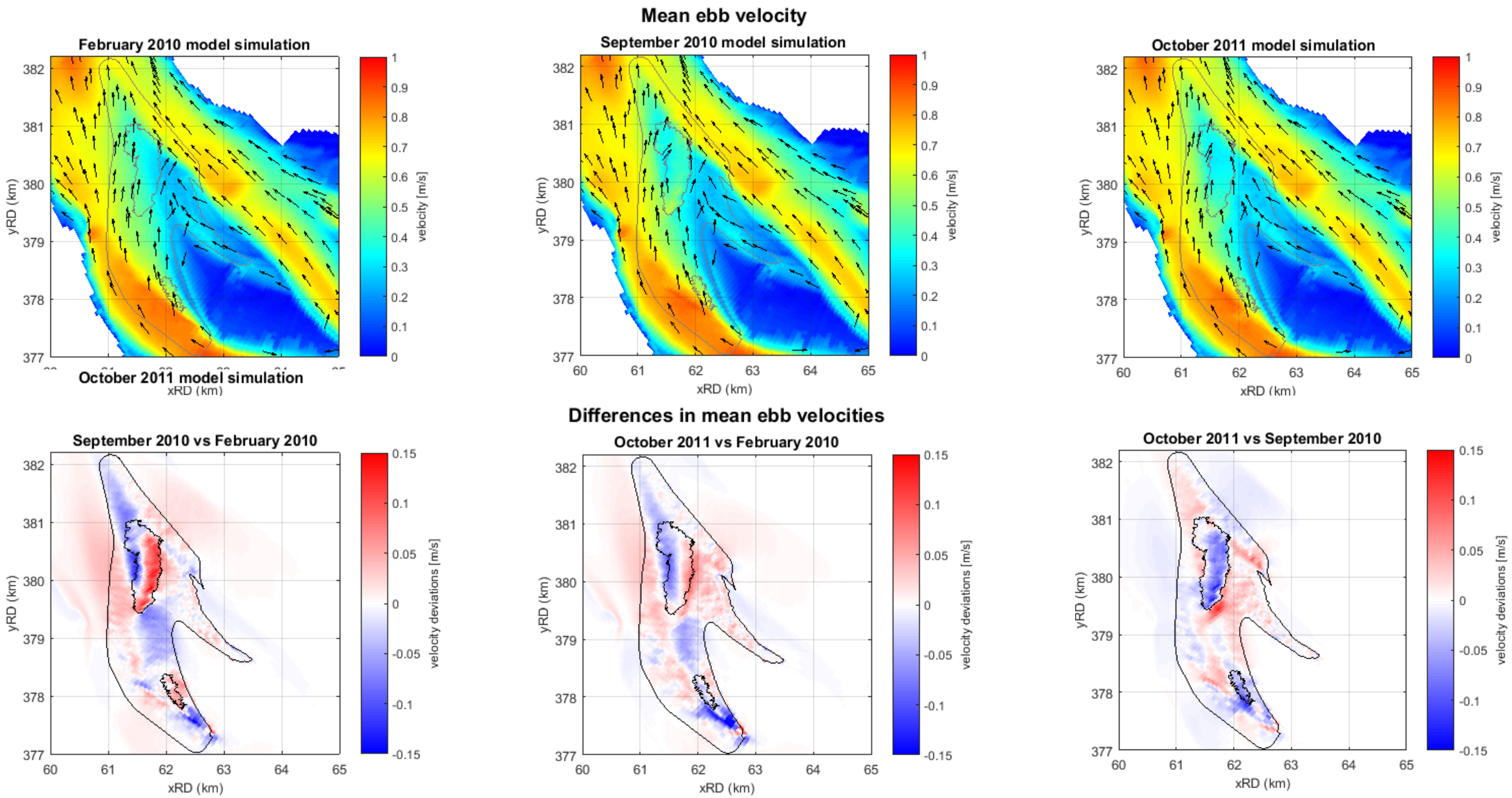

Figure 5-4 Mean ebb velocities of the three model simulations (top) and the differences between the simulations (bottom). The black lines indicate the control polygon and the 2.0 m difference contour line between the bathymetry of February 2010 and September 2010.model.Note that the arrows in the figures do only indicate the direction and not the magnitude of the flow. The magnitude of the flow is indicated by the colour.

5.1.2 *Observation points*

Figure 5-5 shows the locations of five observation points for which the flow velocity will be analysed. This has been done for a neap tide and a spring tide.

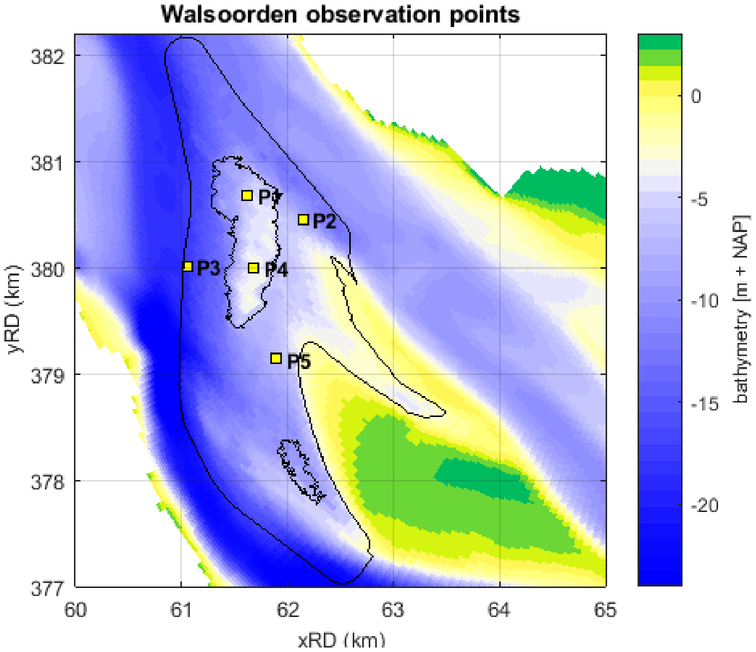

Figure 5-5 Locations of the points for which the local flow velocities have been observed through time. The black lines indicate the control polygon and the 2.0 m difference contour line between the bathymetry of February 2010 and September 2010.

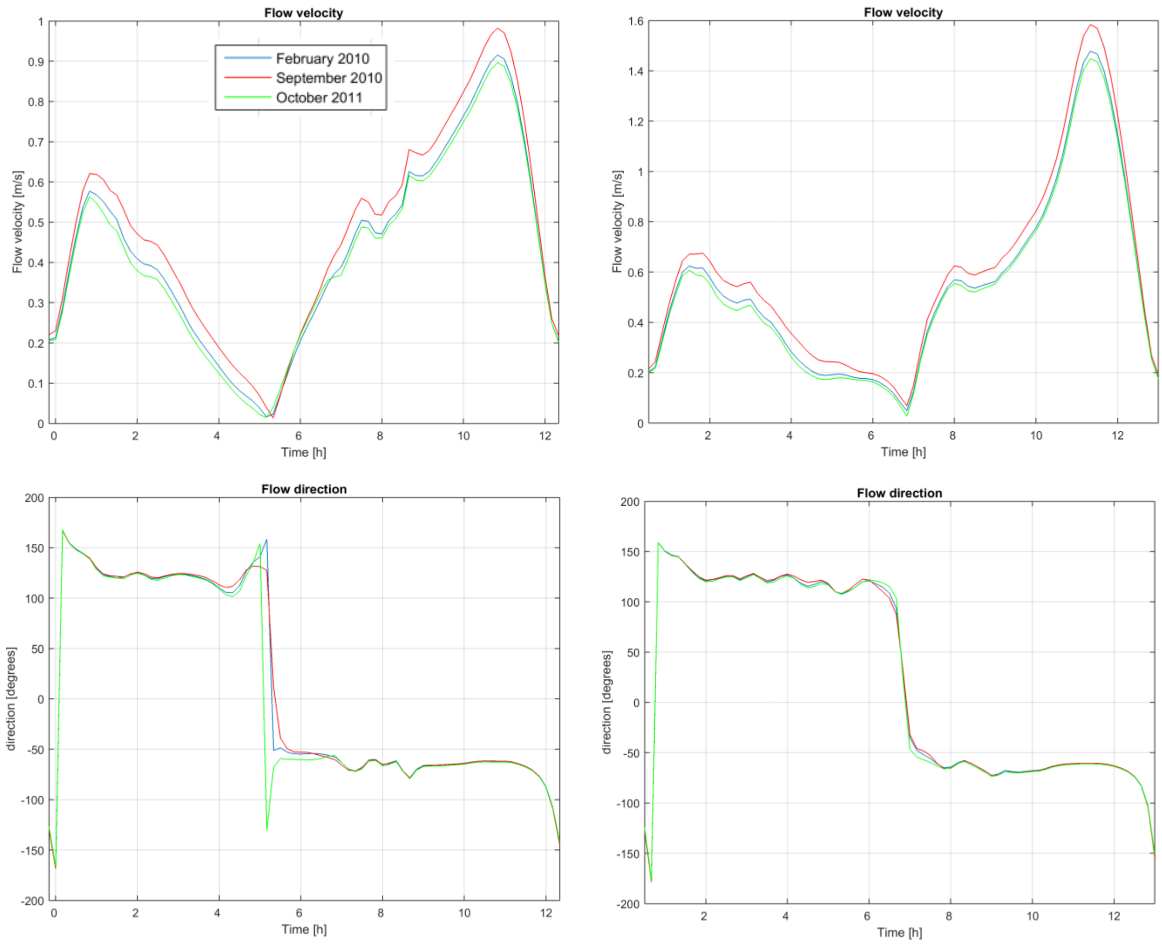

Figure 5-6 Flow velocity (top) and direction (bottom) at observation point 1 during neap (left) and spring (right) tidal conditions

Figures 5-6 shows the simulated flow velocity for neap and spring tidal conditions at observation point 1. The situation before the sediment disposal in February 2010 is indicated by the blue lines, while the red and the green lines are the model results of respectively the September 2010 and October 2011 model simulations. Figures for the water levels and flow velocities of all the observation points can be found in Appendix C. These profiles give an indication of the flow variations over time.

These figures confirm that the peak velocities for flood (right) are higher than for ebb (left). Due to the nonlinear relation between flow velocity and sediment transport, this indicates that the flood direction is the dominant transport direction for the coarse sediment. For the finer sediments the slack water periods can be important as well. Especially for the shallower parts, the slack water period is longer after ebb than after flood. This can be seen in Figures 5-6 and 5-7. Due to the smaller settling velocity of fine sediments, this enhances the sediment transport of fine sediments in the ebb direction. Moreover, the flow velocities of control points 1 and 4 after flood do not drop below 0.2 m/s.

The initial impact of the disposal on the velocity is most profound in observation points 1 and 4. This can be explained by the fact that the differences in bathymetry are the largest in these locations. In both of these observation points the ebb and the flood velocities increase. After one year of morphological development, the velocity increase is cancelled out, and the increase has even turned into a small decrease. As can be seen from figures 5-1 to 5-4 the mean and peak velocities at observation point 5 have both decreased as a result of the disposed sediment.

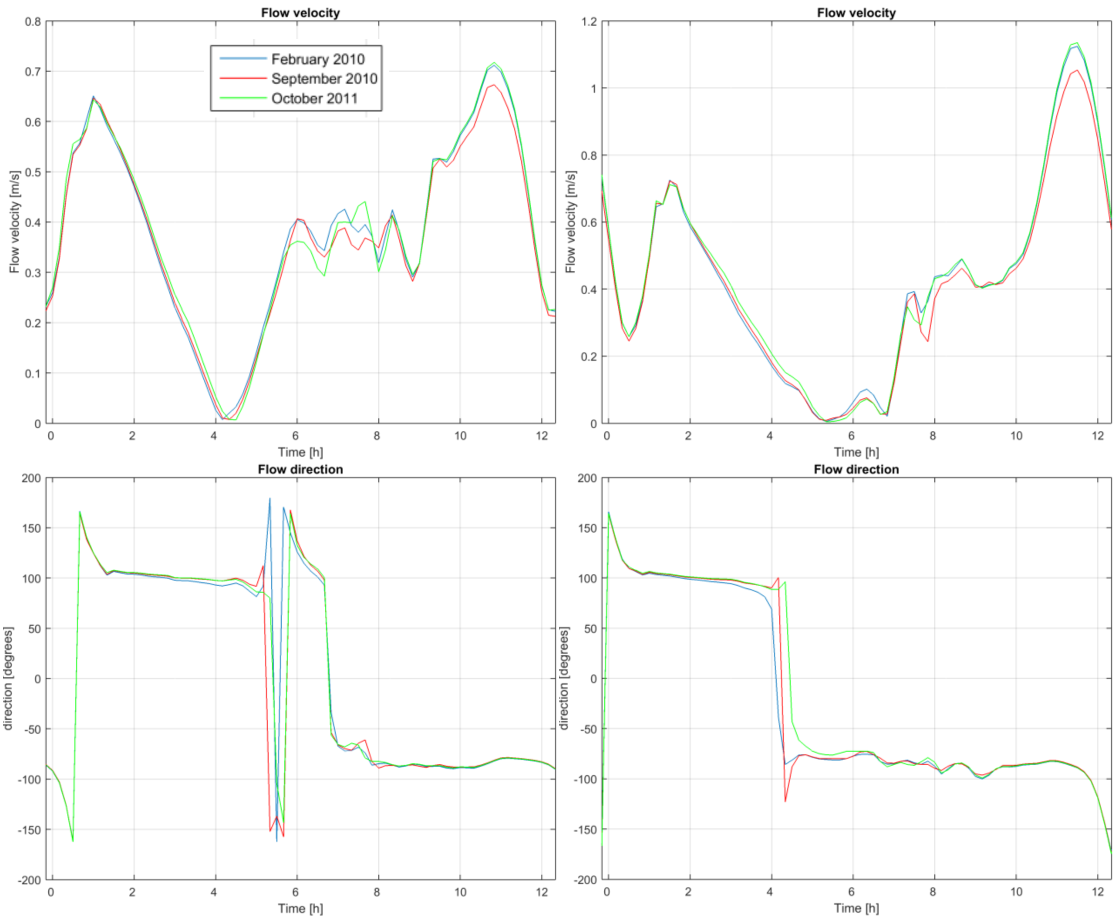

Figure 5-7 Flow velocity (top) and direction (bottom) at observation point 5 during neap (left) and spring (right) tidal conditions

This initial decrease in flow velocities can be seen in Figure 5-7 as well. Figure 5-7 emphasizes that the differences in flow velocities are most clear at the peak flood velocities. This decreased flood peak velocities lead to lower sediment transports in the flood direction. The differences in ebb velocity are much smaller. The green lines in the plots show that this initial decrease has almost fully disappeared after one year. In control point 2 a similar phenomenon occurs with an initially decreased ebb velocity. The flow velocities in control point 3 are only very little influenced by the sediment disposal.

Figures 5-6 and 5-7 show that the differences between the ebb and flood peak velocities are larger during spring tide than during neap tide. This in combination with the higher peak flood velocities indicate that the subtidal and intertidal zone north of intertidal shoal *Walsoorden* is more flood dominated during spring tide than during neap tide. The larger flood dominance during spring tide can be explained by the larger tidal range. As stated in Chapter 2, frictional interaction between the tide and channel bottom causes relatively shorter flood periods. Because the tidal range increase, the ratio of the tidal amplitude and the channel depth increases (R/h). This enhances the flood dominance.

5.1.3 Periods during which a Velocity of 0.5 m/s is Exceeded

In order to get an indication of the sediment transport capacity not only the magnitude of the flow but also the duration during which a threshold value is exceeded is important. In this study a depth averaged threshold value of 0.5 m/s was adopted from Plancke, et al. (2009b). This value represents a threshold value for which the initiation of motion for the local sediment was obtained during measuring campaigns (WLB, 2007). Figure 5-8 and 5-9 show the fraction of the ebb and flood period during which the threshold value of 0.5 m/s is exceeded. It should be noted that the total ebb period in this region is longer than the flood period. Similar fractions thus indicate a longer period during which the threshold value is exceeded for ebb.

In the area of interest the period during which the threshold value is exceeded is larger in during flood than during ebb. Besides, Figure 5-8 clearly show the creation of a sheltered zone between the disposal and the shoal behind the disposed sediment in the flood period. On the 2.0 m difference polygon an increase of the fraction during which 0.5 m/s is exceeded can be observed in the ebb period. From the difference plots it can also be noticed that exceeding periods are also increased in the neighbouring channels. This is in line with the results of the flow velocities.

5.1.4 Dominance

To identify whether the residual transport will be in the ebb or the flood direction, the dominant flow direction has to be found. Because the sediment located at the tip of intertidal shoal *Walsoorden* is relatively coarse (200-300 µm), the flow velocity is more important than the duration of the slack water here. An important parameter to check the dominance is the ratio between the flood and the ebb peak velocity. As can be seen from Figure 5-10, most part of the tip of intertidal shoal *Walsoorden* is flood dominated (higher flood velocities). The differences between the three figures show a clear influence of the disposal on the dominant flow. The ratio between the flood - and ebb velocity increases on the northwest side - and decreases of southeast of the disposal. This is the result of the decrease in flow velocities at the lee-side of the disposed sediment in the flood direction. The neighbouring channels have a much smaller increase in flood dominance.

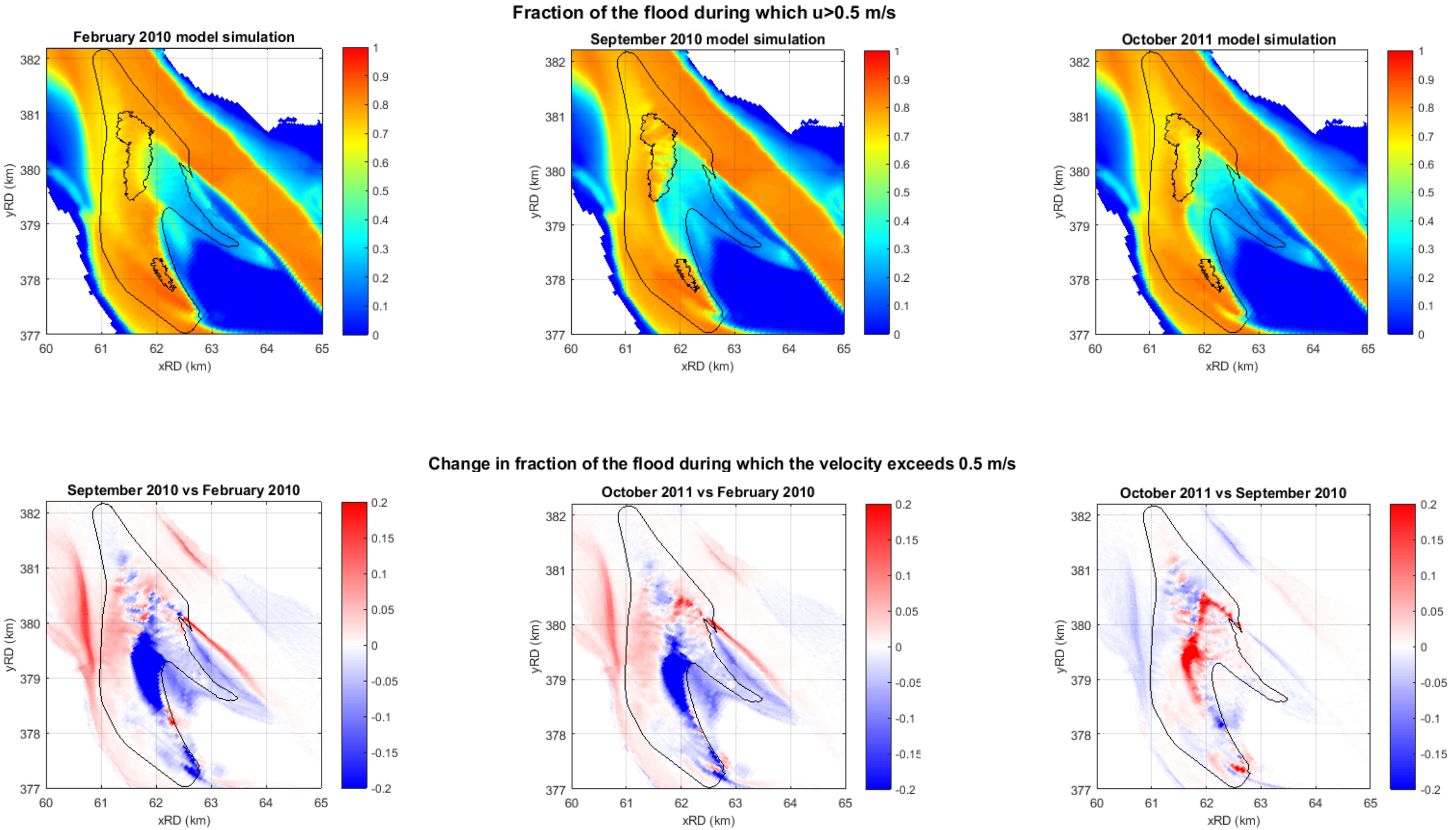

Figure 5-8 Period during which a threshold value of 0.5 m/s is exceeded during flood (top) and the differences between the three model simulations (bottom)

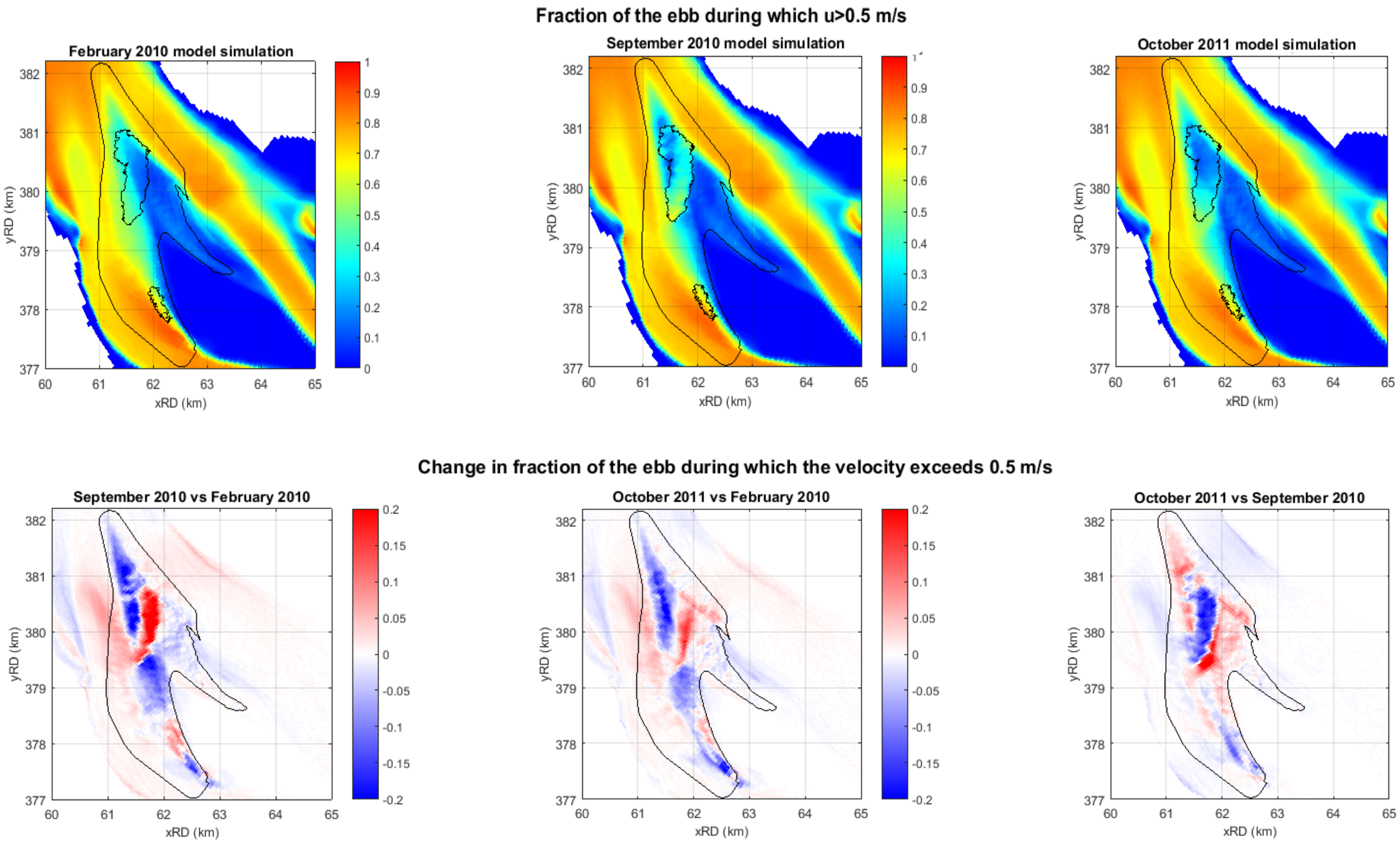

Figure 5-9 Period during which a threshold value of 0.5 m/s is exceeded during ebb (top) and the differences between the three model simulations (bottom)

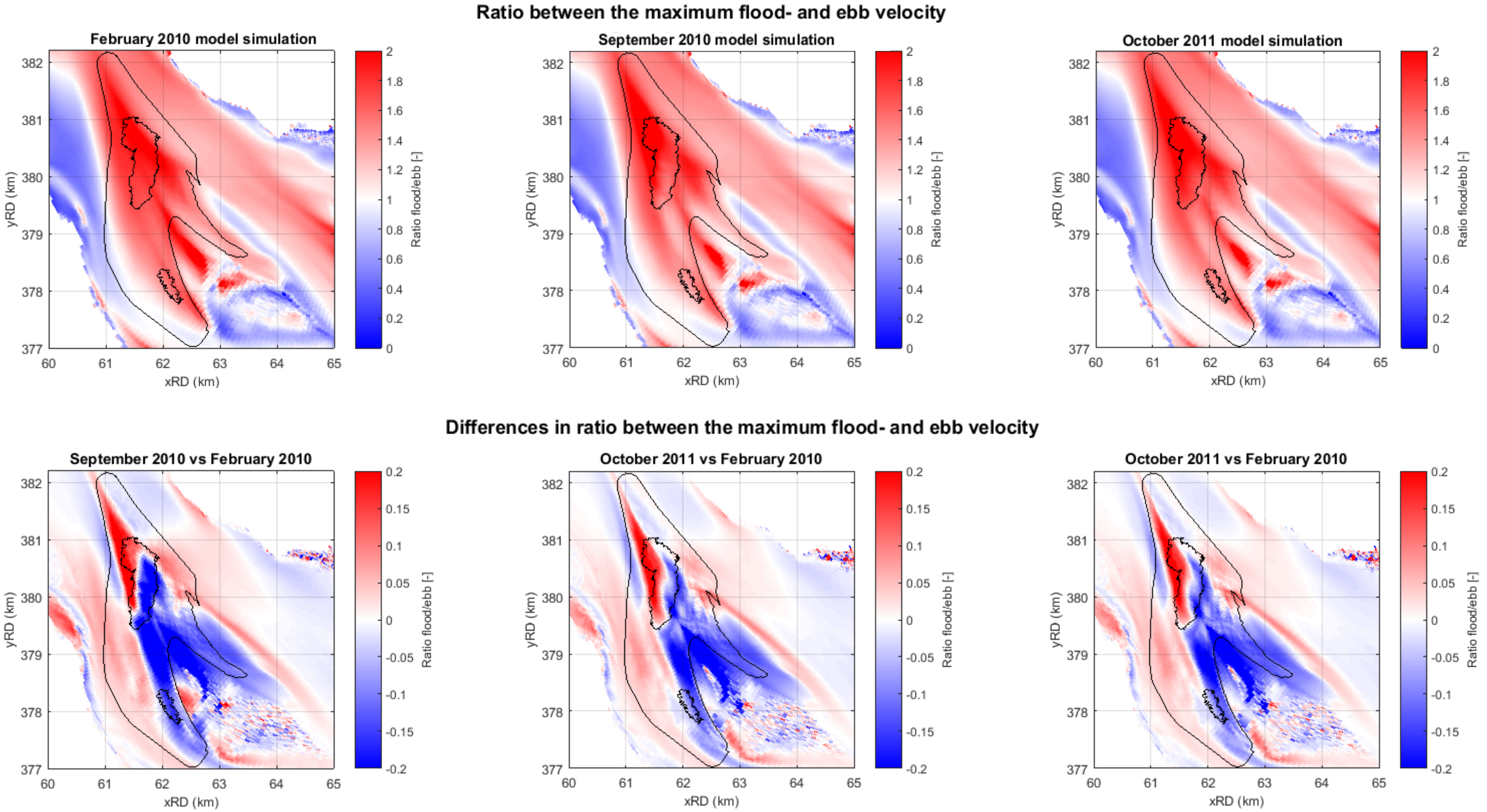

Figure 5-10 Ratio between the flood - and ebb peak velocities (top) and the differences between the ratios between the three model simulations (bottom)

5.1.5 *Flow distribution*

Besides the main goals of the sediment disposals, an increase of the flow velocities in the adjacent channels would lead to a more self-erosive capacity and a reduction of the dredging activities. Figure 5-11 gives an overview the flow velocities in three cross-sections near the sediment disposal for the different model simulations. The arrows indicate the positive flow direction. The figure shows that the impact of the sediment disposals on the flow velocities in the adjacent is very small. The peak flow velocities in cross-section 1 *(Zuidergat)* do initially increase by the sediment disposals, but in October 2011 this effect has fully disappeared again. The flow velocity in cross-section 2 shows that the flood velocities decrease. This is in line with what has been observed from the other figures in this Chapter. The flow velocities in cross-section 3 *(Schaar van Waarde)* are hardly influenced by the sediment disposals.

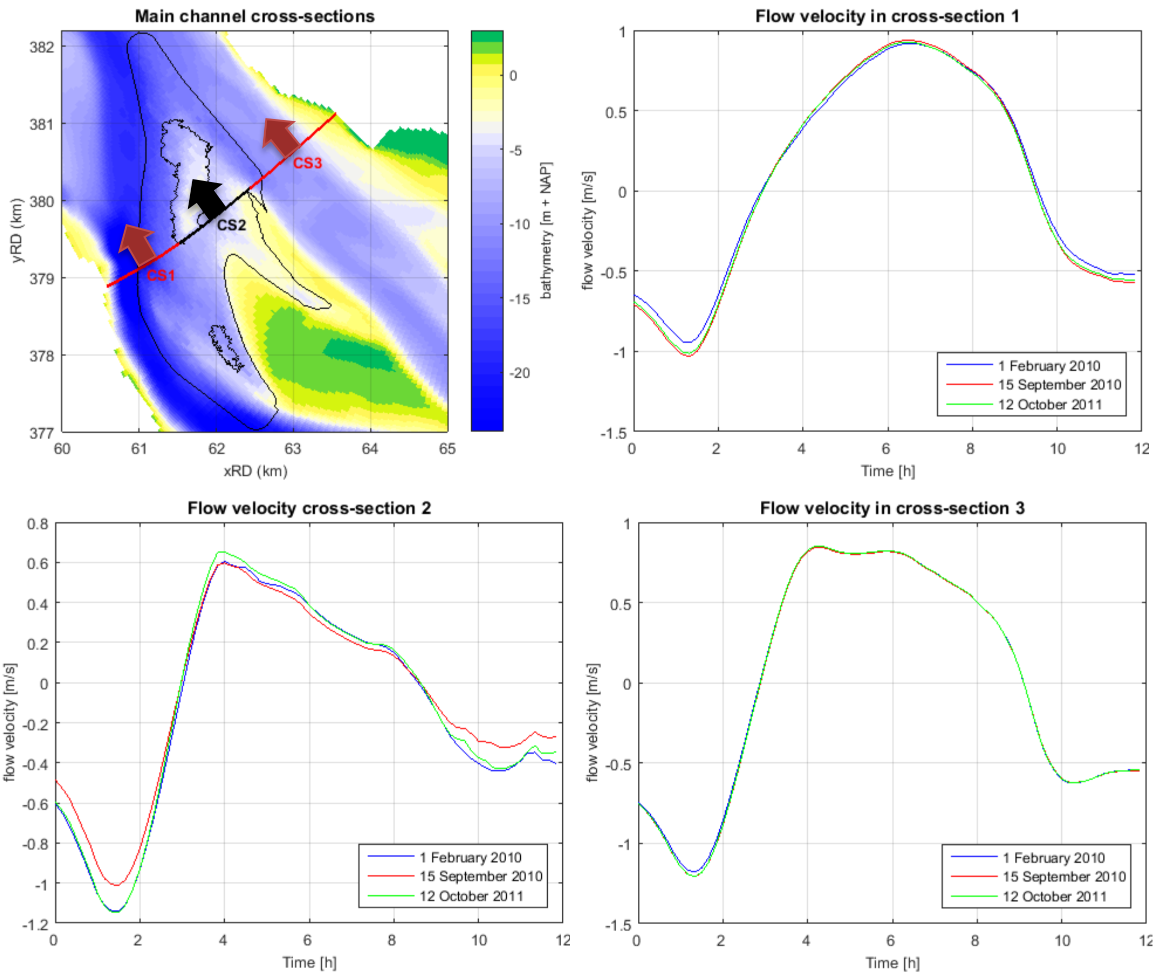

Figure 5-11 Location of three cross-sections that were observed to assess the flow velocities in the adjacent channels with the flow velocities (top left) and the flow velocities for the three cross-sections over one tidal cycle (top right and bottom). The colours of the lines indicate the used model simulations.

5.2 Bed Shear Stress

As mentioned before the bed shear stress is an important indicator for the sediment transport. Sediment transport is initiated when the bed shear stress exceeds a certain threshold value. The magnitude of the critical bed shear stress depends on the local flow velocities and the grain size diameter. According to Berenbrock & Tranmer (2008) a grain size with a D_{50} of 200 μm coincides with a critical bed shear stress of approximately 0.2 N/m^2. As can be seen from Figure 5-12 and 5-13, the average bed shear stresses are much higher than the threshold value in very large parts of the system. Especially the channels are morphologically very active and sediment transports in both directions can be expected. On the tip of the intertidal shoal the bed shear stresses do also exceed the threshold value of 0.2 N/m^2. The plots that show the differences between the various model simulations show similar patterns as with the flow velocities. The shear stress at the location of the disposals is increased by the disposed sediment. In October 2011 the initial impact has reduced.

Plots with the fraction of the time during which the threshold bed shear stress is exceeded and the difference plots can between these plots can be found in Figure 5-14 and 5-15. Figure 5-14 shows that at the location of the sediment disposals this threshold value is exceeded during almost the whole flood period. As a result of the sediment disposals this fraction increases even more. Figure 5-15 shows that the period during which the bed shear stress is exceeded during the ebb period initially increases at the location of the sediment disposal. After September 2010, the system is slowly returning towards the situation before the sediment disposals.

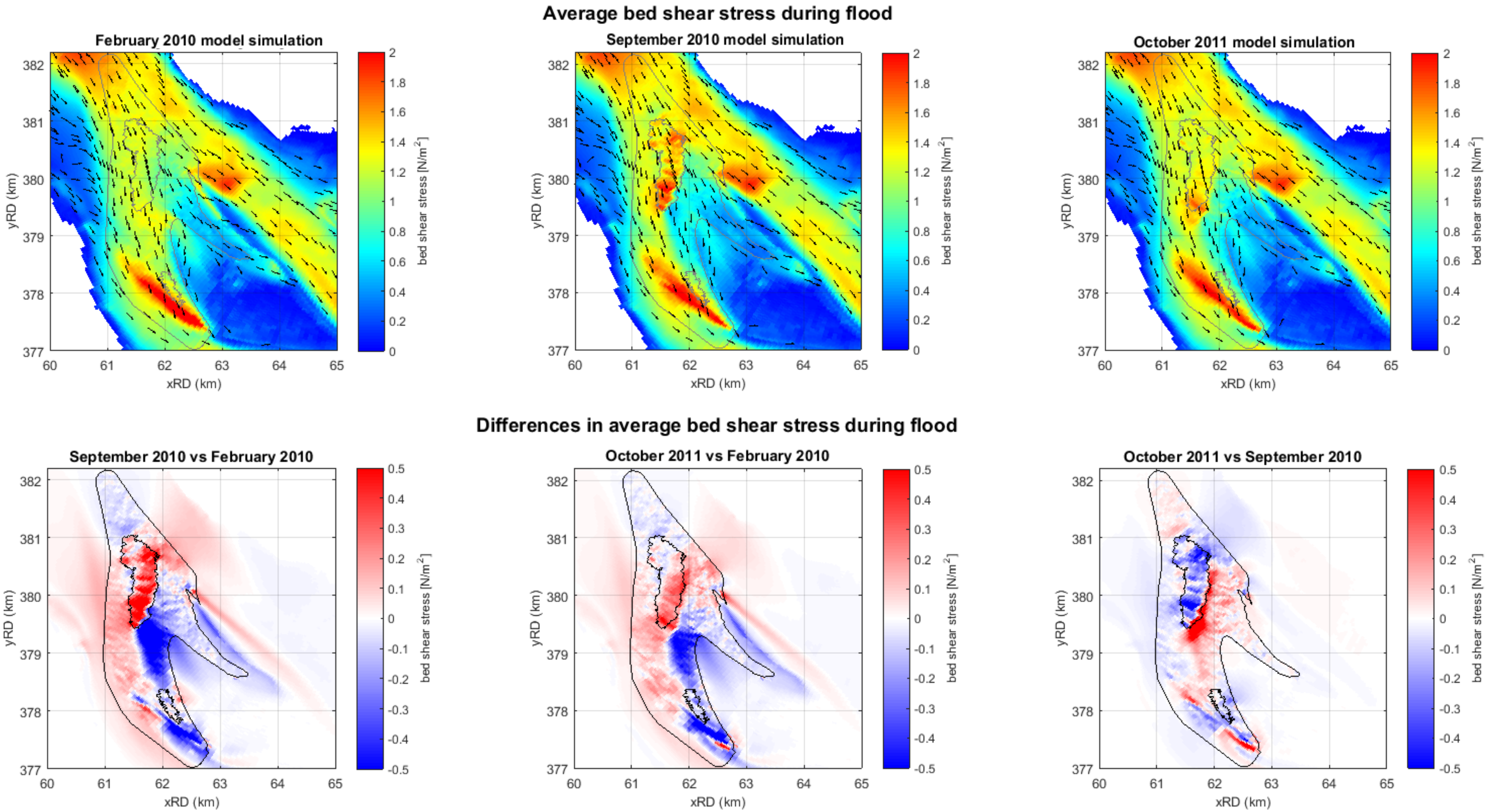

Figure 5-12 Average bed shear stress during flood of the three model simulations (top) and the differences between the simulations (bottom). The black lines indicate the control polygon and the 2.0 m difference contour line between the bathymetry of February 2010 and September 2010 model. Note that the arrows in the figures do only indicate the direction and not the magnitudes. The magnitude of the bed shear stress is indicated by the colour.

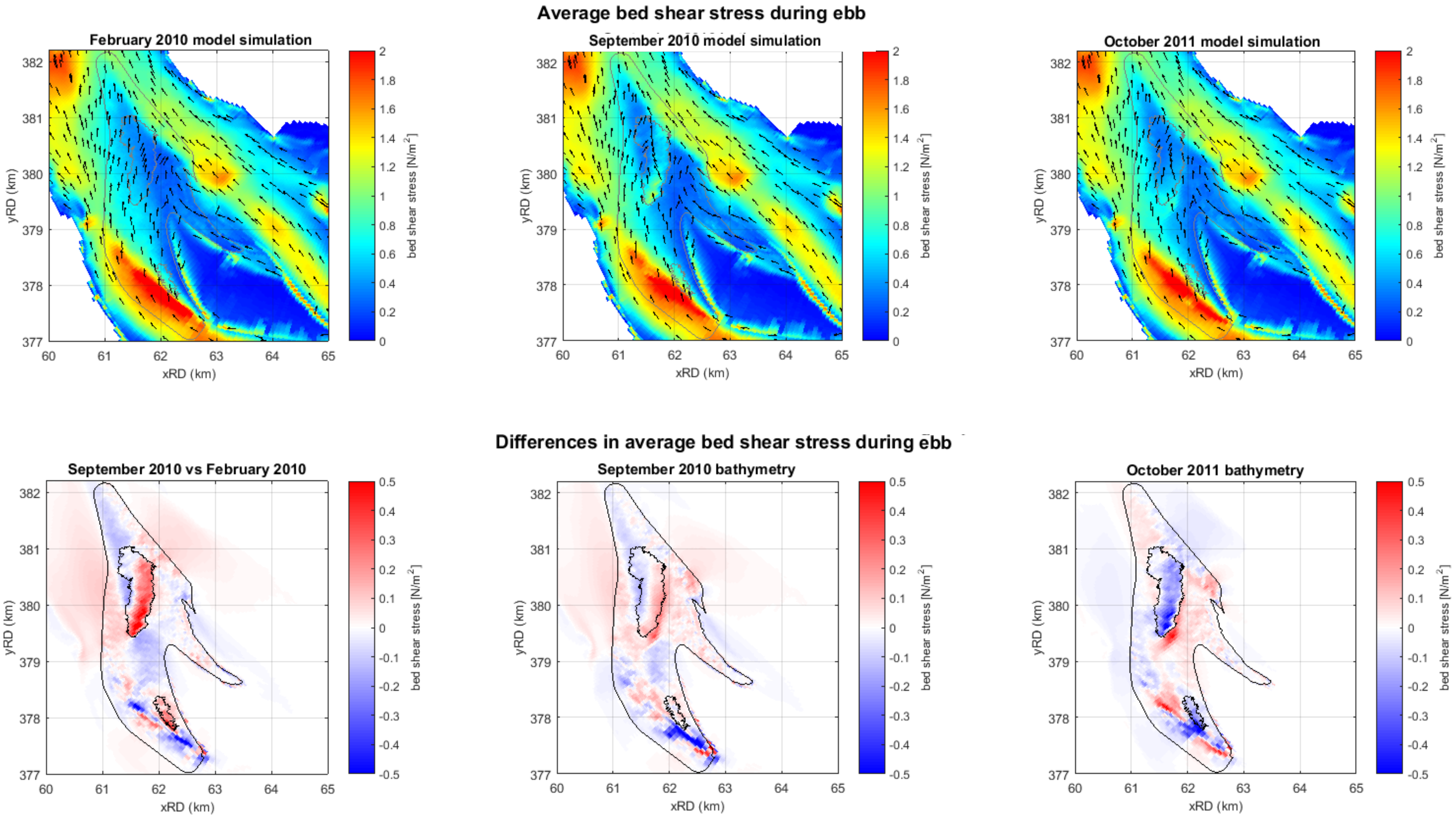

Figure 5-13 Average bed shear stress during ebb of the three model simulations (top) and the differences between the simulations (bottom). The black lines indicate the control polygon and the 2.0 m difference contour line between the bathymetry of February 2010 and September 2010 model. Note that the arrows in the figures do only indicate the direction and not the magnitudes. The magnitude of the bed shear stress is indicated by the colour.

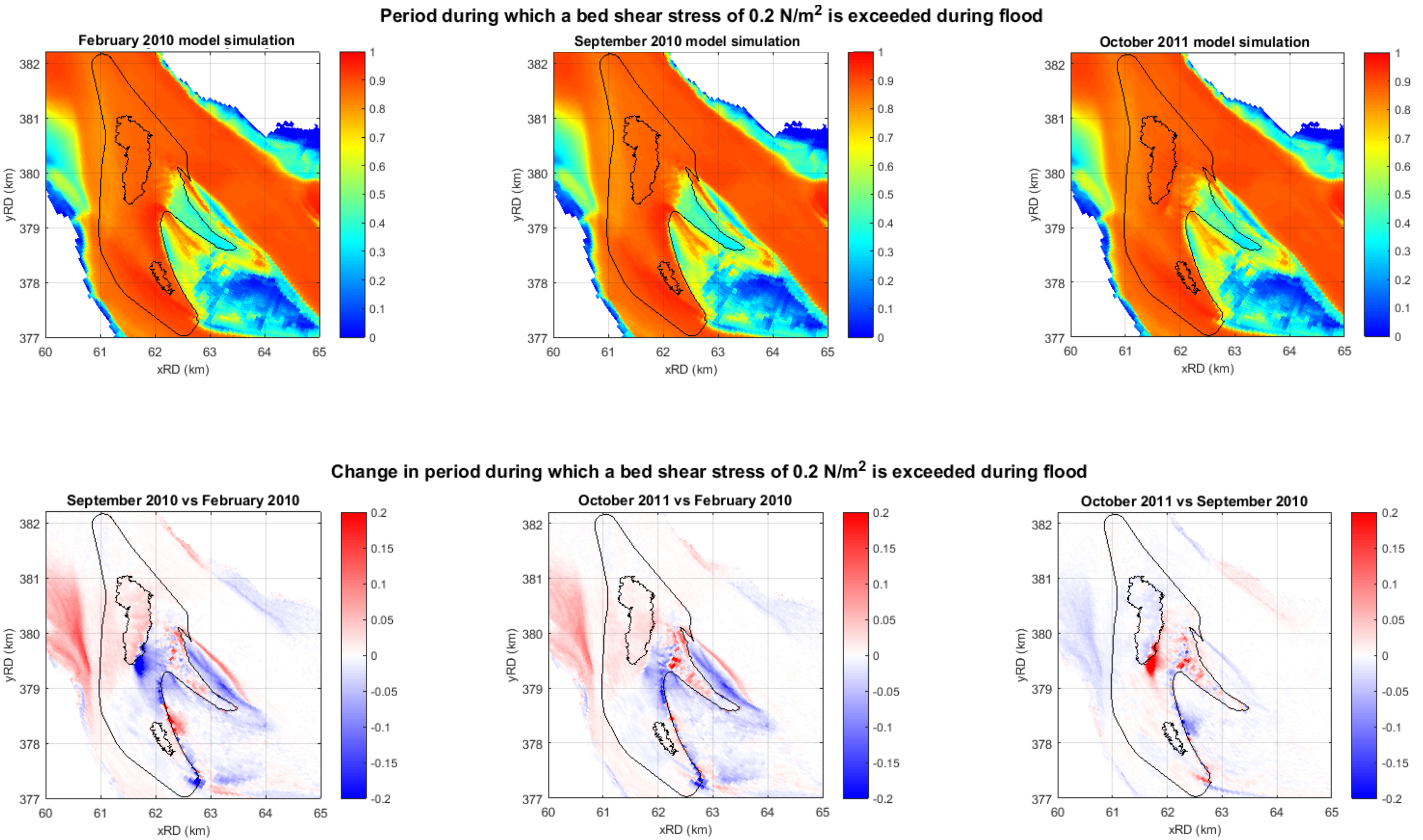

Figure 5-14 Fraction of the flood during which a threshold value of 0.2 N/m^2 is exceeded at ebb (top) for the three model simulations and their differences (bottom)

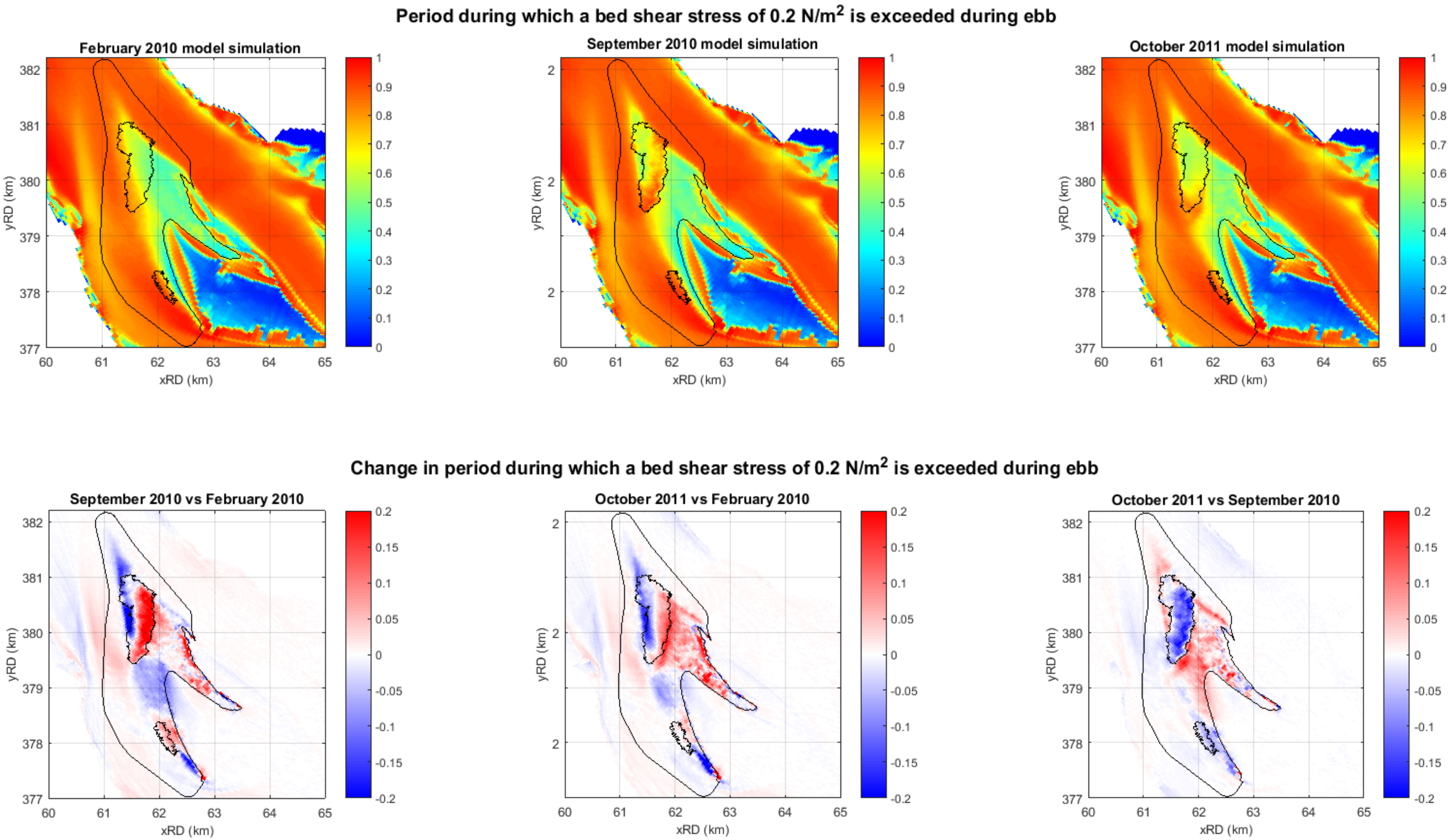

Figure 5-15 Fraction of the ebb during which a threshold value of 0.2 N/m^2 is exceeded at ebb (top) for the three model simulations and their differences (bottom)

5.3 Conclusions

Hydrodynamic Reference Situation

From the February 2010 model simulation it can be seen that the in subtidal zone north of intertidal shoal *Walsoorden* and in the channel *Schaar van Waarden* the peak flood velocity is higher than the peak ebb velocity. This indicates that the flood direction is the dominant transport direction. Besides, the period during which a threshold velocity of 0.5 m/s is exceeded during flood is larger than during ebb. This indicates that more sediment is transported in the flood direction than in the ebb direction as well. In the observation points it is shown that the low water slack period is longer than the high water slack period. This enhances the transport of fine sediments in the ebb direction. Finally, the average bed shear stress at the location of the disposal is larger than the critical bed shear stress during ebb and flood. This means that sediment transport in both directions can be expected.

Initial Hydrodynamic Response

As a result of the disposed sediment, the flow velocity and of bed shear stress magnitudes, and thus also sediment transport capacity, at the location of the sediment disposals increase for the ebb as well as the flood period. At the upstream and downstream sides of the disposal the magnitudes of the flow velocity and bed shear stress decrease. In this way the flow can erode sediment from the front of the disposal and bring it to the back. The area with the largest decrease in velocities is located between the location of the disposed sediment and the intertidal shoal. This is at the downstream end of the sediment disposals during the flood period.

The direction of the flow changes only a little due to the disposed sediment. The ebb flow is strongly guided onto and over the disposed sediment while the flood flow is partly guided around the disposed sediment. In the neighbouring channels a small increase in the velocity is observed. This effect is most evident in the flood period.

However, all the above mentioned impacts diminish due to the morphological development between September 2010 and October 2011. In October 2011 the initial impact of the sediment disposal on the local flow and bed shear stress is reduced. As the sediment is smoothening out, the patterns and magnitudes of the flow and bed shear stress are returning towards the situation before the sediment was disposed.

6 SEDIMENT TRANSPORT MODEL RESULT

6.1 Variations in Sediment Transport

Both the spatial, and the temporal variation in sediment transport will be addressed here. The spatial variations will be considered with the help of the averaged sediment transport rates over ebb and flood. The temporal variations will be considered with the help of five observation points. These observation points are the same as the observation points that were used in the previous Chapter. The period of the spring tide is the same as the period used in the chapter with hydrodynamic results. For both the spatial and the temporal variations a distinction is made between ebb and flood of neap tide and spring tide. As for the hydrodynamic model results, the ebb and flood period is defined by rise or fall of the water level per grid cell.

6.1.1 Temporal Variations

In order to get an idea of the magnitudes and the distribution of the sediment transport over time the sediment transport profiles of five observation points have been analysed (see Figure 5-5). Figure 6-1 shows the total sediment transport of observation points 1 and 5 for the three model simulations for a neap and a spring tide. Figures for the sediment transport of all the observation points can be found in Appendix C.

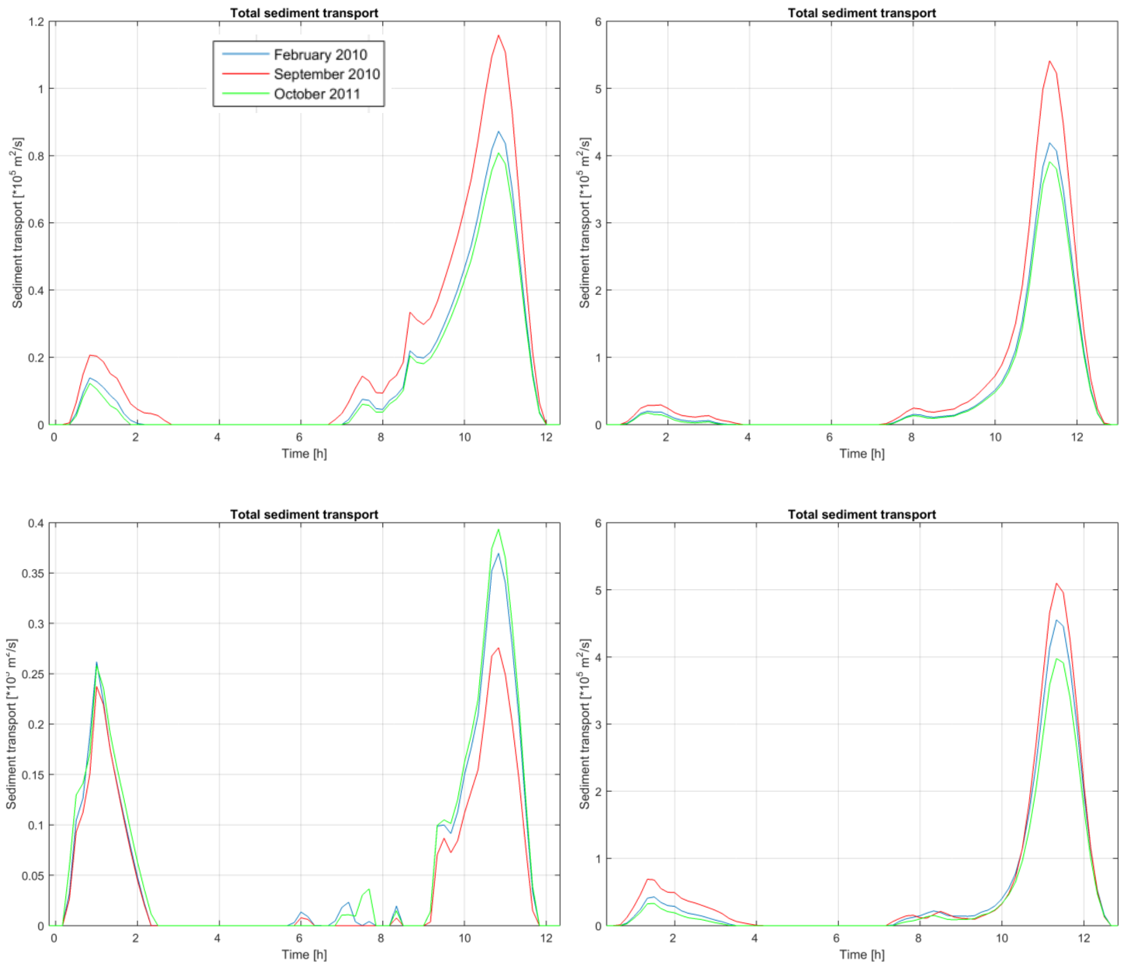

Figure 6-1 Time series of the sediment transport for observations points 1(top) and 5 (bottom) for a neap (left) and spring tide. The locations of the observation points can be found in Figure 5-5.

Figure 6-1 clearly shows two distinct peaks for the sediment transport. The peaks on the left in the figures display the sediment transport during ebb and the peaks on the right show the sediment transport during flood. For all observation points the sediment transport during flood is larger than during ebb. This asymmetry is larger during spring than during neap tide and is most evident in observation points 1, 2 and 4. Furthermore, the sediment transport during spring tide is significantly larger than during neap tide. The largest differences between the sediment transport during spring and neap tide are found in the flood period. The difference between the peak transport during spring tide and neap tide is approximately a factor five. If the plots of the local sediment transport are compared with the plots of the local flow velocities, it can be seen that the threshold velocity above which sediment is transported, is approximately 0.4 m/s. Figures that contain the sediment transport and the flow velocity for the various observation points are included in Appendix C.

6.1.2 Spatial Variations

As mentioned in Chapter 2, bed level changes occur due to a sediment transport gradients. The alternating direction and magnitude of the flow due to the ebb and flood currents creates a situation where the sediment transport continuously varies. An estimate of the sediment transport and the locations where sedimentation or erosion can be expected during ebb and flood will be made in this paragraph. Figures 6-1 and 6-2 show the average sediment transport for a neap and spring tide during flood conditions for the three different model simulations and their differences. Figures 6-3 and 6-4 show this for the ebb period. From this figures, the magnitude and the direction of the sediment transport can be found. To find the locations where erosion and sedimentation can be expected, a gradient in the magnitude of the sediment transport in the flow direction needs to be identified. (Note that gradient in magnitude of the sediment transport, and not the magnitude itself, are responsible for the change in bed level.)

It can be derived from the figures that the sediment transport in the deeper channels (red) are larger than in the shallower intertidal areas (blue) due to the higher flow velocities. When the flow direction is from the areas with higher (lower) sediment transport to areas with lower (higher) sediment transport, accretion (sedimentation) can be expected. The arrows in the figures indicate that during flood conditions sediment is transported towards the shoal to settle on higher grounds (from red to blue). During ebb a less strong gradient is directed off the shoal indicating sediment being eroded from the shallow water north of the shoal into the channels (from blue to red). If the accretion during flood and erosion during ebb are not balanced, accretion or erosion will occur over the time span of one tidal cycle.

Beside the differences in ebb and flood, it also needs to be noticed that the sediment transport, and thereby the gradients in sediment transport, are much larger during spring tide than during neap tide. This is clearly noticeably when the scale bars of Figures 6-1 and 6-2, and 6-3 and 6-4 are compared. Therefore, it is most likely that the largest developments in bed level occur during spring tide.

The lower plots in Figures 6-2 and 6-3 show the response of the sediment transport during flood to different bathymetries during neap and spring tide. The figures show that the sediment transport initially increases on the location of the disposed sediment and decreases in the leeward zone of the disposal (left). As a result of this, the gradient of the sediment transport in flood direction decreases. This means that more sediment is deposited in the flood direction of the disposal than before. The difference plots between October 2011 and February 2010 (middle) show that this effect has reversed after one year. Less sediment is thus transported towards the shoal than in the initial situation. The patterns in Figures 6-2 and 6-3 are similar but the magnitudes of the differences are much smaller during neap tide (Figure 6-3).

The lower plots in Figures 6-4 and 6-5 show the response of the sediment transport during ebb to different bathymetries during neap and spring tide. As can be seen from the scale of the colorbars in these figures, the responses are much smaller than is the case for flood. Nevertheless, a clear increase of the sediment transport at the location of the disposal can be observed. The increased sediment transport creates a local increase in the gradient of the sediment transport. The gradient provides a migration of the disposed sediment in the ebb direction. A clear statement about the differences between the October 2011 and the February 2010 situation (middle) cannot be made because the differences in sediment transport are very small. What can be concluded from this is that the situation is evolving towards the situation where the sediment was not disposed yet. A comparison between the difference plots in Figures 6-4 and 6-5 show that the response of the ebb sediment transport to the sediment disposals is almost identical for neap and spring tide.

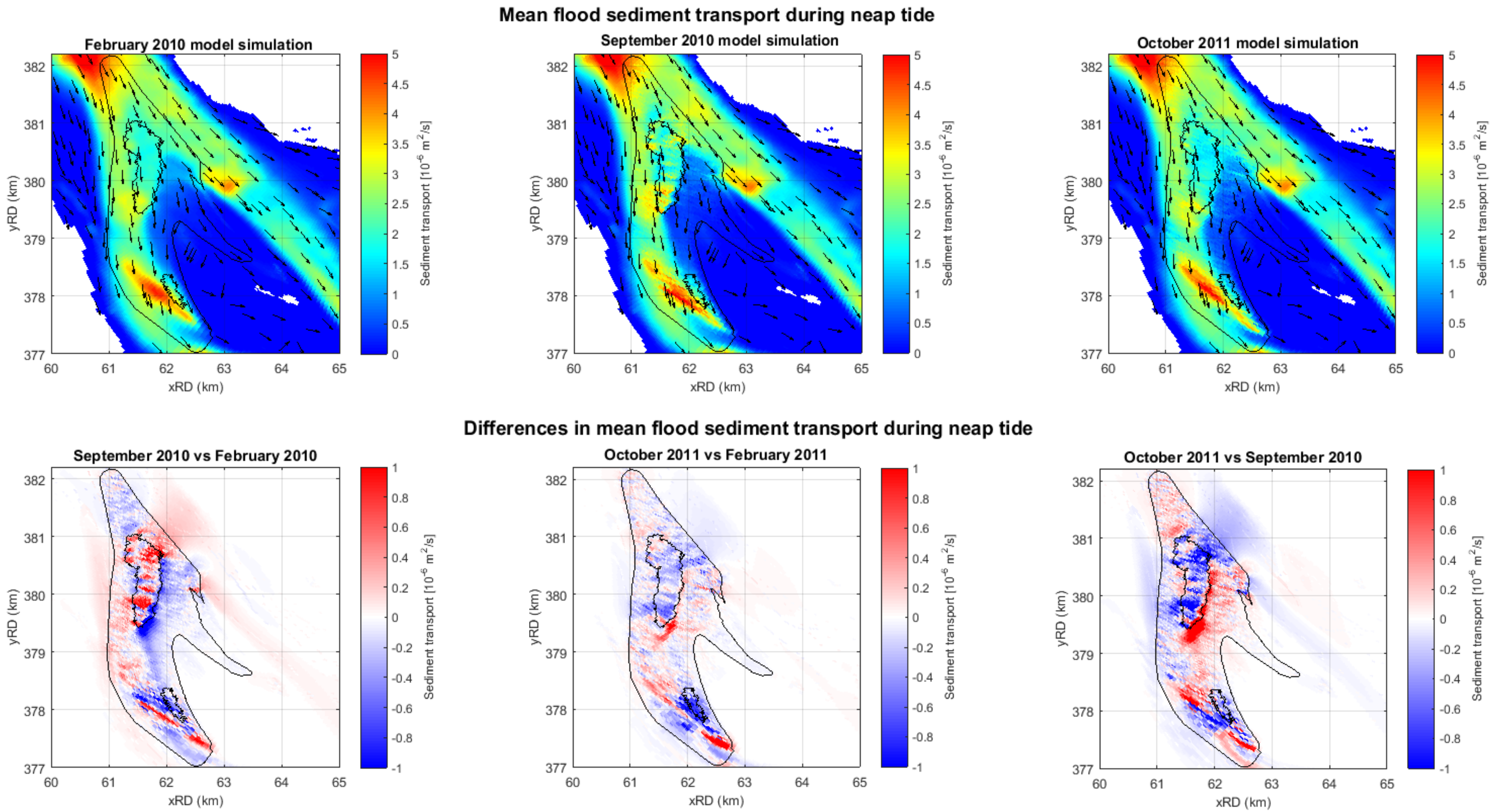

Figure 6-2 Mean flood sediment transport during neap tide of the three model simulations (top) and the differences between the three model simulations (bottom). The black lines indicate the control polygon and the 2.0 m difference contour line between the bathymetry of February 2010 and September 2010 model. Note that the arrows in the figures do only indicate the direction and not the magnitude of the flow. The magnitude of the flow is indicated by the colour.

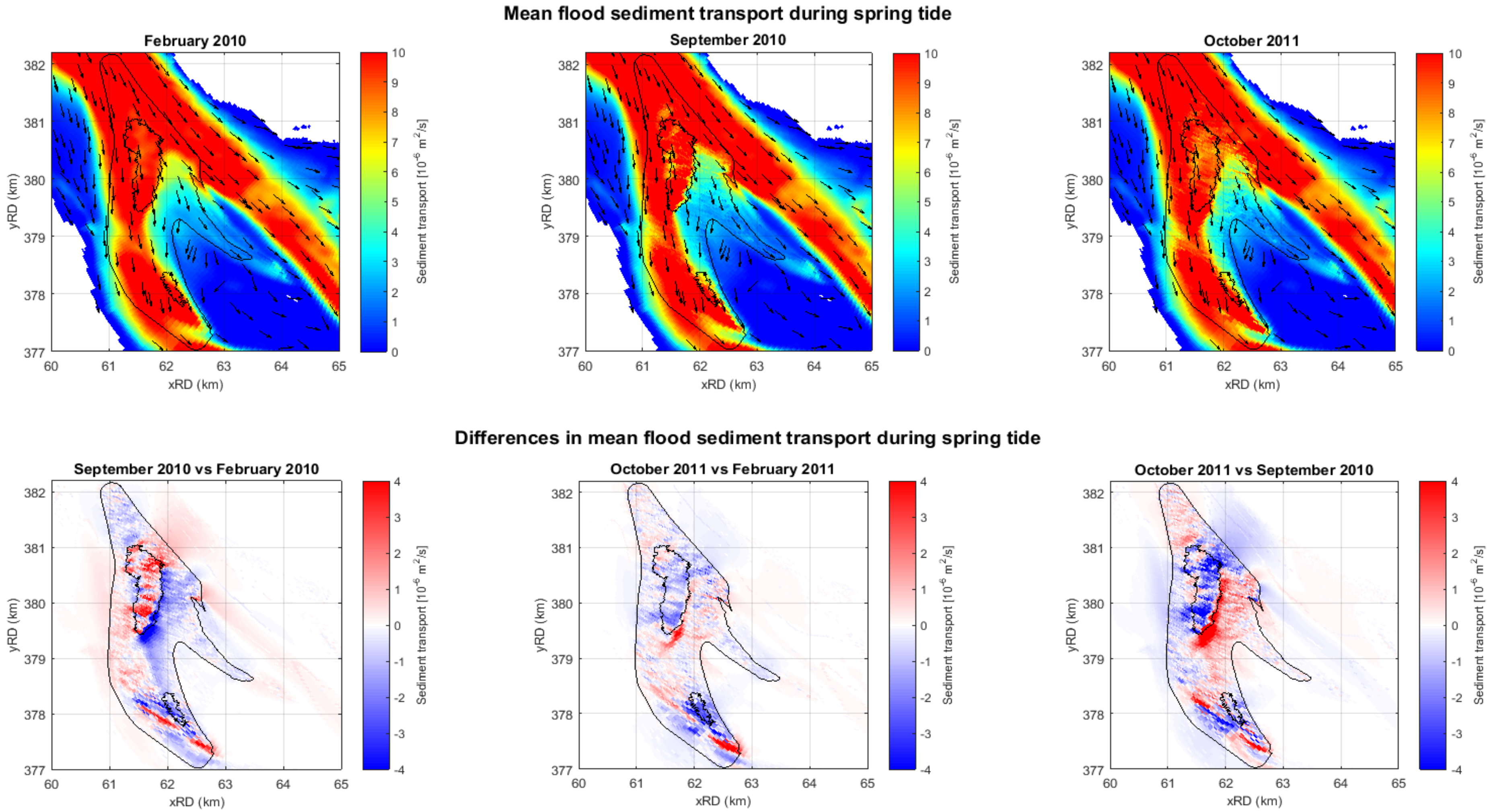

Figure 6-3 Mean flood sediment transport during spring tide of the three model simulations (top) and the differences between the three model simulations (bottom). The black lines indicate the control polygon and the 2.0 m difference contour line between the bathymetry of February 2010 and September 2010 model. Note that the arrows in the figures do only indicate the direction and not the magnitude of the flow. The magnitude of the flow is indicated by the colour.

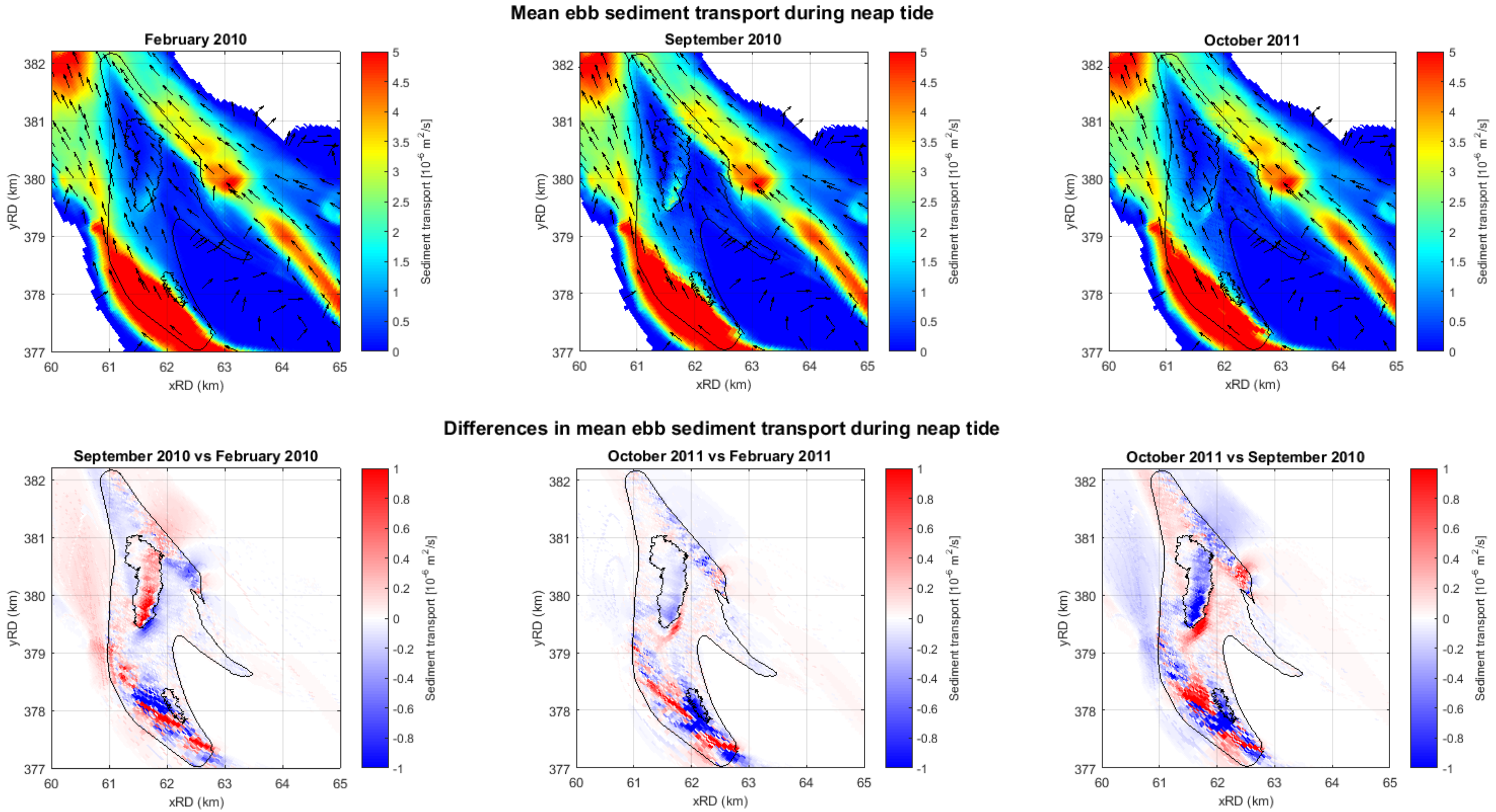

Figure 6-4 Mean ebb sediment transport during neap tide of the three model simulations (top) and the differences between the three model simulations (bottom). The black lines indicate the control polygon and the 2.0 m difference contour line between the bathymetry of February 2010 and September 2010 model. Note that the arrows in the figures do only indicate the direction and not the magnitude of the flow. The magnitude of the flow is indicated by the colour.

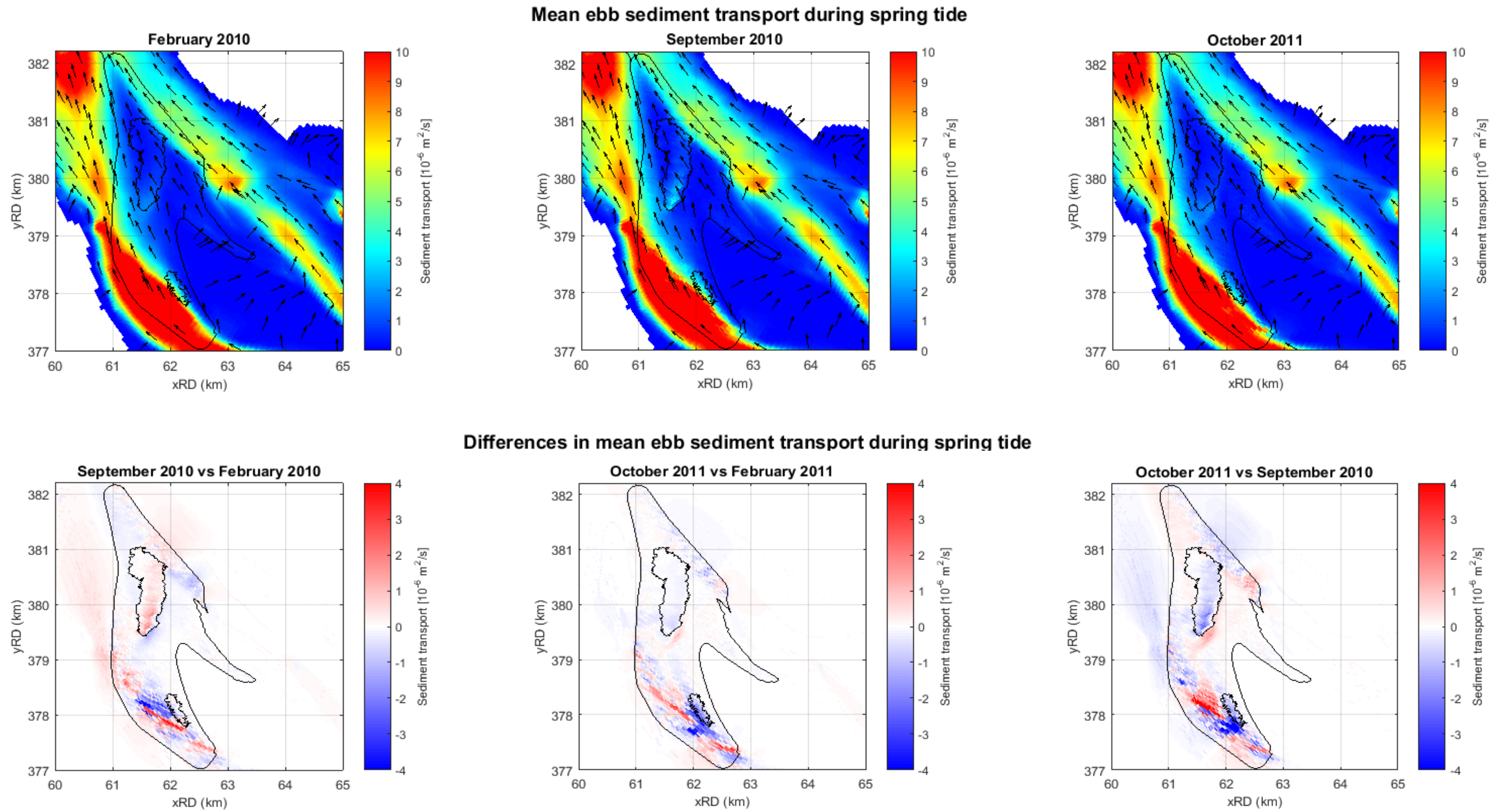

Figure 6-5 Mean ebb sediment transport during spring tide of the three model simulations (top) and the differences between the three model simulations (bottom). The black lines indicate the control polygon and the 2.0 m difference contour line between the bathymetry of February 2010 and September 2010 model. Note that the arrows in the figures do only indicate the direction and not the magnitude of the flow. The magnitude of the flow is indicated by the colour.

6.2 Residual Transport

As referred to in chapter 2, changes in bed level occur when the gradients in net sediment transport during a characteristic period of natural forcing are nonzero. The characteristic period of natural forcing that is evaluated here is one tidal cycle. In order to explain the developments of the bed level, the residual transport over this period have to be examined. A gradient in the residual sediment transport points out where a change in bed level can be expected. To include the variability of the residual transport over a spring neap tide cycle, an analysis of the residual transport is made for a spring tide as well as a neap tide. Figure 6-6 shows the residual transport for a spring and neap tide for the three different model simulations. A similar figure for neap tide can be found in Appendix B.

The residual flow clearly shows that the residual transport direction at the northern tip of the intertidal shoal is flood directed. This holds for both spring and neap tide conditions. The residual sediment transport in the channel south of the shoal (*Zuidergat*) is ebb directed for both spring and neap tide. In the channel north of the shoal (*Schaar van Waarde*) there is a less clear residual transport direction. During spring tide conditions the residual transport is flood directed, while during neap tide conditions the residual sediment transport is ebb directed. Given that the magnitude of the residual sediment transport is larger for a spring tidal cycle than for a neap tidal cycle, the residual transport over a full spring neap tidal cycle shall look more like the residual sediment transport during spring tide. This results in a similar spatial distribution of the residual sediment transport as the ratio between the ebb and flood peak velocities in Figure 5-10 (p48).

As before, the spatial gradients in sediment transport in the direction of the residual sediment transport indicate that a change in bed level can be expected. At the subtidal zone north of the intertidal shoal a negative gradient in the flood direction is present in the direction towards the shoal (from large sediment transport to smaller sediment transport). From Equation 2-2 (p 10) it follows that a negative gradient in sediment transport corresponds with an increase of the bed level. This means that an increase in bed level can be expected at subtidal zone north of the shoal in the direction of the negative gradient. At the shoal itself the residual transport, and therefore also the gradient, is very small. This means that a transport of the sediment on to the shoal itself is very unlikely.

At the southward end of the control polygon a loss of sediment from the shoal to the channel is indicated by the direction of the residual transport at this location. In the flood dominated region the sediment is steered towards the channel where the transport is pointed towards the north. From here on the sediment is transported towards more downstream regions in the estuary. The arrows perpendicular to the flow direction of the channel in the top three plots in Figure 6-6 clarify that sediment is transported from the tip of the shoal to the channel.

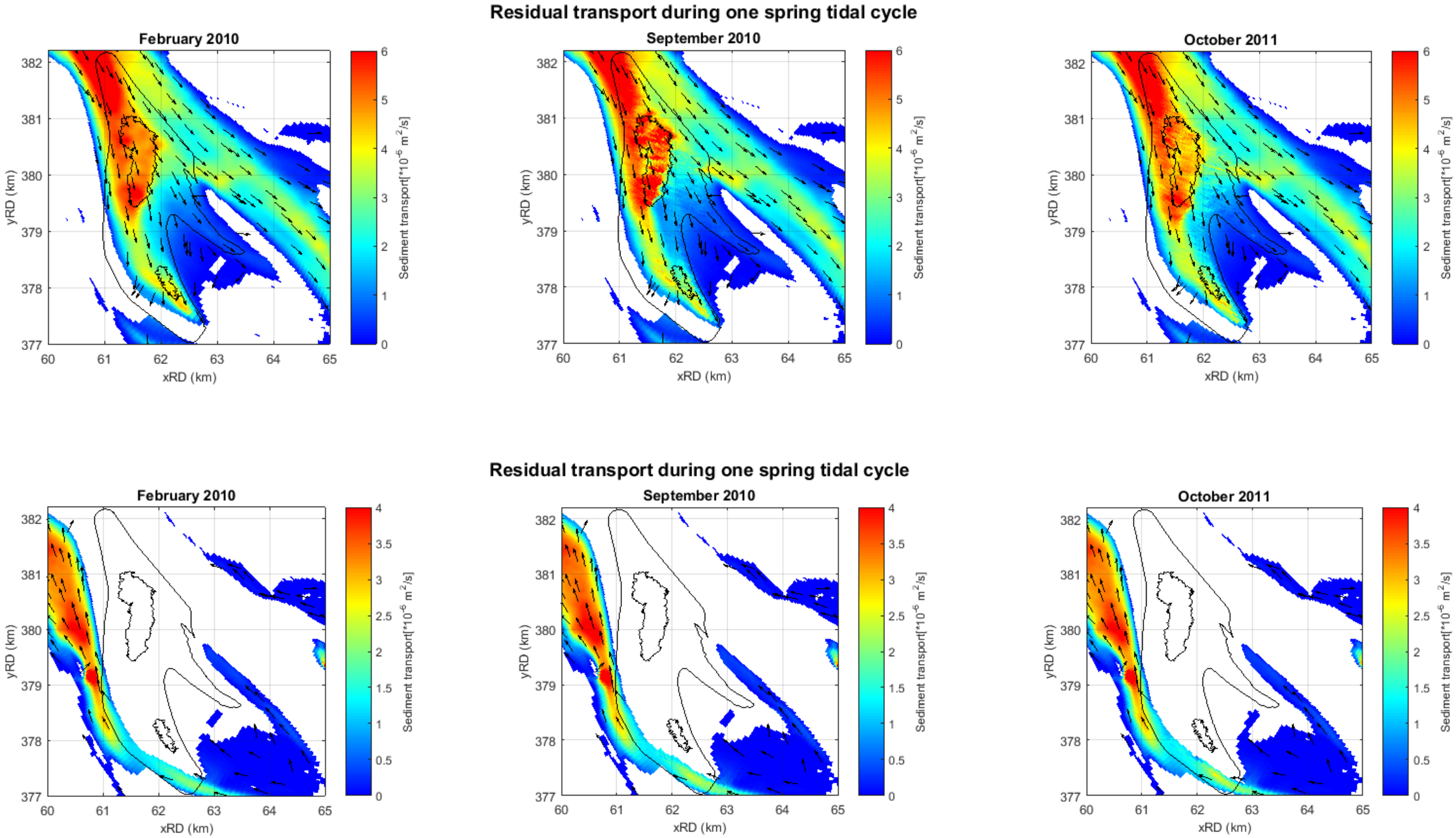

Figure 6-6 Residual flood (top) and ebb transport (bottom) during spring tide for the different model simulations. The magnitude is expressed by the colour and the arrows indicate the direction.

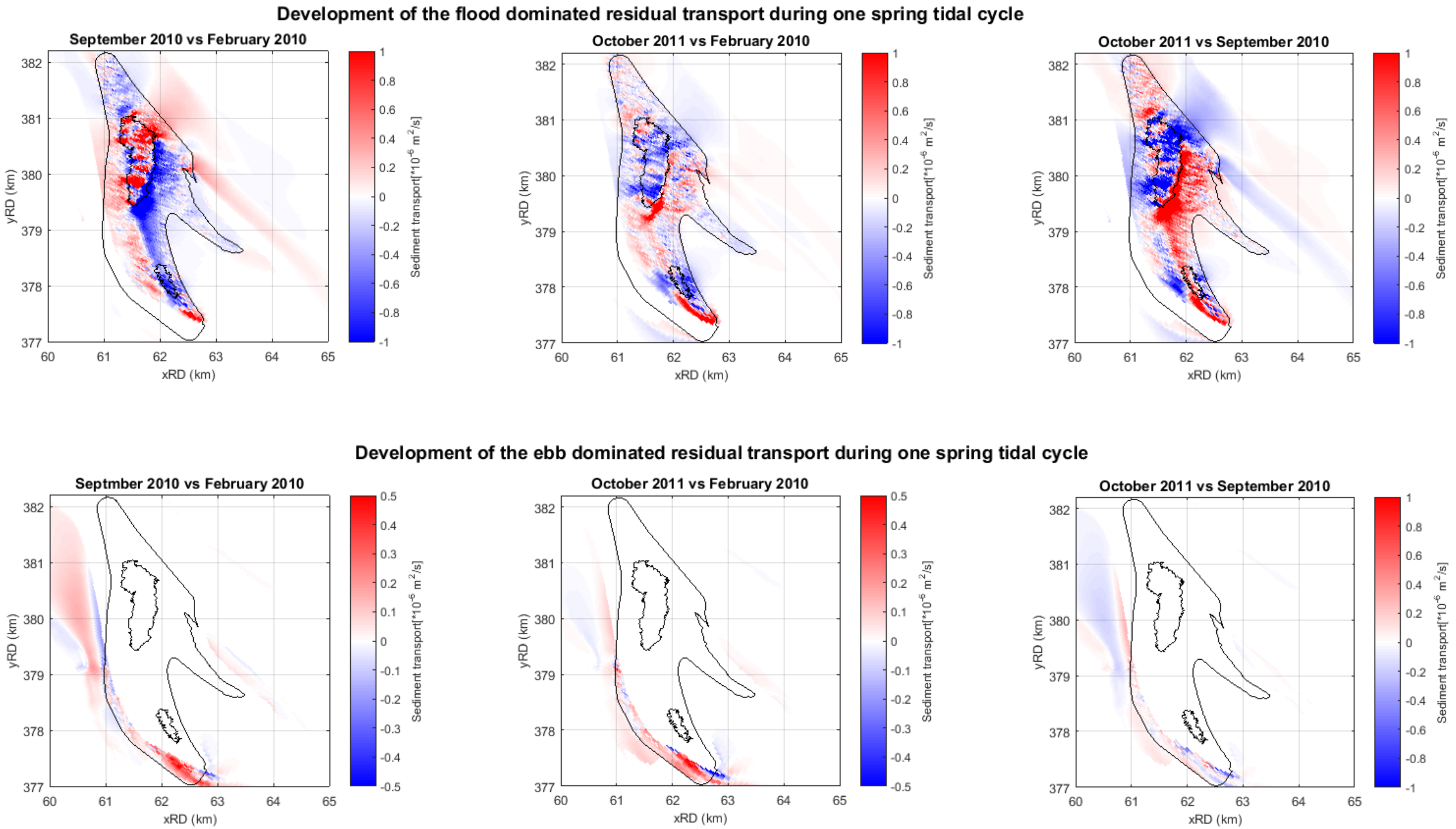

Figure 6-7 Differences in the magnitude of the residual sediment transport for a spring tide between the three model simulations

The consequences of the disposal on the residual sediment transport for spring tide can be obtained from 6-7. As with the previous figures a similar figure for neap tide can be found in Appendix B. The two plots on the left side of Figure 6-7 show the initial response of the residual sediment transport to the disposal. They show an increase of the transport towards the shoal at the location of the disposed sediment and a decrease in transport between the shoal and the disposal location. These two together provide a larger negative gradient in the direction of the residual transport. Consequently an increase in bed level at this boundary is to be expected. In the ebb dominated region an increase in sediment transport can be seen at the south side of the control polygon. This can be due to the sediment that is transported into the channel from the flood dominated region.

The two plots in the middle of Figure 6-7 show the differences between the reference situation and the situation after one year of morphological development. What directly stands out it that the pattern of the flood dominated region is almost opposite to the pattern of the initial response. This reveals that the initial gradient in sediment transport that was created by the disposal has smoothed out and has even decreased in comparison with the initial situation. An explanation for this is that the flow velocities in this location have decreased. The highest parts of the created dune have been eroded while the centre of mass has migrated towards the shoal. As a result of this, the earlier created sheltered zone behind the dune has disappeared and the flow velocity, and thus the sediment transport capacity, at this location has increased again. The little red dot in the middle of the control polygon indicates a location where the top of the dune has migrated to.

The decrease in residual sediment transport at the initial location of the disposal is a result of a decrease in sediment transport during flood. As can be seen from the flow velocity profiles of the control points on the disposal, the peak flood velocities have decreased. The water that is flowing towards the migrated dune is obstructed by the dune and therefore decreases in speed. This results in lower sediment transport during flood and thus smaller residual sediment transport. The increase in sediment transport at the south side of the control polygon in the ebb dominated zone is still present.

6.3 Balance

To find out where the disposed sediment is transported to, a balance polygon around the disposed sediment is introduced in Figure 6-8. Table 6-1 shows the difference in average depth and sediment volume with the February 2010 situation within this polygon. What can be observed is that the sediment volume within this polygon has a decreasing trend.

Table 6-1 Difference in average depth and sediment volume with the February 2010 bathymetry within the balance polygon that is displayed in Figure 6-8 for three different moments in time.

Date	Difference in average depth with the February 2010 bathymetry [m]	Difference in sediment volume with the February 2010 bathymetry [$*10^6$ m^3]
15 September 2010	1.02	2.61
14 April 2011	0.98	2.49
12 October 2011	0.91	2.32

Table 6-2 shows the average sediment transports through the boundaries of the balance polygon for the different model simulations as displayed in figure 6-8. The arrows indicate the direction of the sediment transport through the boundaries that are defined positive. Show the average incoming, outgoing and resulting sediment transport during these model simulations.

What can be seen from the last column in Table 6-2 is that there is an inflow of sediment into the balance polygon for all the model simulations for both spring and neap tidal conditions. This would lead to an increase of the sediment volume within the polygon instead of the observed decrease. However the magnitude of the residual transport into the balance polygon is very small. Given that the area of the balance polygon is 255 hectare, a resulting sediment inflow of $5*10^{-4}$ m^3/s would result in an increase of the average bed level of less than 1 cm/year.

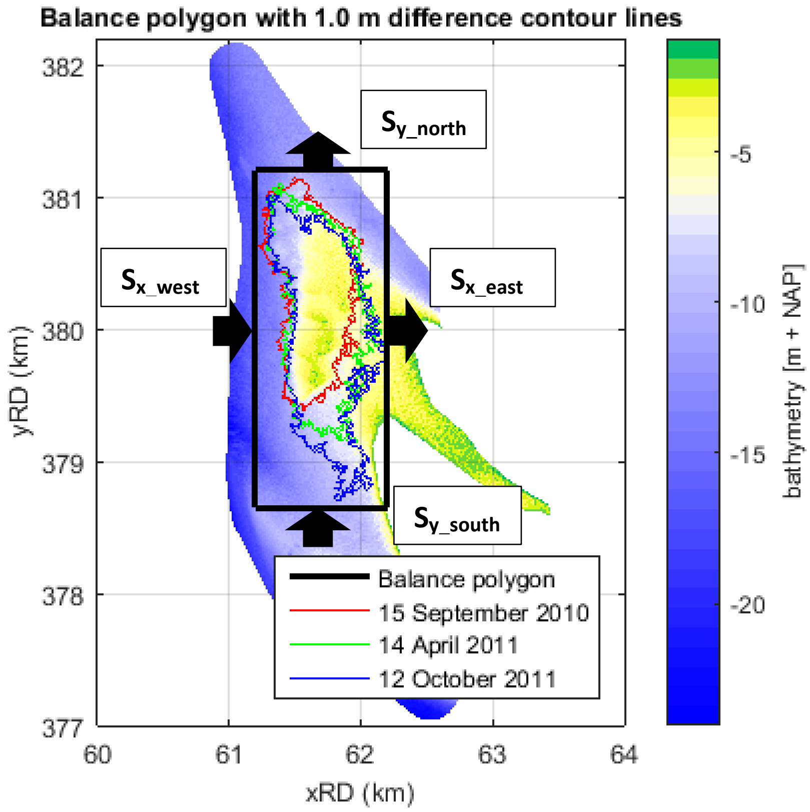

Figure 6-8 Balance polygon for which the in- and outflowing sediment transport for the different sediment transport model simulations is analysed. The red, green and blue polygons indicate the development of the 1.0 m difference contour line with the February 2010 bathymetry.

Table 6-2 Average sediment transport through the boundaries of the balance polygon in Figure 6-8 for the different model simulations. The cells that are shaded in green (red) display sediment that is transported into (out of) the polygon. The last three columns display the incoming, outgoing and residual transport for the concerned simulations.

Scenario	S_{x_west} [m^3/s]	S_{x_east} [m^3/s]	S_{y_north} [m^3/s]	S_{y_south} [m^3/s]	S_{IN} [m^3/s]	S_{OUT} [m^3/s]	S_{RES} [m^3/s]
M1.1	1.47*10-4	$-6.18*10^{-5}$	$-3.73*10^{-4}$	-1.28*10-5	$5.82*10^{-4}$	$1.28*10^{-5}$	**$+5.69*10^{-4}$**
M1.2	$1.75*10^{-3}$	2.69*10-3	$-3.39*10^{-3}$	$-2.09*10^{-3}$	$5.14*10^{-3}$	$4.78*10^{-3}$	**$+3.55*10^{-4}$**
M2.1	$1.31*10^{-4}$	$-4.6*10^{-5}$	$-3.34*10^{-4}$	$6.32*10^{-6}$	$5.17*10^{-4}$	0	**$+5.17*10^{-4}$**
M2.2	$1.75*10^{-3}$	$2.52*10^{-3}$	$-3.27*10^{-3}$	$-2.04*10^{-3}$	$5.02*10^{-3}$	$4.56*10^{-3}$	**$+4.65*10^{-4}$**
M3.1	$1.45*10^{-4}$	$-6.81*10^{-5}$	$-3.87*10^{-4}$	$-3.08*10^{-5}$	$6.01*10^{-4}$	$3.08*10^{-5}$	**$+5.70*10^{-4}$**
M3.2	$1.73*10^{-3}$	$2.65*10^{-3}$	$-3.44*10^{-3}$	$-2.11*10^{-3}$	$5,18*10^{-3}$	$4.76*10^{-3}$	**$+4.21*10^{-4}$**

6.4 Concluding Remarks on the Modelled Sediment Transport

At a flow velocity of 0.4 m/s, the transport of the sediment in the model (D_{50}=200 µm) is initiated. The sediment transport can be divided into two distinct peaks: a large peak in the flood direction and a smaller peak in the ebb direction. The peak flood transport is approximately 5 times larger with springtide than during neap tide.

The residual transport at the location of the sediment disposal is flood dominated during neap and spring tide conditions. Compared to the situation during neap tide the flood dominance increases during spring tide. A comparison of the residual sediment transport that is calculated by the model with the sediment transport found by Vandenbruwaene, et al. (2012) as displayed in Figure 3-5, shows a large resemblance in spatial patterns. The magnitude of the residual sediment transport that is calculated by the sediment transport model in this study is a factor 5 to 10 smaller than the magnitude of the sediment transport that is derived by Vandenbruwaene, et al.

As could be expected from the analysis of the flow velocities, the impact of the sediment disposal is exhibited by an increase of sediment transport at the location of the sediment disposals and a decrease in sediment transport in the leeward zone of the disposed sediment during flood. As a result of this, a gradient in residual transport at the boundary of the disposal site that imposes a migration of the disposed sediment in the flood direction is developed. This gradient explains the migration of the disposed sediment into the flood direction.

The balance polygon that was introduced in Chapter 6.3 did not find an evident cause for the part of the disposed sediment that disappeared from the polygon between September 2010 and October 2011. A reason for this discrepancy might be found in the assumptions that were made in the model setup.

7 Discussion

7.1 Model results

The analysis of the bathymetric data showed that the bathymetric development of the disposed is responsible for only a part of the sediment that has disappeared from the control polygon. The rest of the sediment that is lost from the control polygon is due to the autonomous morphological development of shallow waters north of the intertidal shoal of Walsoorden. The decrease in sediment volume of the disposed sediment cannot be explained by the sediment transport that is simulated by the sediment transport model. A sediment transport balance over the area around the disposed sediment showed that during both neap and spring tidal conditions the sediment transport into the balance polygon is larger than the transport out of the balance polygon. This implies that the sediment volume within the balance polygon increases while a decrease of the sediment volume is observed in reality.

A reason for the discrepancy between the observed data and the modelled sediment transport must be found in the assumptions that were made in the model setup. Modelling the sediment transport is very sensitive for deviations in hydrodynamics. Due to the higher order relationship between flow velocity and sediment transport, seemingly small variations in flow velocities can have major impact on the direction and magnitude of the (residual) sediment transport. Although the resemblance of the model simulations and the measured hydrodynamic data in the subtidal zone near the intertidal shoal of Walsoorden is accurate, an underestimation of the peak flood velocities was observed by Tiessen, et al. (2016). The reduction of the number of grid cells of the model that calculates the sediment transport introduces another error in the flow velocity. The errors in flow velocities have their impact on the sediment transport as well. The fact that the boundary conditions of the year 2013 are used while the sediment was disposed in 2010 is not considered as a problem because representative tidal conditions are used in the modelling approach.

While the influence of waves is not included in the model, it is likely that waves have their effects on the sediment transport (e.g. by the stirring up of sediment and wave current interactions). As stated in Chapter 2, the wave energy of non-dissipative waves induces a seaward transport of sediment and increases in the landward direction (Friedrichs & Aubrey 1996 & Friedrichs, 2011). This means that especially during low water waves are likely to influence the sediment transport. The erosive effect of wind waves on the disposed sediment could explain why the model without waves cannot reproduce the decrease of sediment in the balance polygon. However, it needs to be taken into account that the theory that emphasizes the erosive trend of waves represents a simplified situation. In reality the situation is much more complex and a lot of variables that have their impact are not taken into account in this approach (e.g. wave breaking and local hypsometry). The exact impact of wind waves on the local hydrodynamics is difficult to assess due to the large variability of the hydrodynamics. The only way to investigate the impact of waves would be by running a model where waves are included. With the used software this was not possible (yet).

Besides this, the used model is a 2D depth averaged model. This model only takes a simplified representation of secondary flow effects and spiral motion into account (Deltares, 2016). The effects of these flows can strongly vary over depth. However, due to the location of the study area and the time and spatial scales of the simulations, these effects are considered to have only a little influence on the results of this work. Therefore, it is not likely that the use of a 2D depth-averaged model is responsible for the fact that the sediment transport model is not able to reproduce the sediment balance in the polygon.

Additionally, the used model roughness and composition and distribution of the sediment are a subject for debate. In the model the roughness is described with a Manning coefficient that spatially varies in the longitudinal direction of the estuary. This parameter is used to calibrate the water levels on a large scale. For morphological calculations this parameter is not necessarily the best value as well. The prediction of sediment transport is strongly dependent on the bed roughness whereas the bed roughness in turn depends on the sediment transport generated by the bed forms migrating over the bed (Van Rijn,2007). Important parameters that influence the bed roughness are particle size and particle mobility. Plancke, et al. (2009b) showed the presence of a seasonal variation of the roughness of the bed. Better sediment transport model results could be gained if a more realistic spatial distribution of the roughness would be included.

The composition and distribution of the sediment that is used in the model is represented by one sediment fraction with a grain size of 200 µm. This grain size is used because it is a good representation for the grains of the disposed sediment as well as for the grains in the shallow waters near the shoal. However, in reality the sediment is composed of a distribution of sediment with different grain sizes. All sediment types have different properties when it comes to sediment transport. The use of multiple sediment fractions, or even a sediment distribution in the calculations of the sediment transport, is likely to result in a different magnitude or direction of the sediment transport. What the effect of different sediment fractions will be is again difficult to predict. A model simulation including multiple grain size fractions could clarify this. The cohesive properties sediments is not considered to have a large impact because only a very small fraction (<2%) of the sediment consists of fine cohesive sediment (D<63µm) (WLB, 2008).

Apart from the decrease of sediment volume of the disposed sediment, it was concluded that the disposed sediment is transported in the flood direction. In line with what could be expected from literature (Vandenbruwaene, et al., 2012), the model simulates flood dominance in the shallow water north of intertidal shoal *Walsoorden*. The disposed sediment particularly causes an increase of the sediment transport in the flood direction at the location of the disposals that is most profound during spring tidal conditions. This can be explained by the increased ratio between the tidal amplitude and the channel depth (R/h). The gradient in residual sediment into the flood direction explains why the disposed sediment is transported into the flood direction.

7.2 Modelling Software

This present study makes us of the Delft3D Flexible Mesh (DFM) software package for the numerical model simulations. During the time of writing the software was still under development and several features such as the implementation of wave modelling and morphology were still under development. Nevertheless, this study uses DFM software because it allows the user to locally refine the grid and increase the level of detail without a significant increase in computational times. However, for the morphological model it was not possible to simulate a DFM model in parallel mode (i.e. running a single simulation on multiple computers to decrease the computational time). Due to the large size of the model, the numerical grid had to be reduced in order to execute a simulation in serial mode. This was at the cost of the accuracy of the model (Chapter 4.3.2).

Furthermore, a simulation where bed level updating was included was performed. This simulation was found to be unstable at the boundaries of the model. If the bed level updates at the boundaries of the model were switched off in the model, the instabilities were shifted upstream. For this reasoning, no calculations with bed level updates could be made and the available bathymetric data could not be used to validate the model.

8 Conclusions and Recommendations

8.1 Conclusions

Between February and September 2010 3.72 million m^3 sand was disposed at the subtidal zone north of intertidal shoal *Walsoorden*. The most important goals were maintaining the multiple channel system and creating and preserving ecologically valuable areas. During the execution works over 0.88 million m^3 of the sand was already lost from the control polygon. The morphological development of the remaining sediment in the subsequent 13 months is a migration of a large part of the sediment in the flood direction. Besides, the monitoring programme of the Flemish government indicated a loss of 0.57 million m^3 sediment from the control polygon in this period.

In this study a smaller polygon around the disposed sediment shows that only part of this sediment is due to a loss of sediment of the disposed sediment. The development of the contour lines that indicate a difference with the reference bathymetry show that the disposal smoothens out, this happens mainly into the flood direction. Table 3-2 shows the development of the area and the sediment volume within the contour lines that indicate the difference with the February 2010 bathymetry. Between September 2010 and October 2011, 0.24 million m^3 of the 2.55 million m^3 sediment has disappeared from the 1.0 m difference polygon while the area has increased from 80 hectares to 100 hectares. This is much less than the 0.57 million m^3 sediment that has disappeared from the control polygon.

The various model simulations gave clarifying results about the impact of the changed bathymetry. At the location of the sediment disposal the water depths decrease considerably. Nevertheless, the whole sediment disposal stays under the low water line. As a result of the decreased water depth, the flow velocities and magnitude of the bed shear stress increase. This results in a larger sediment transport and erosion of the sediment at the location of the disposal. This trend is present in the ebb and the flood period and is the largest during flood. In the downstream flood direction of the sediment disposal a sheltered zone is introduced where the flow velocity decreases for the ebb and the flood period. Observation point 5 showed that the reduction in flow velocities can associated with the decrease in flood peak velocities. However, the peak flood velocities do still exceed 0.8 m/s while velocities higher than 0.8 m/s are undesired for ecologically valuable shallow water areas (Plancke, et al., 2009b).

As a result of the increased sediment transport on the sediment disposal and the decreased sediment transport in the sheltered zone a gradient in residual sediment transport arises. As a result, a migration of the disposed sediment in the flood direction is initiated. This gradient is the result of the larger tidal flow velocities, and thus sediment transport, on the location of the sediment disposal; and the decreased flow velocities, and thus sediment transport, in the resulting sheltered zone. The increase and decrease of the flow velocities is most profound for the peak flood velocities. From this it can be concluded that the variation in tidal flow initiates the migration of the disposed sediment into the flood direction. The loss of sediment from the control polygon cannot be explained by the model simulations. In Chapter 6.3 it was emphasized that all model simulations showed a residual sediment transport into the balance polygon. In order to find out which processes are responsible for the loss of sediment from the control and balance polygon, further investigation is needed.

The decrease in sediment of within the polygons in combination with the flow velocities above 0.8 m/s show that the sediment disposals did not succeed in creating new ecologically valuable areas. However, the areas with flow velocities below 0.8 m/s were preserved. This can partially be due to the sediment that is added to the system by the sediment disposals. Considering the magnitude of the losses of sediment from the polygons between September 2010 and October 2011 it can be said that the subtidal zone north of the intertidal shoal of Walsoorden is a suitable location for sediment disposal. In this way the sediment that is dredged from the navigational channel can be disposed more evenly over the estuary in order to stop the jeopardising of the multiple channel system.

Delft3D Flexible Mesh is promising modelling software package that could very well be suited for the modelling of meso-scale developments. The hydrodynamic model showed that relatively large models with a great level of detail could be simulated much faster than the conventional modelling software packages (Delft3D Flow). However, at this stage the absence of functionalities like waves and bed-level updating supress the advantages that the modelling software gives relative to its alternatives. A large step forward could be made by adding the functionality of running the morphological model simulations in parallel mode.

8.2 Recommendations

As mentioned before, the used numerical modelling software was still being developed at the time of this study. The missing functionalities that would contribute to the most to the meso-scale morphological modelling are the option of running a model in parallel mode, the bed-level update and the inclusion of wind waves in the simulations. Therefore it is advised to focus on implementing these functionalities into DFM.

If bed level updates are included, the changed bed levels can be compared with the data to validate the model. When this is done the hydrodynamic boundary conditions need to be taken into account. The hydrodynamics that will be used need to be a good representation of the hydrodynamics that occurred between September 2010 and October 2011. As for the tidal conditions, a representative spring neap tidal cycle could provide an appropriate period. However, the wind and wave conditions need to be taken into account as well. The representative conditions for this do not necessarily occur simultaneously with the representative neap spring tidal cycle. An artificial set of hydrodynamic data could be constructed in order to reproduce the correct morphological development of the sediment disposal.

Taking wind waves into account will lead to a better representation of the hydrodynamics and sediment transport. Running a model with and without wind waves in the calculations can give a good insight in the importance of wind waves for sediment transport in intertidal areas. Given the local water depth it is very likely that waves have an impact on the sediment transport.

For further improvements of the results it is recommended to run the calculations with multiple sediment fractions. The sensitivity of the morphological developments for the used grain sizes can be investigated. The deviations in settling velocity and critical bed shear stress might have their effects on the magnitudes of the sediment transport and bed level changes.

An adjustment of the roughness of the model could help to further improve the local flow. Includinga spatially varying roughness could help to improve the local flow velocities. In this way the local flow velocities can be improved without influencing the water levels and tidal propagation throughout the estuary. Tiessen, et al. (2016) already concluded that the flow velocities on intertidal areas are influenced by the local roughness. A good step towards a realistic roughness field could be made if the Van Rijn roughness parameter would be used (Van Rijn, 2007).

Besides measurements of the flow velocities and bathymetry, more sediment transport measurements could help to validate and calibrate the numerical model. Because sediment transport is very sensitive for changes in flow velocity, measuring errors in the flow velocity can have an effect on the sediment transport.

9 CITED LITERATURE

Allen, J. & Duffy, M., 1998. Medium-term sedimentation on high intertidal mudflats and salt marshes in the Severn estuary, SW Britain: the role of wind and tide.. *Marine Geology,* Volume 150, pp. 1-27.

Berenbrock, C. & Tranmer, A., 2008. *Simulation of Flow, Sediment Transport, and Sediment Mobility of the Lower Coeur d'Alene River, Idaho,* Reston: United States Geological Survey.

Berlamont, J. et al., 2003. *An Alternative Strategy for Dumping in the Scheldt Estuary - Comments of the expert team,* s.l.: s.n.

Bosboom, J. & Stive, M. J. F., 2015. *Coastal Dynamics I - lecture notes.* 0.5 ed. Delft: Delft Academic Press.

Cleveringa, J., 2013a. *LTV V&T rapport G02 - Grootschalige sedimentbalans van de Westerschelde,* s.l.: Consortium Deltares, IMDC, Svašek, Arcadis.

Cleveringa, J., 2013b. *LTV V&T rapport K16: Ontwikkelingen mesoschaal Westerschelde,* s.l.: Consortium Deltares, IMDC, Svašek, Arcadis.

Cleveringa, J., 2013c. *LTV V&T rapport K17: Samenhang ontwikkelingen op verschillende tijd- en ruimteschalen,* s.l.: Consortium Deltares, IMDC, Svašek, Arcadis.

Coen, I., 2008. *De eeuwige Schelde? Ontstaan en ontwikkeling van de Schelde,* s.l.: Waterbouwkundig laboratorium.

Consortium ARCADIS - Technum, 2007a. *Milieueffectrapport Verruiming vaargeul Beneden-Zeeschelde en Westerschelde. Achtergronddocument - Systeembeschrijving Schelde-estuarium. Een visie op de macro-morfologische ontwikkeling.,* s.l.: Technische Scheldecommissie.

Consortium ARCADIS - Technum, 2007b. *Milieueffectrapport Verruiming vaargeul Beneden-Zeeschelde en Westerschelde. Achtergronddocument morfologische ontwikkelingen Westerschelde. Femenologisch onderzoek naar de ontwikkelingen op meso-schaal,* s.l.: Technische Scheldecommissie.

Dam, G., 2013. *LTV V&T rapport A26: Actualisatierapport Finel 2D Schelde-estuarium,* s.l.: Consortium Deltares, IMDC, Svasek, Arcadis.

De Swart, H. E. & Zimmerman, J., 2009. Morphodynamics of Tidal Inlet Systems. *Annual Review of Fluid Mechanics,* Volume 41, pp. 203-229.

De Vriend, H.J. l. Wang, Z.B. Ysebaert, T. Herman, P.M.J. Ding, P. 2011. Eco-Morphological Problems in the Yangtze Estuary and the Western Scheldt. *Society of Wetland Scientists,* Volume 33, pp. 1033-1042.

Deltares, 2016. *D-Flow Flexible Mesh User Manual, Draft version 1.1.0,* Delft: Deltares.

Depreiter, D. Maris, T. Cleveringa, J. Ysebaert, T. Wijnhoven, S. van der Laan, T., 2013. *T2009-RAPPORT SCHELDE-ESTUARIUM,* Bergen op Zoom: Consortium IMDC, ARCADIS, NIOZ, UA.

Dronkers, J., 1986. Tidal asymmetry and estuarine morphology. *Netherlands Journal of Sea Research,* Volume 20, pp. 117-131.

Friedrichs, C. D. & Aubrey, D., 1996. Uniform Bottom Shear Stress and Equilibrium Hypsometry of Intertidal flats. *Coastal and Estuatine Studies,* 50(24), pp. 405-429.

Friedrichs, C. T., 2011. Tidal Flat Morphodynamics: A Synthesis. *Estuarine and Coastal Science,* 3(Estuarine and Coastal Geology and Geomorphology), pp. 137-170.

Friedrichs, C. T. & Aubrey, D. G., 1988. Non-linear Tidal Distortion in Shallow Well-mixed Estuaries: A Synthesis. *Estuarine Coastal and Shelf Science,* Volume 27, pp. 521-545.

Grasmeijer, B., 2013. *LTV V&T-rapport A27: Actualisatierapport Delft3D Schelde-estuarium,* s.l.: Consortium Deltares, IMDC, Svasek, Arcadis.

Henderson, S. M. & Mullarney, J. C., 2013. Wave mixed, wind-generated near-surface shear observed over a tidal flat. *Continental Shel fResearch,* Volume 60S, pp. 22-29.

Hunt, S., Bryan, K. R. & Mullarney , J. C., 2015. The influence of wind and waves on the existence of stable intertidal morphology in meso-tidal estuaries. *Geomorphology,* Volume 228, pp. 158-174.

IMDC, 2012. *Monitoringprogramma flexibel storten - Tweemaandelijkse rapportage september-oktober 2011,* Antwerp: IMDC.

IMDC, 2013. *Monitoringprogramma flexibel storten - Derde Verruiming Schelde: Voortgangsrapport data 2010-2011 ,* Antwerp: IMDC.

Janssen-Stelder, B., 2000. The effect of different hydrodynamic conditions on the morphodynamics of a tidal mudflat in the Dutch Wadden Sea. *Continental Shelf Research,* Volume 20, pp. 1461-1478.

Jeuken, M. Hordrijk, D. Ides, S. Kuijper, C Peeters, P. de Sonneville, B Vanlede, J., 2007. *Koploperproject LTV-O&M – Thema Veiligheid – deelproject 1: Inventarisatie historische ontwikkeling van de hoogwaterstanden in het Schelde estuarium.* Delft, Delft Hydraulics.

Jeuken, M. & Wang, Z., 2010. Impact of dredging and dumping on the stability of ebb–flood channel systems. *Coastal Engineering,* pp. 553-566.

Kuijper, K., 2013. *LTV V&T rapport G05: Data-analysis water levels, bathymetry Western Scheldt,* s.l.: Consortium Deltares, IMDC, Svašek, Arcadis.

Mastbergen, D. & Schrijvershof, R. 2015. *Sedimentatiepatronen Plaat van Walsoorden na plaatval 22 juli 2014.* Delft: Deltares

Palaiogianni, N., 2015. *MSc thesis: Modelling the impact of large scale sediment dumping on the meso-scale hydro- and morphodynamics in the Western Scheldt,* Delft: Deltares.

Peters, J., Meader R, H., Parker, W. R. & Stevens, M., 2001. *Improving navigation conditions in the Westerschelde and managing its estuarine environment - How to harmonize accessibility safetyness and naturallness,* s.l.: s.n.

Pieters, T., 2002. *Het Scheldegetij – Beschrijving en analyse van het getij in het Schelde-estuarium,* Middelburg: Bureau getijdewateren.

Plancke, Y., Sas, M., Heins, F. & Ides, S., 2008. *Westerschelde Nota Plaatrandstortingen: Verruiming vaargeul Westerschelde,* Antwerpen: Waterbouwkundig Laboratorium.

Plancke, Y. M. G., Ides, S. J., Peters, J. J. & Vos, G., 2009a. *The Walsoorden pilot project: a first step in morphological management of the Western Scheldt, conciliating nature preservation and port accessibility.* Paris, s.n.

Plancke, Y., Vos, G., De Mulder, T. & Mostaert, F., 2009b. *Habitatmapping Westerschelde - deelrapport 1 - Classificatie op basis van bodemvormen en hydrodynamica,* Antwerpen: Waterbouwkundig Laboratorium.

Plancke, Y., Vos, G., Taveniers, E. & Mostaert, F., 2011. *Overleg Flexible Storten - T0 morfologie plaatranden,* Borgerhout: Waterbouwkundig Laboratorium.

Postma, H., 1954. Hydrography of the Dutch Wadden Sea. *Archives Néerlandaises de Zoologie,* Volume 13, pp. 405-511.

Pritchard, D. & Hogg, A. J., 2003. Cross-shore sediment transport and the equilibrium morphology of mudflats under tidal currents. *Journal of Geophysical Research,* C10(108), pp. 11-1 - 11-15.

Ridderinkhof, H., van der Ham, R. & van der Lee, W., 2000. Temporal variations in concentration and transport of suspended sediment in a channel-flat system in the Ems-Dollard estuary. *Continental Shelf Research,* Volume 20, pp. 1479-1493.

Rijkswaterstaat, 2012. *Presentation: Plaat van Walsoorden - Ontwikkelingen in de omgeving van de Plaat van Walsoorden,* s.l.: s.n.

Santermans, J., 2013. *LTV V&T rapport A31 - Achtergrondrapport Baggeren en Storten,* s.l.: Consortium Deltares, IMDC, Svašek, Arcadis.

Schroevers, M., 2013. *Stroming in de Westerschelde-Inventarisatie van de informatiebehoefte en informatievoorziening,* Delft: Deltares.

Soulsby, R., 1997. *Dynamics of marine sands.* 1st ed. London: Thomas Telford Publications.

Swinkels, C. M., Jeuken, C. M. C. J. L., Wang, Z. B. & Nicholls, R. J., 2009. Presence of Connecting Channels in the Westerns Scheldt Estuary. *Journal of Coastal Research,* 25(3), pp. 627-640.

Taal, M., Wang, Z. B. & Cleveringa, J., 2013. *LTV V&T rapport G13 - Synthese en conceptueel model,* s.l.: Consortium Deltares, IMDC, Svašek, Arcadis.

Tiessen, M., Vroom, J. & van der Werf, J., 2016. *Ontwikkeling van het Delft3D FM NeVla model voor het Schelde estuarium-Waterbeweging in de Westerschelde en stroming over de plaat van Walsoorden. 1220095-000-ZKS-0023,* Delft: Deltares.

Van der Werf, J. & Briere, C., 2013. *LTV V&T rapport G04: Influence morphology on tide and sand transport,* s.l.: Consortium Deltares, IMDC, Svašek, Arcadis.

van Leeuwen, B., 2013. *LTV V&T rapport G10 - Probleemanalyse zandwinning,* s.l.: Consortium Deltares, IMDC, Svašek, Arcadis.

Van Rijn, L. C., 2007. A Unified View of Sediment Transport by Currents and Waves Part 1: Initiation of Motion, Bed Roughness and Bed-Load Transport. *Journal of Hydraulic Engineering,* 6(133), pp. 649-667.

van Straaten, L. & Kuenen, P., 1957. Accumulation of fine grained sediments in the Dutch Wadden Sea. *Netherlands Journal Of Geosciences,* 19(3), pp. 29-54.

Vandenbruwaene, W., Vos, G., Plancke, Y. & Mostaert, F., 2012. *Werkgroep O&M - Projectgroep Veiligheid en Toegankelijkheid: Onderzoek naar de morfologie op meso-schaal ter hoogt van stortlocaties,* Antwerpen: Waterbouwkundig laboratorium.

Vanlede, J; Delecluyse, K; Primo, B; Verheyen, B; Leyssen, G; Plancke, Y; Verwaest, T; Mostaert, F

Vanlede, J. Delecluyse, K. Primo, B. Verheyen, B. Leyssen, G. Plancke, Y. Verwaest, T. Mostaert, F., 2015. *Verbetering randvoorwaardenmodel - Subreport 7 - Calibration of NEVLA 3D,* Antwerp: Flanders Hydraulic Research & IMDC.

VNSC, 2015. *http://www.vnsc.eu/.* [Online]
Available at: http://www.vnsc.eu/projecten/derde-verruiming-van-de-schelde/
[Accessed 15 January 2016].

VNSC, 2015. *www.vnsc.eu.* [Online]
Available at: http://www.vnsc.eu/projecten/flexibel-storten/
[Accessed 9 March 2016].

Vroom, J., de Vet, L. & van der Werf, J., 2015. *Validatie waterbeweging Delft3D-NeVla model Westerschelde monding ,* Delft: Deltares.

Wang, Z. B. Jeuken, M.C.J.L. Gerritsen, de Vriend, H.J. Kornman, B.A., 2002. Morphology and assymetry of the vertical tide in the Westerschelde estuary. *Continental shelf reasearch,* pp. 2599-2609.

Wang, Z. B. & Winterwerp, J. C., 2001. *Impact of dredging and dumping on the stability of ebb-flood channel system.* Obihiro,Japan, Proceedings of the 2nd IAHR symposium on River, Coastal and Estuarine Morphodynamics, pp. 515-524.

Waterbouwkundig laboratorium (WLB), 2006. *Alternatieve stortstrategie Westerschelde - proefstorting Walsoorden eindevaluatie monitoring,* Borgerhout: WLB.

Waterbouwkundig laboratorium (WLB), 2007. *M754/2B Alternatieve stortstrategie Westerschelde – Verslag 13u meetcampagnes Walsoorden,* Borgerhout: WLB.

Istitute fur Wasserbau, 2003. *Current measurements in the Westerschelde – September and October 2002,* s.l.: s.n.

Winterwerp, J.C. Wang, Z.B. Stive, M.J.F. Arends, A. Jeuken, C. Kuijper, C. Thoolen, P.M.C., 2001. *A new morphological schematization of the Western Scheldt estuary, the Netherland.* s.l., s.n., pp. 525-533.

APPENDICES

A. MORPHOLOGICAL DEVELOPMENT OF INTERTIDAL SHOAL WALSOORDEN AFTER THE SEDIMENT DISPOSAL

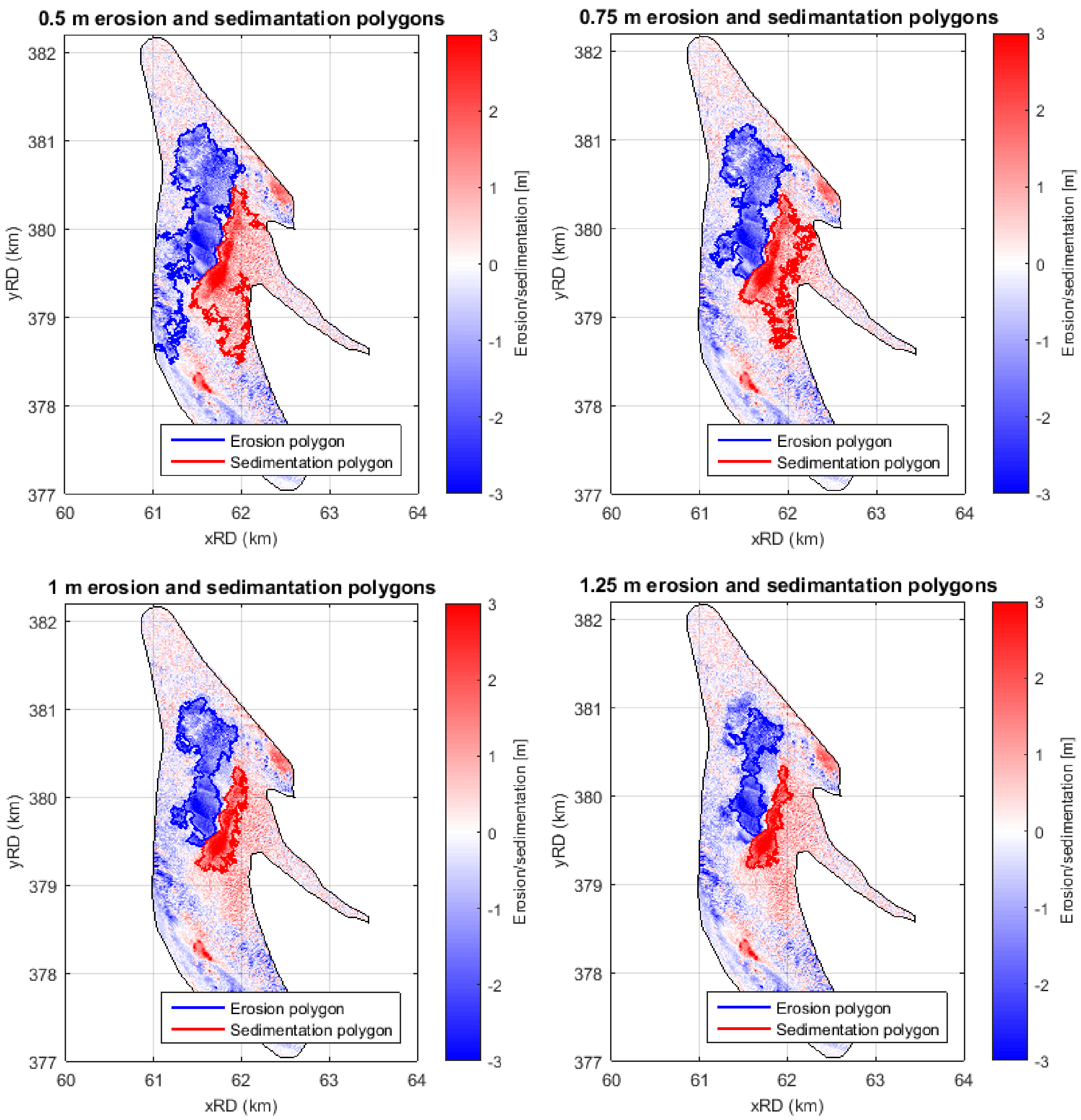

Figure A- 1 Erosion – and sedimentation contour lines for 0.5 m - (top left), 0.75 m - (top right), 1.0 m - (bottom left) and 1.25 m (bottom right) differences

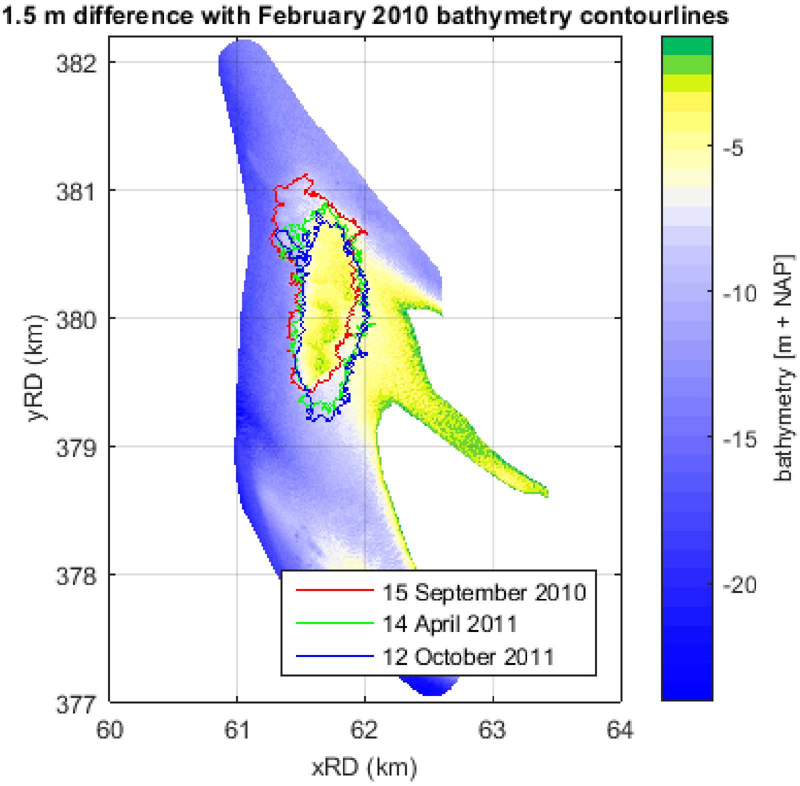

Figure A- 2 Contour lines that indicate a difference in bathymetry that is larger than 1.5 m compared to the February 2010 bathymetry displayed on a September 2010 bathymetry.

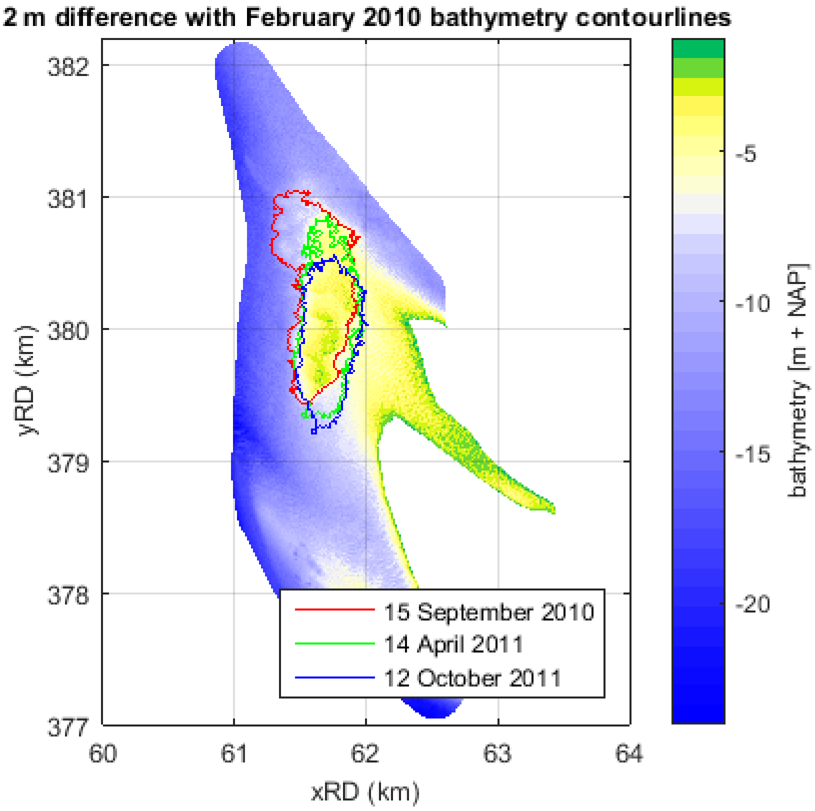

Figure A- 3 Contour lines that indicate a difference in bathymetry that is larger than 1.5 m compared to the February 2010 bathymetry displayed on a September 2010 bathymetry.

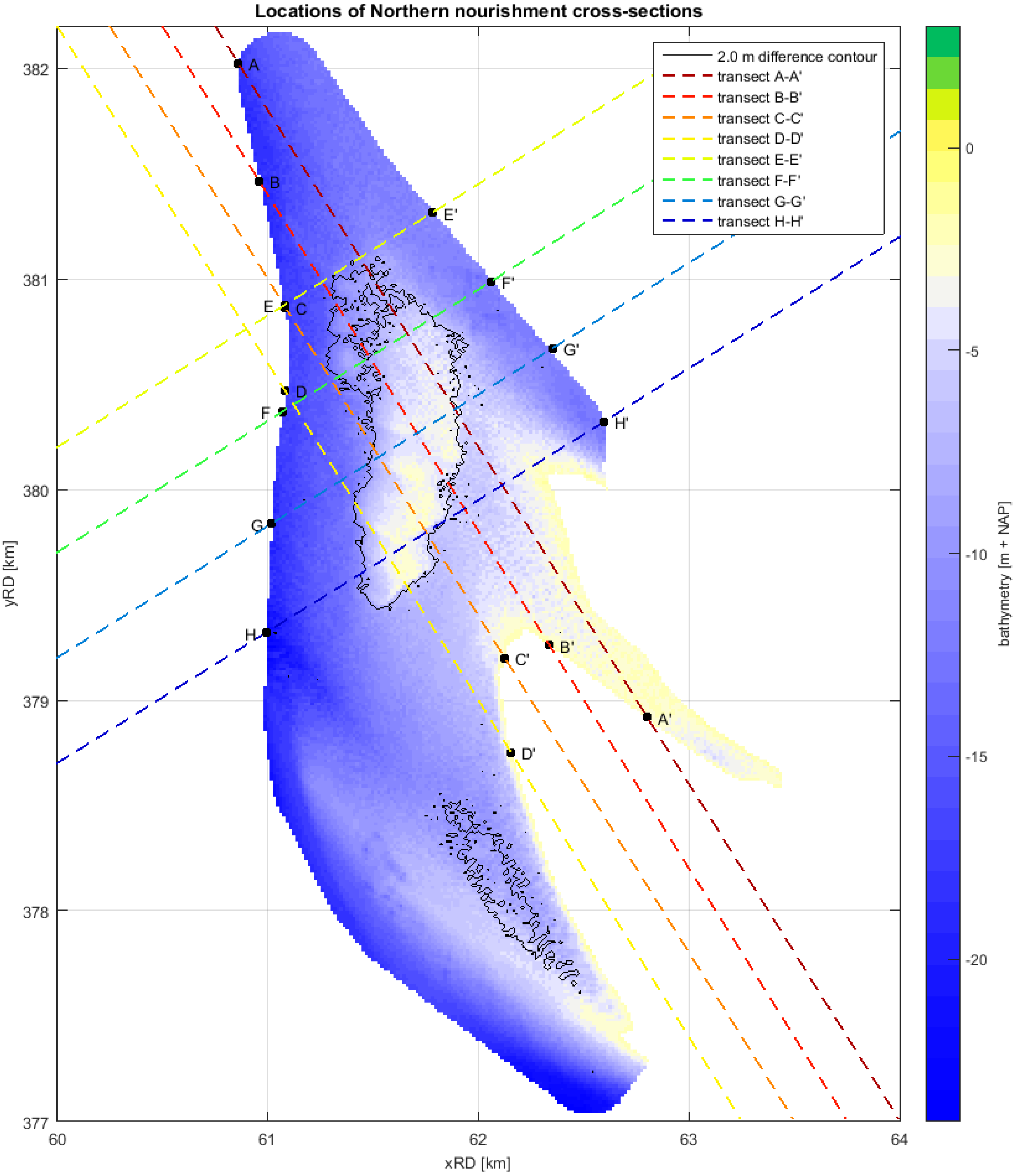

Figure A- 4 Overview of the locations of the cross-sections at the northern sand nourishment plotted on September 2010 bathymetry. The 2.0 m difference contour indicates the difference with the February 2010 bathymetry.

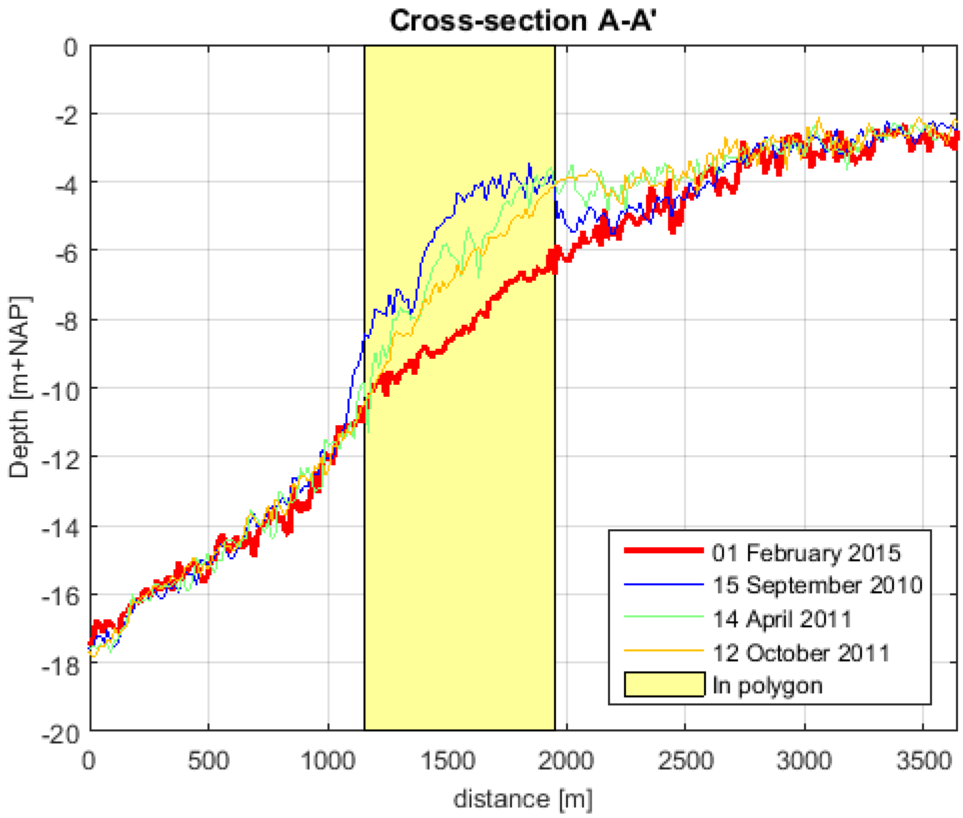

Figure A- 5 Morphological development of cross-section A-A

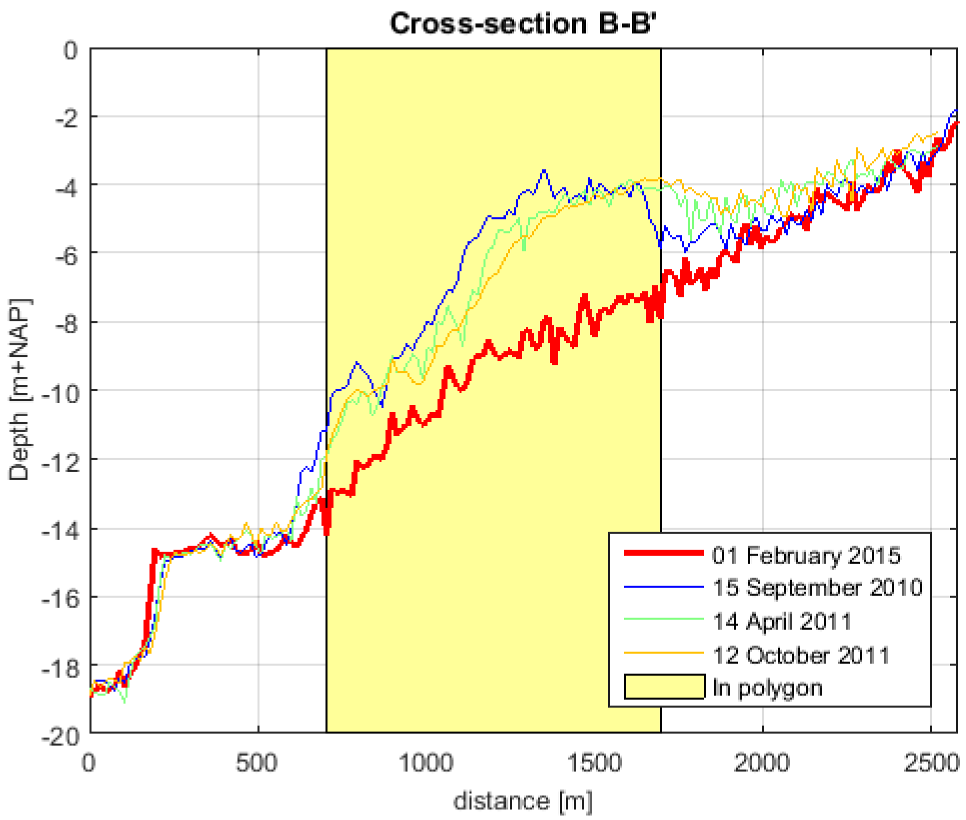

Figure A- 6 Morphological development of cross-section B-B’

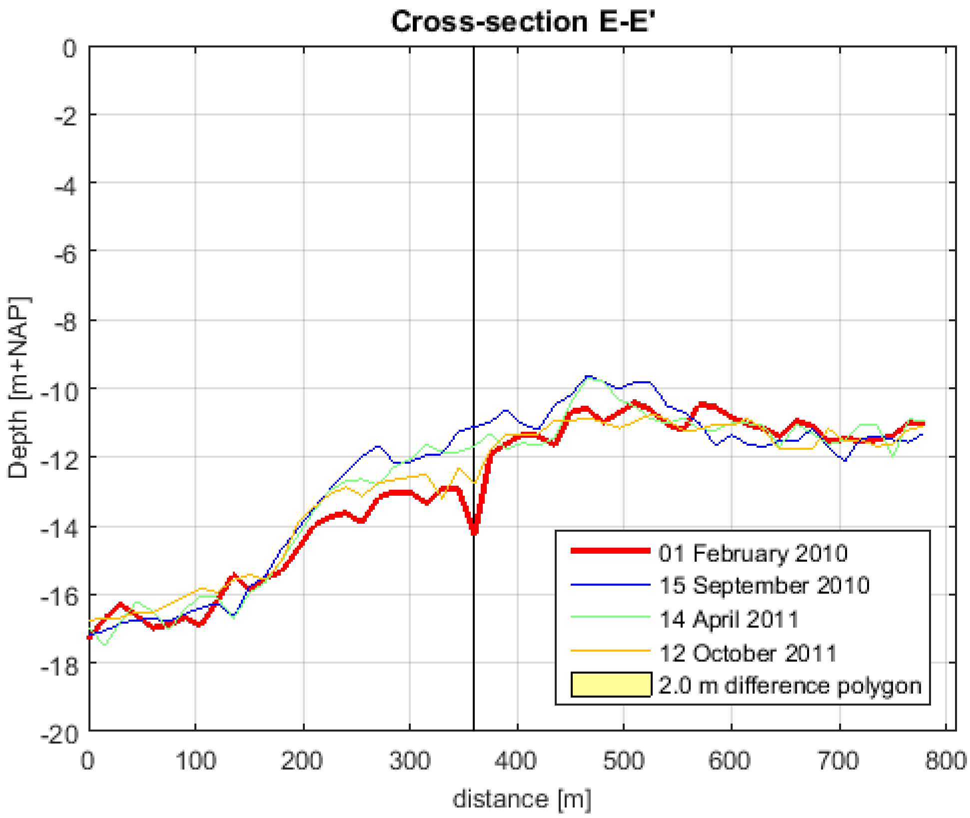

Figure A- 7 Morphological development of cross-section E-E'

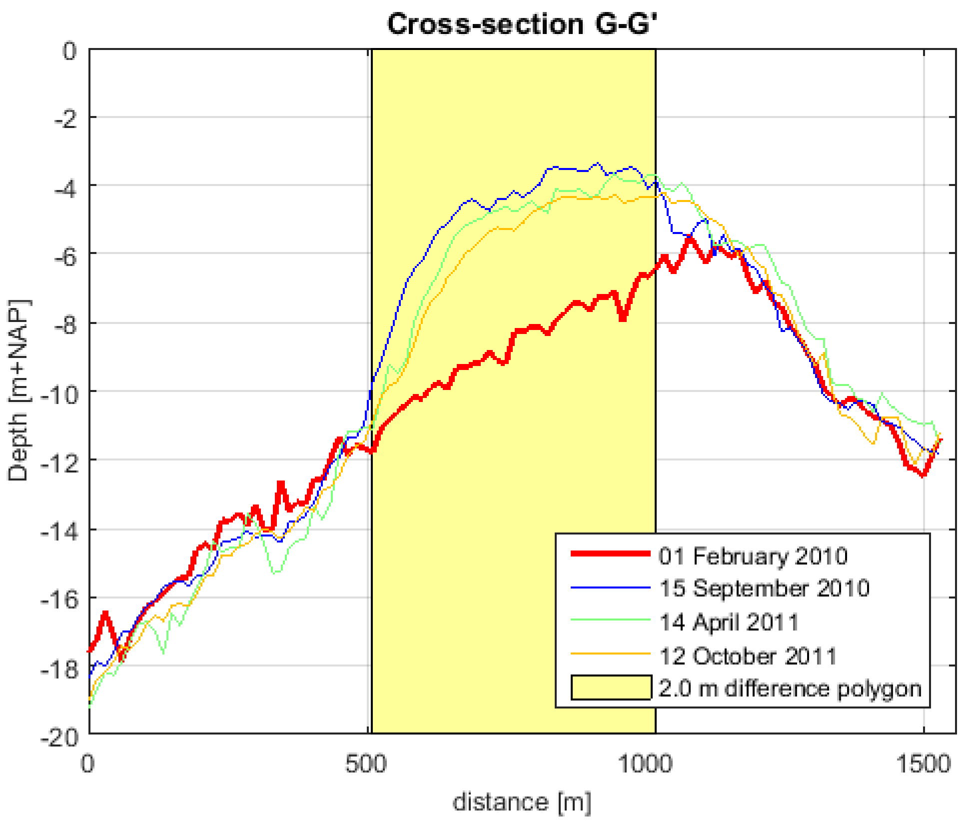

Figure A- 8 Morphological development of cross-section G-G'

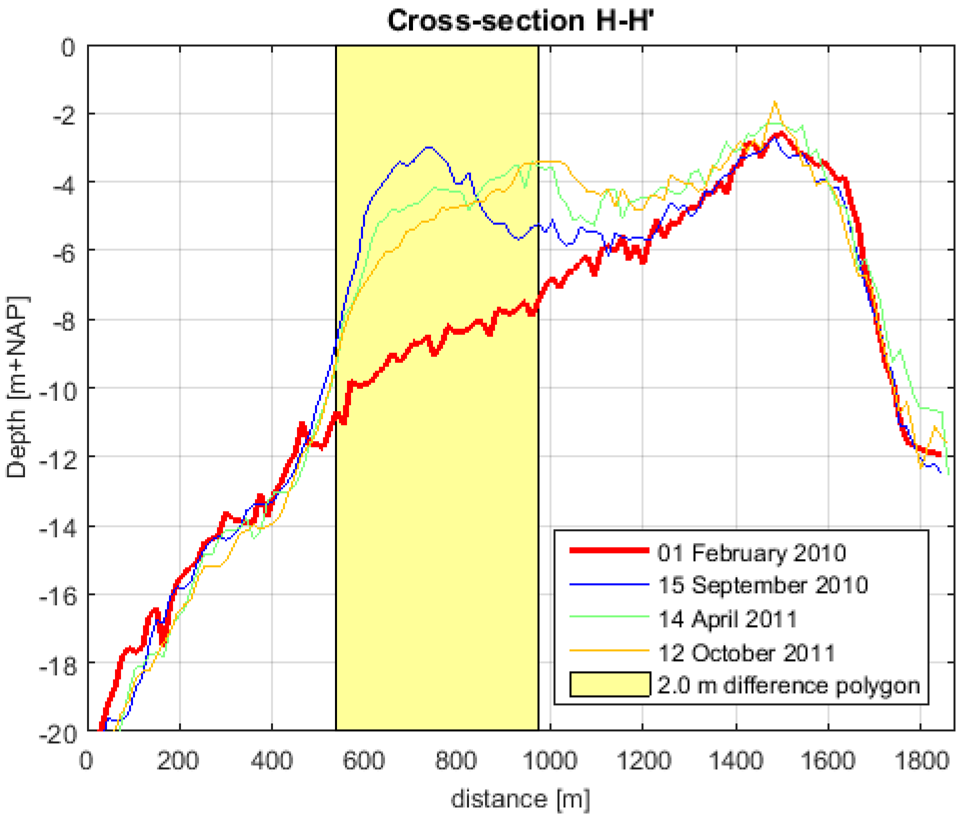

Figure A- 9 Morphological development of cross-section H-H'

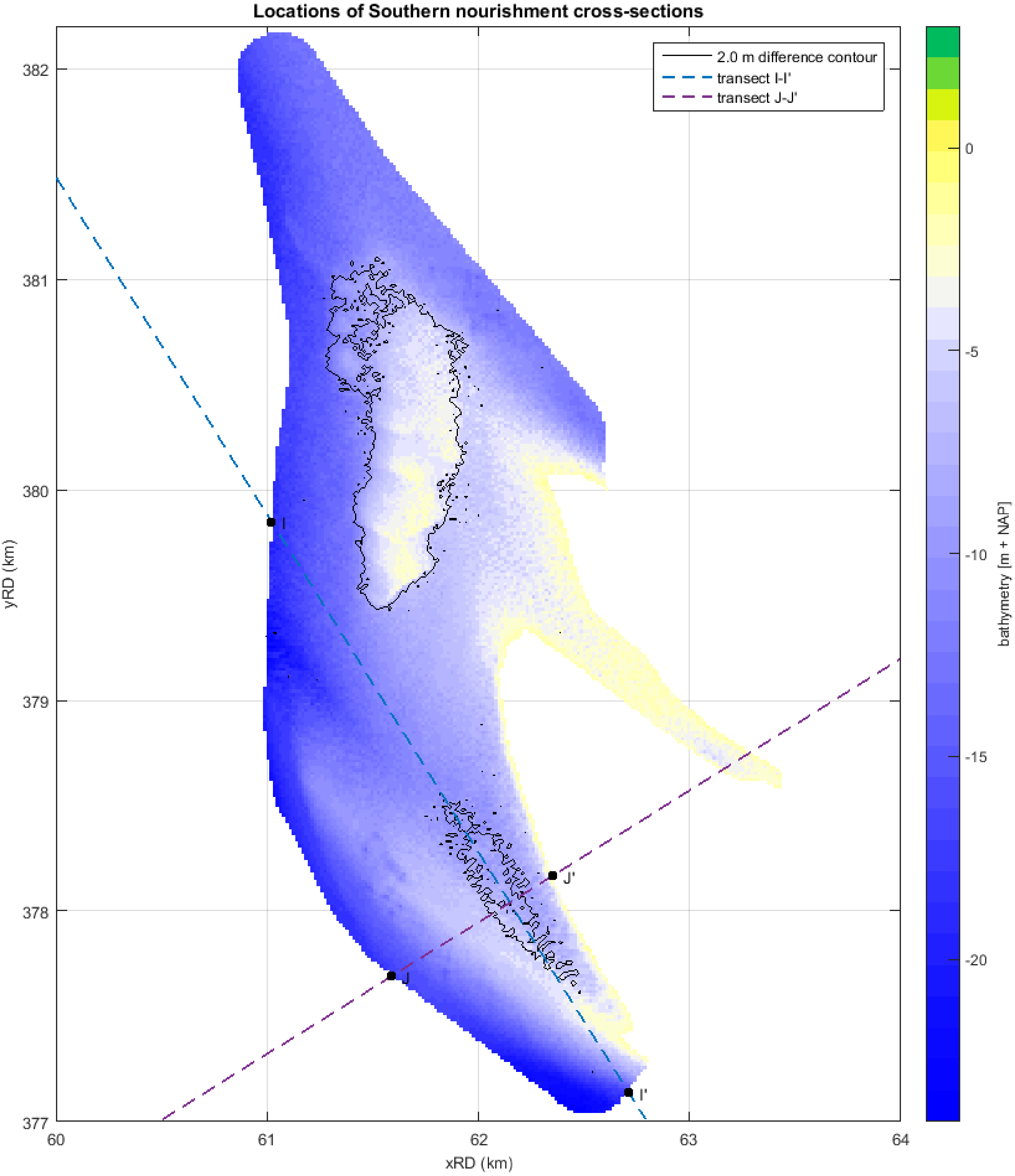

Figure A- 10 Overview of the locations of the cross-sections at the southern sand nourishment.

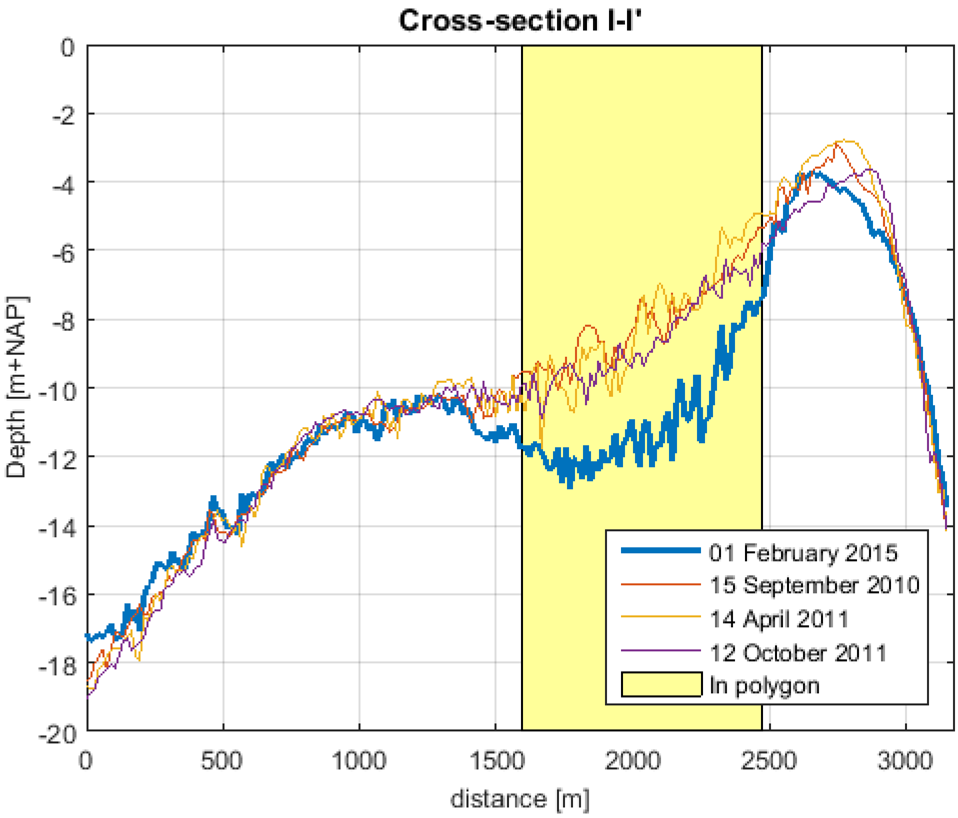

Figure A- 11 Morphological development of cross-section I-I’

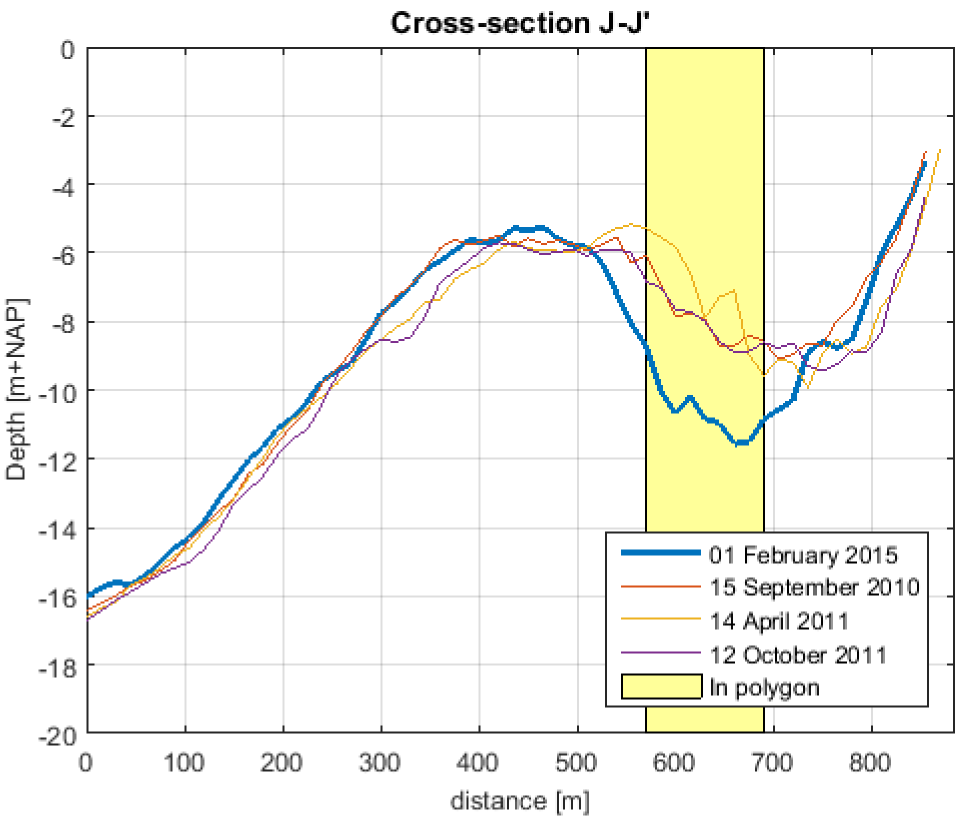

Figure A- 12 Morphological development of cross-section J-J’

B. SUPPLEMENTARY MODEL RESULTS IN SPACE

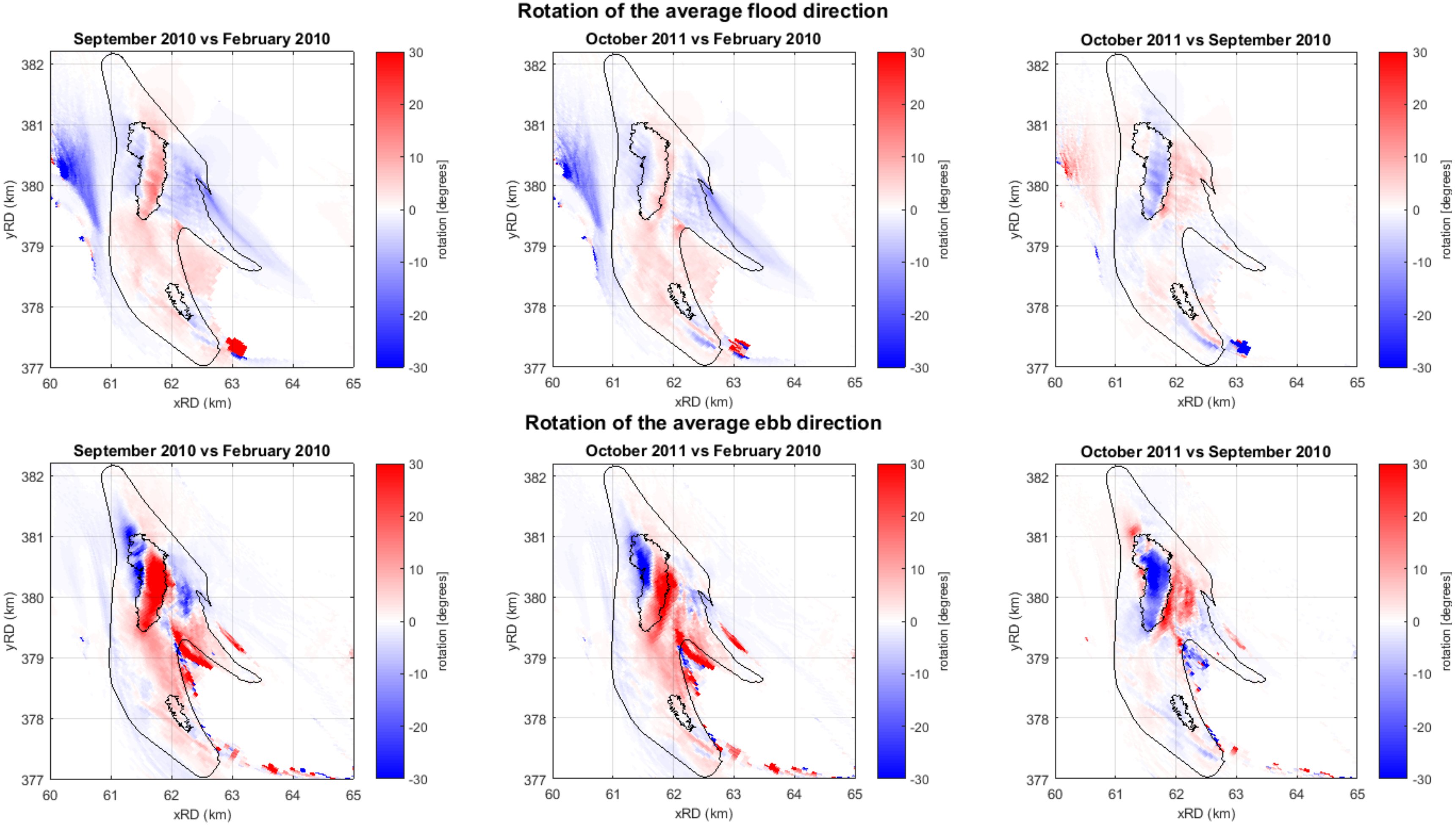

Figure B - 1Difference in average flood - (top) and ebb directions (bottom) between the three model simulations with the counter clockwise direction being the positive angular displacement

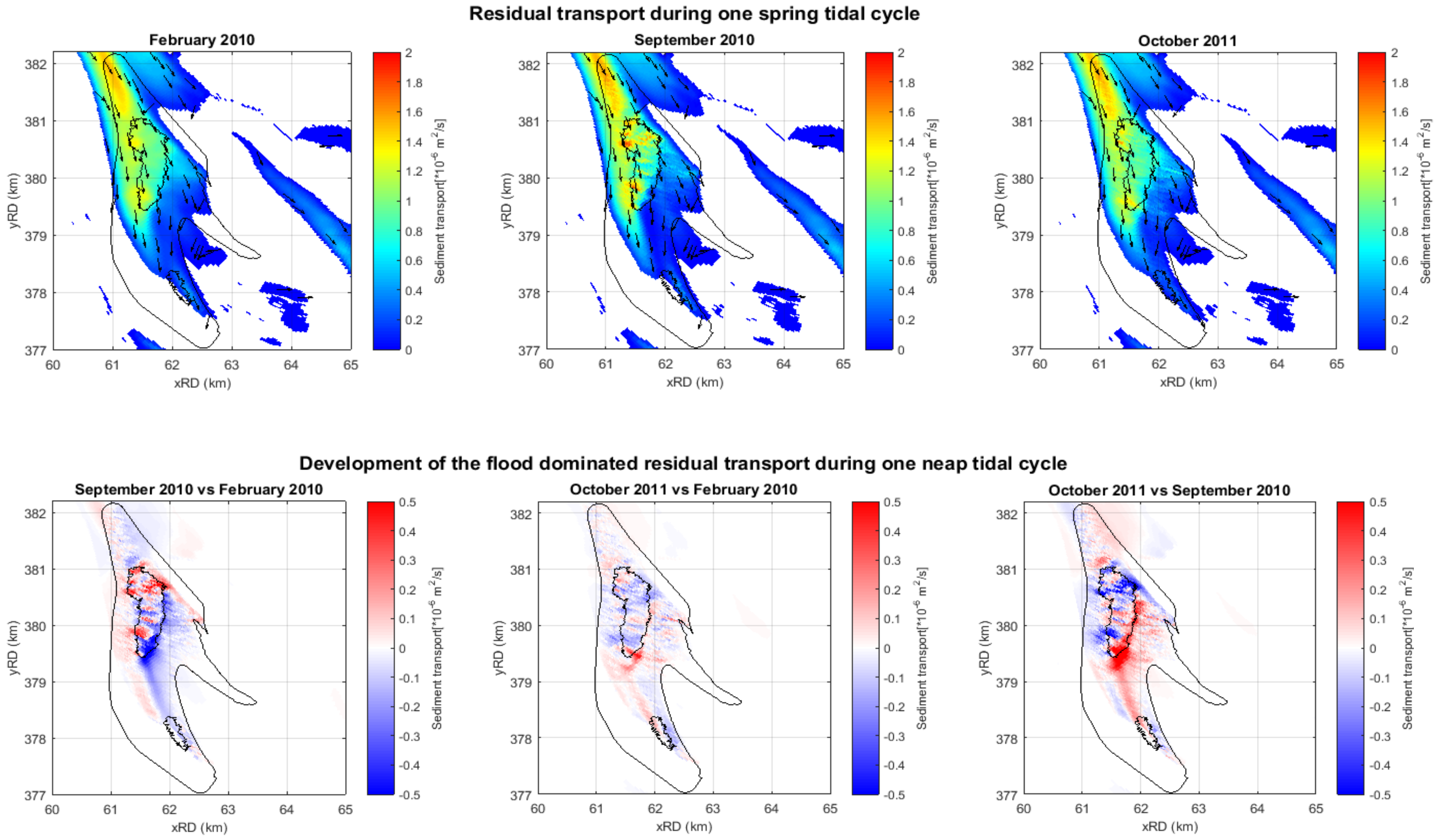

Figure B - 2 Flood dominated residual transport during neap tide for the three model simulations (top) and their differences (bottom)

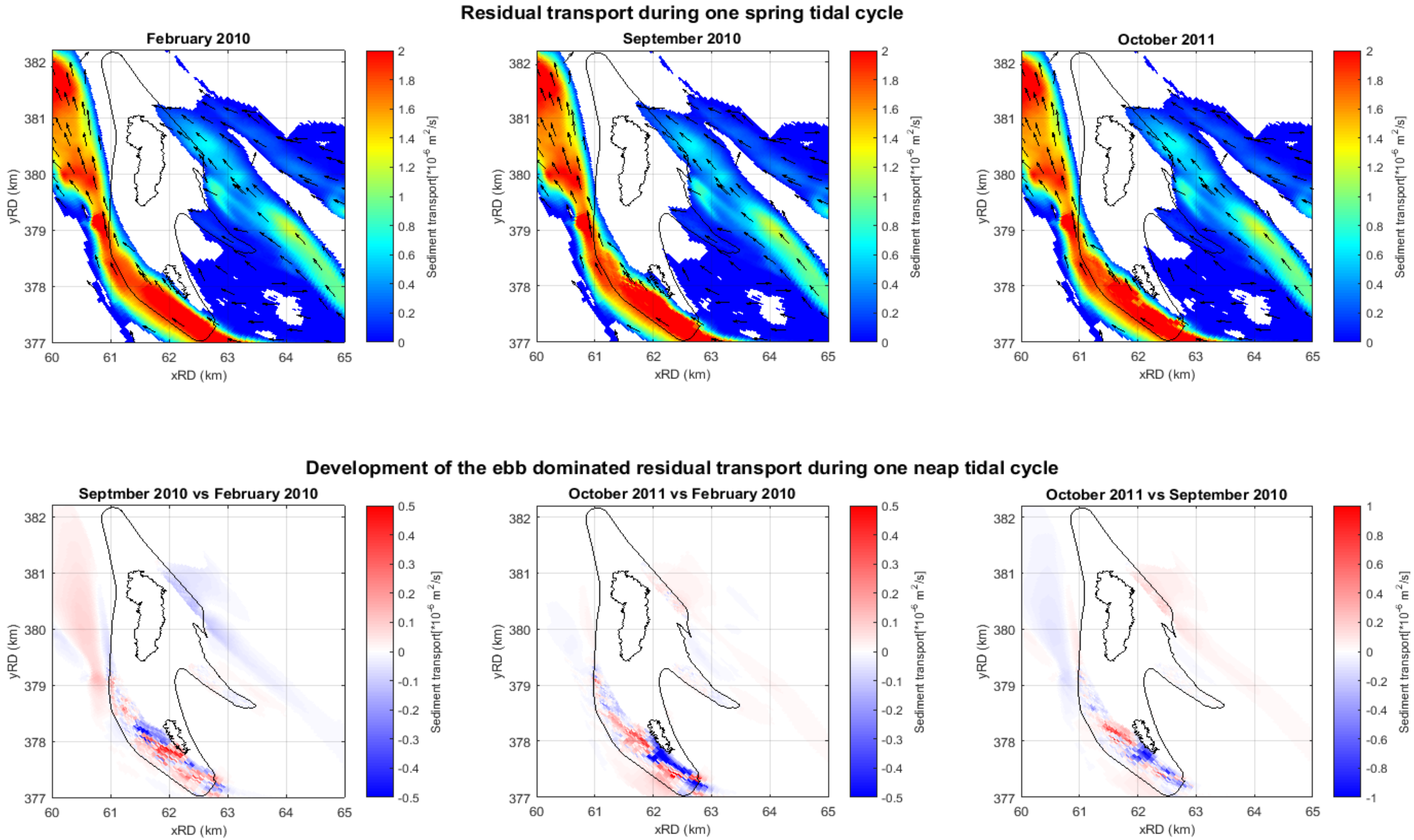

Figure B - 3Ebb dominated residual transport during neap tide for the three model simulations (top) and their differences (bottom)

C. MORPHODYNAMIC CONTROL POINTS

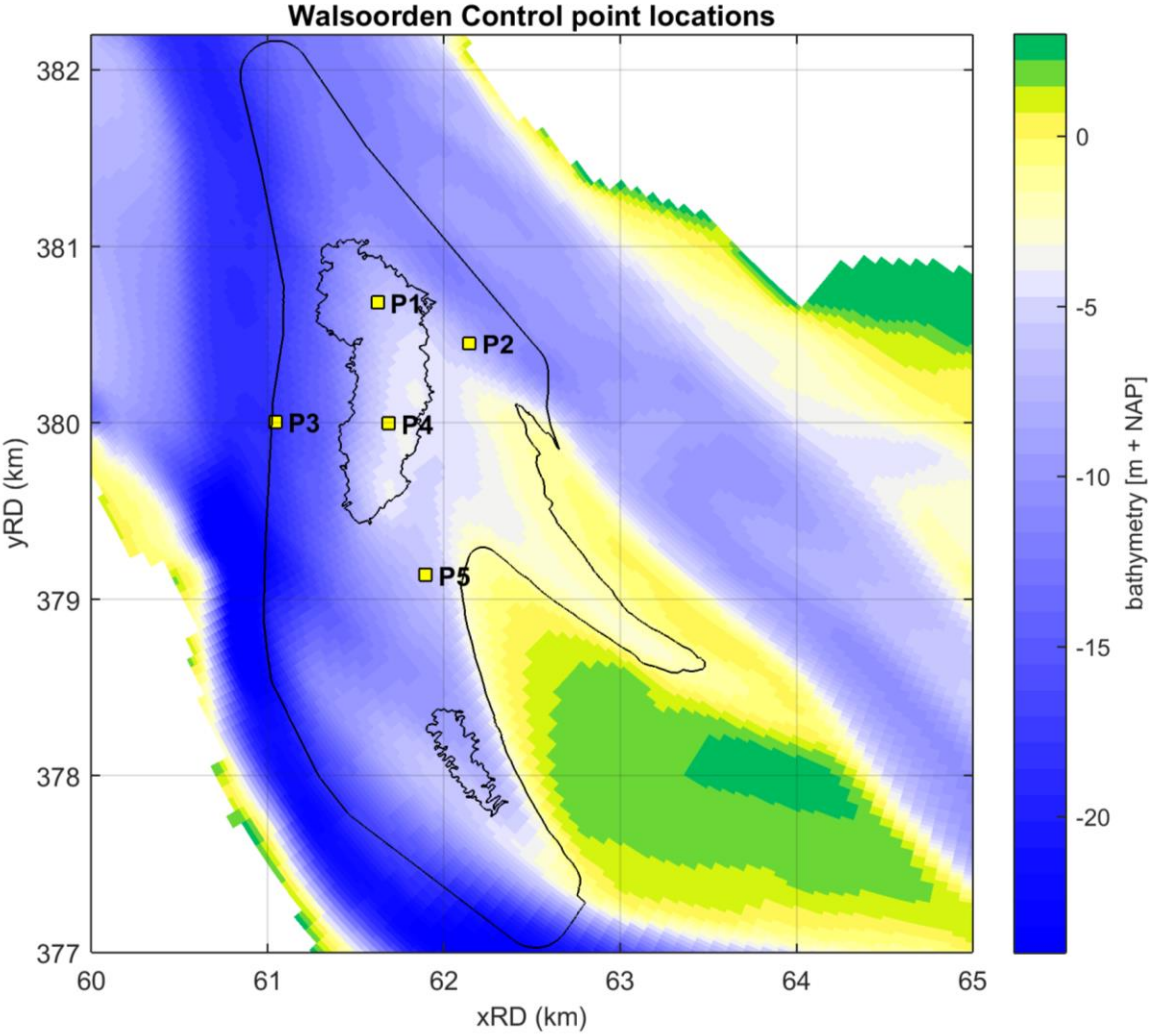

Figure D- 1 Locations of the five control points for which the water levels, flow velocities and sediment transport during a spring tidal cycle and neap tidal cycle are analysed.

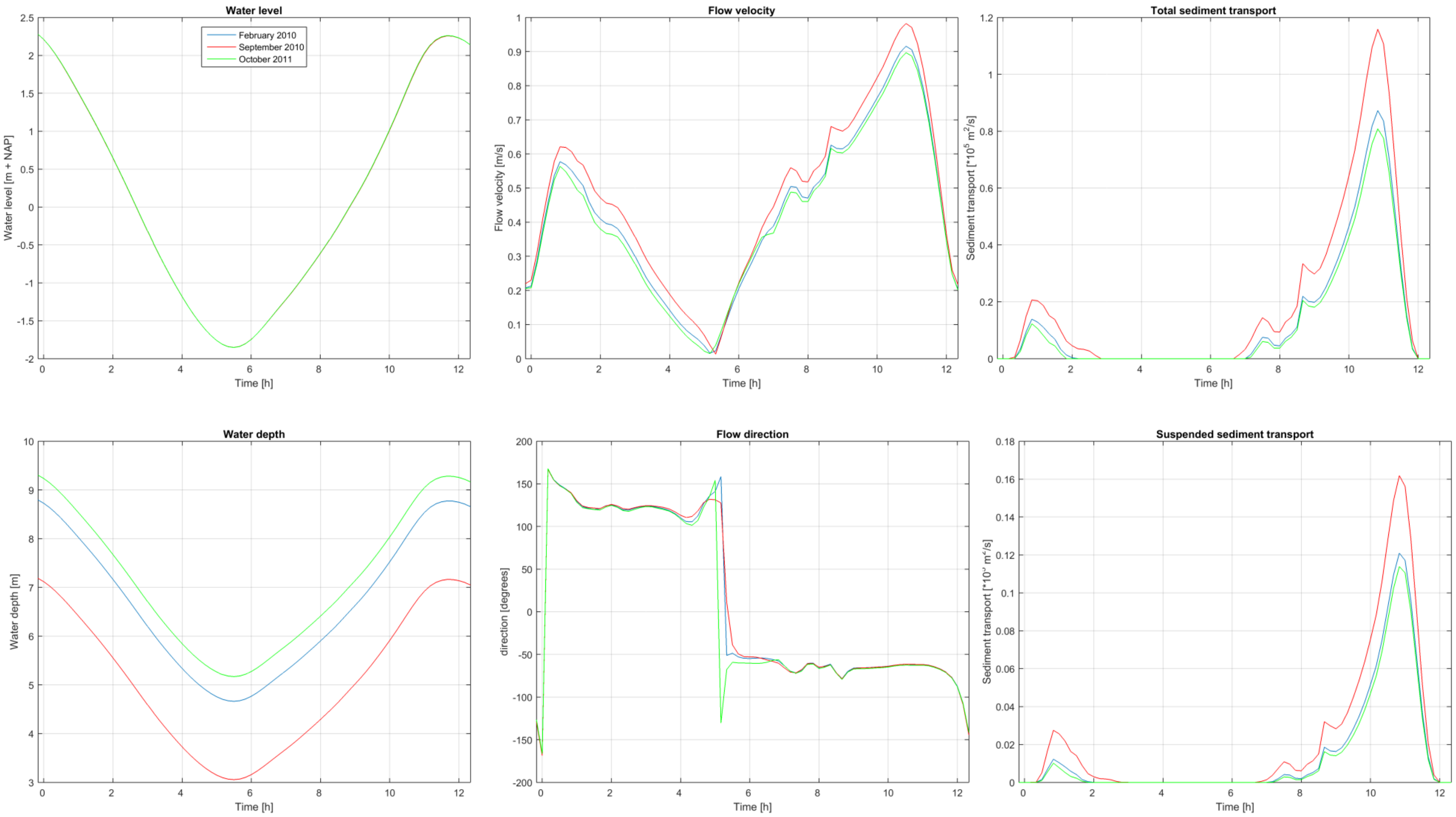

Figure D- 2 Water level (top left), water depth (bottom left), flow velocity (top middle), flow direction (bottom middle), total sediment transport (top right) and suspended sediment transport for control point 1 during neap tide

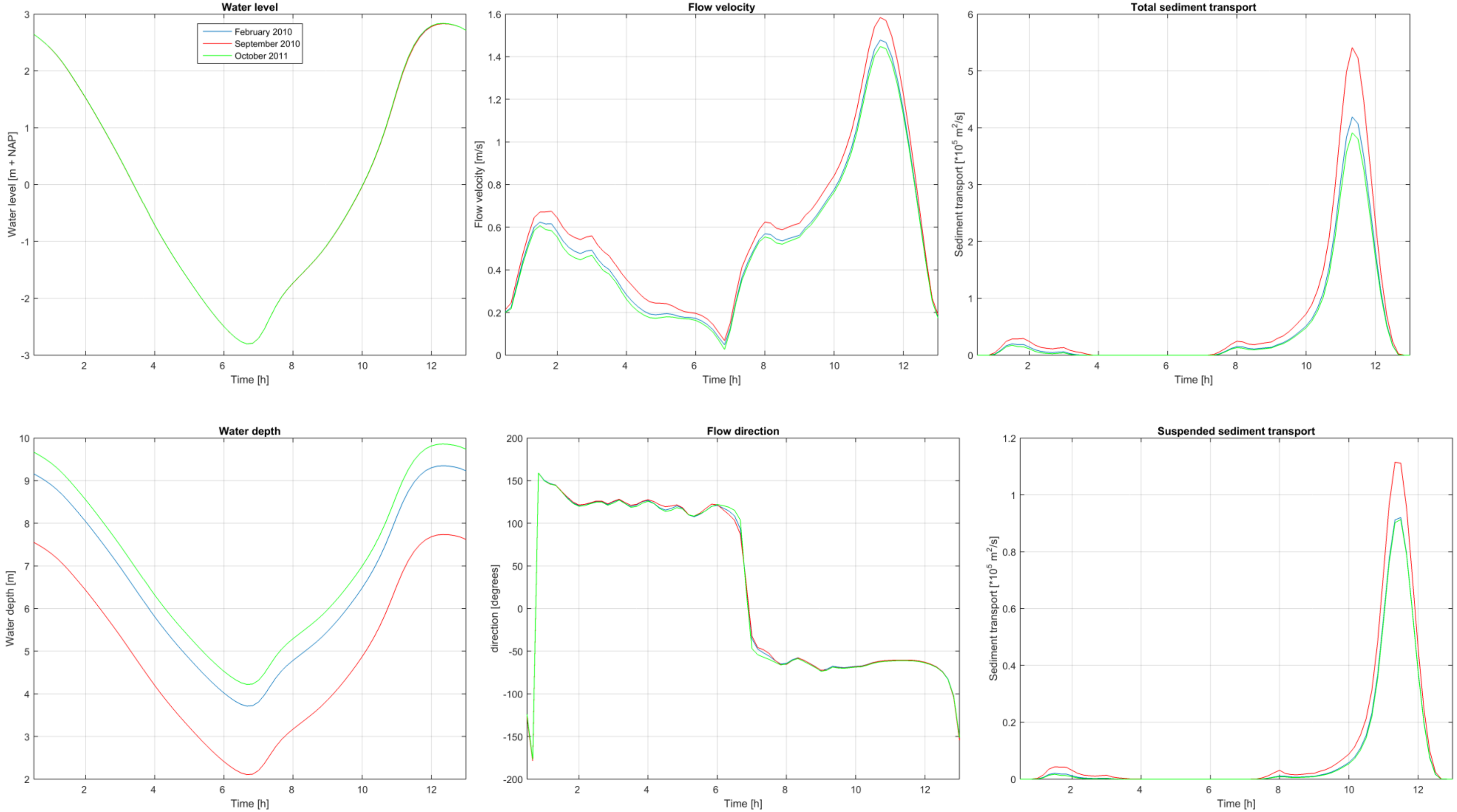

Figure D- 3 Water level (top left), water depth (bottom left), flow velocity (top middle), flow direction (bottom middle), total sediment transport (top right) and suspended sediment transport for control point 1 during spring tide

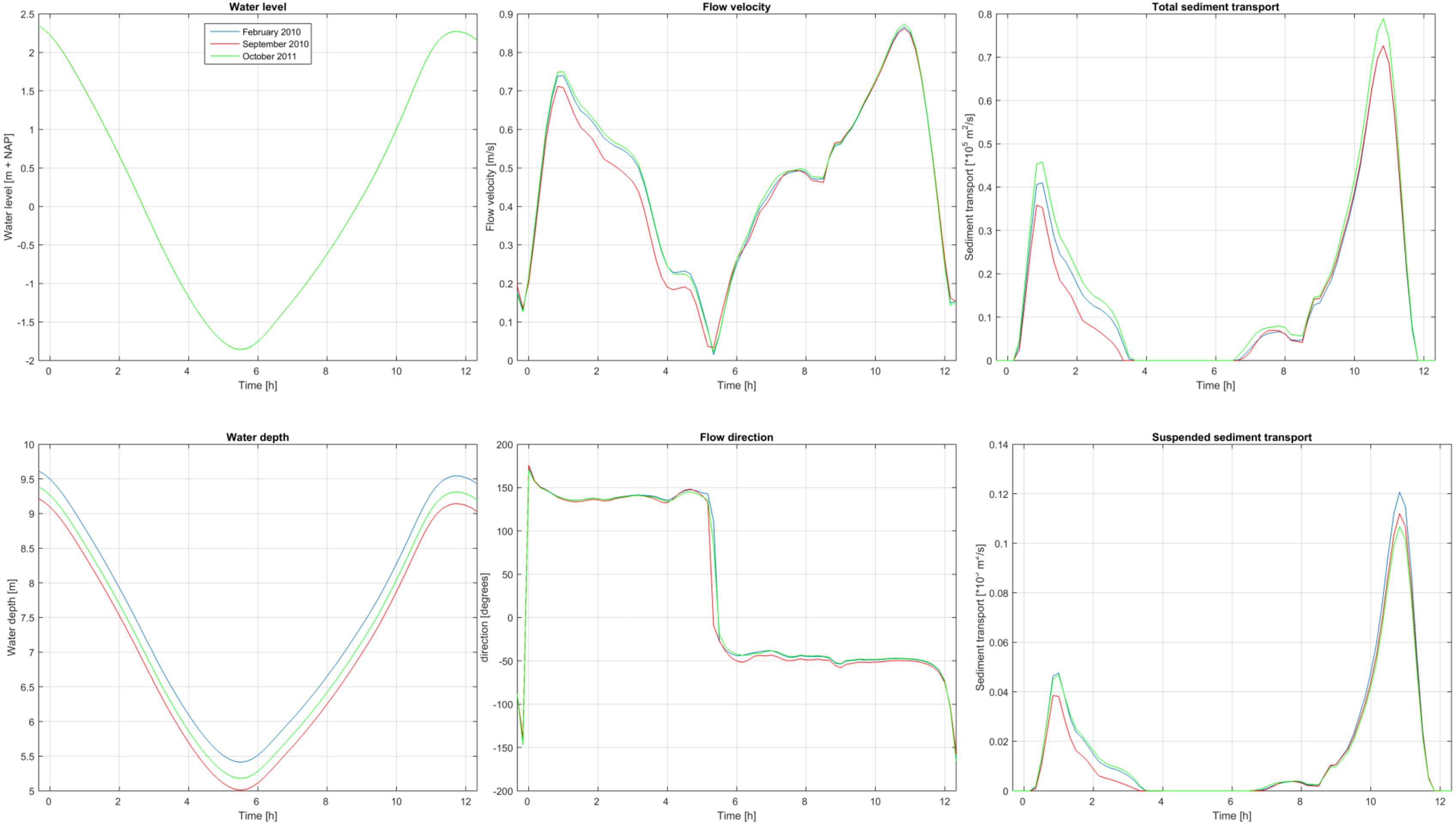

Figure D- 4 Water level (top left), water depth (bottom left), flow velocity (top middle), flow direction (bottom middle), total sediment transport (top right) and suspended sediment transport for control point 2 during neap tide

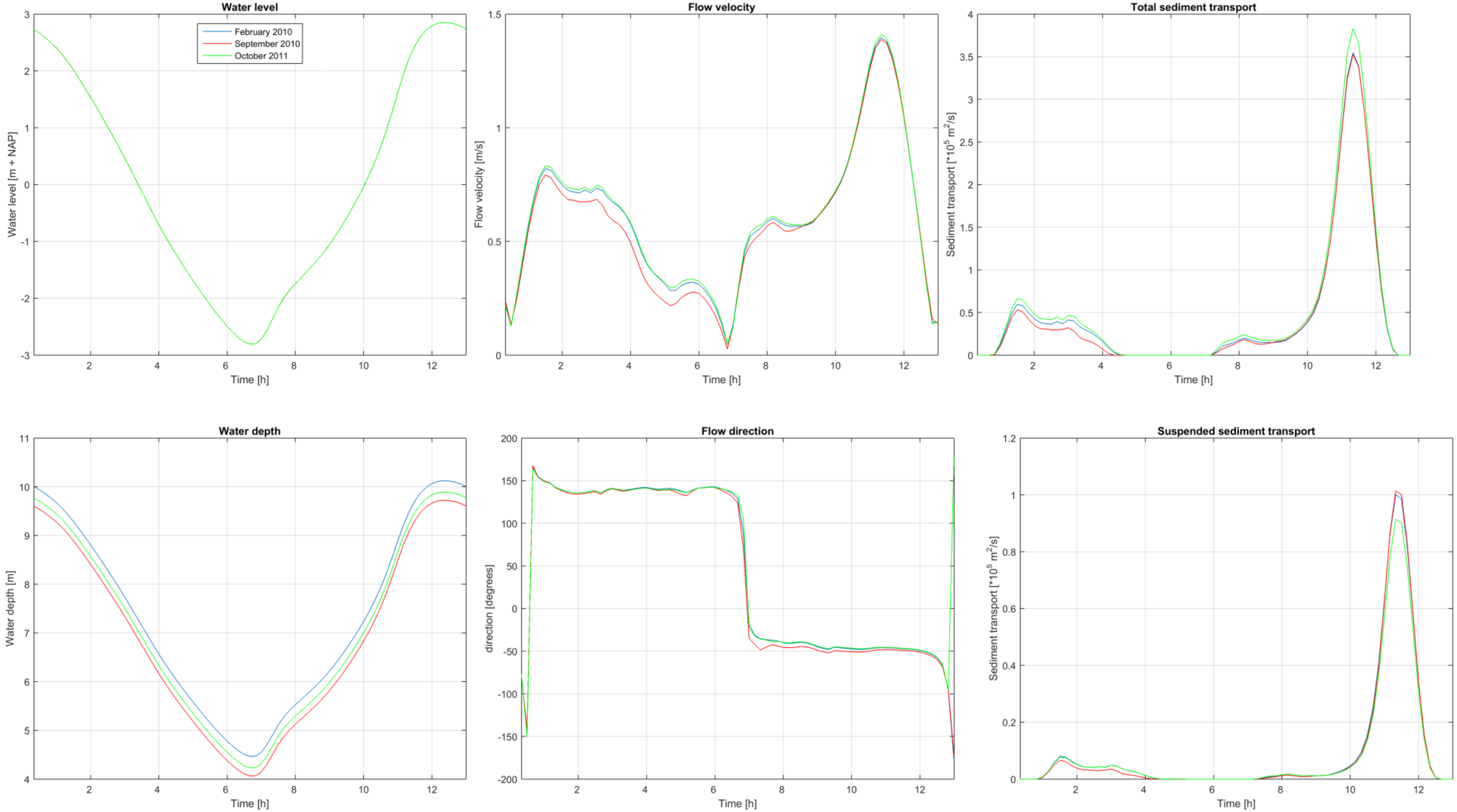

Figure D- 5 Water level (top left), water depth (bottom left), flow velocity (top middle), flow direction (bottom middle), total sediment transport (top right) and suspended sediment transport for control point 2 during spring tide

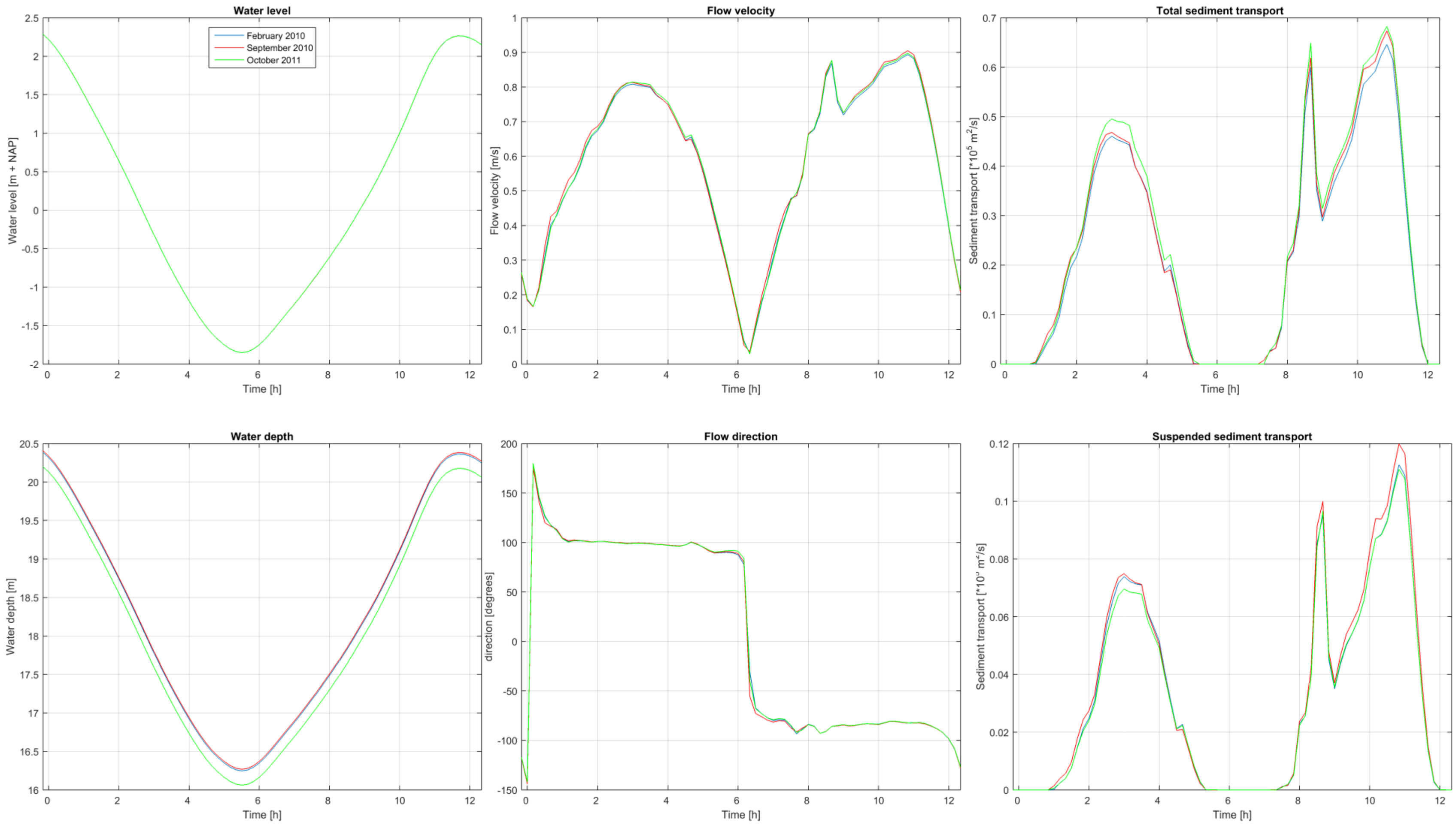

Figure D- 6 Water level (top left), water depth (bottom left), flow velocity (top middle), flow direction (bottom middle), total sediment transport (top right) and suspended sediment transport for control point 3 during neap tide

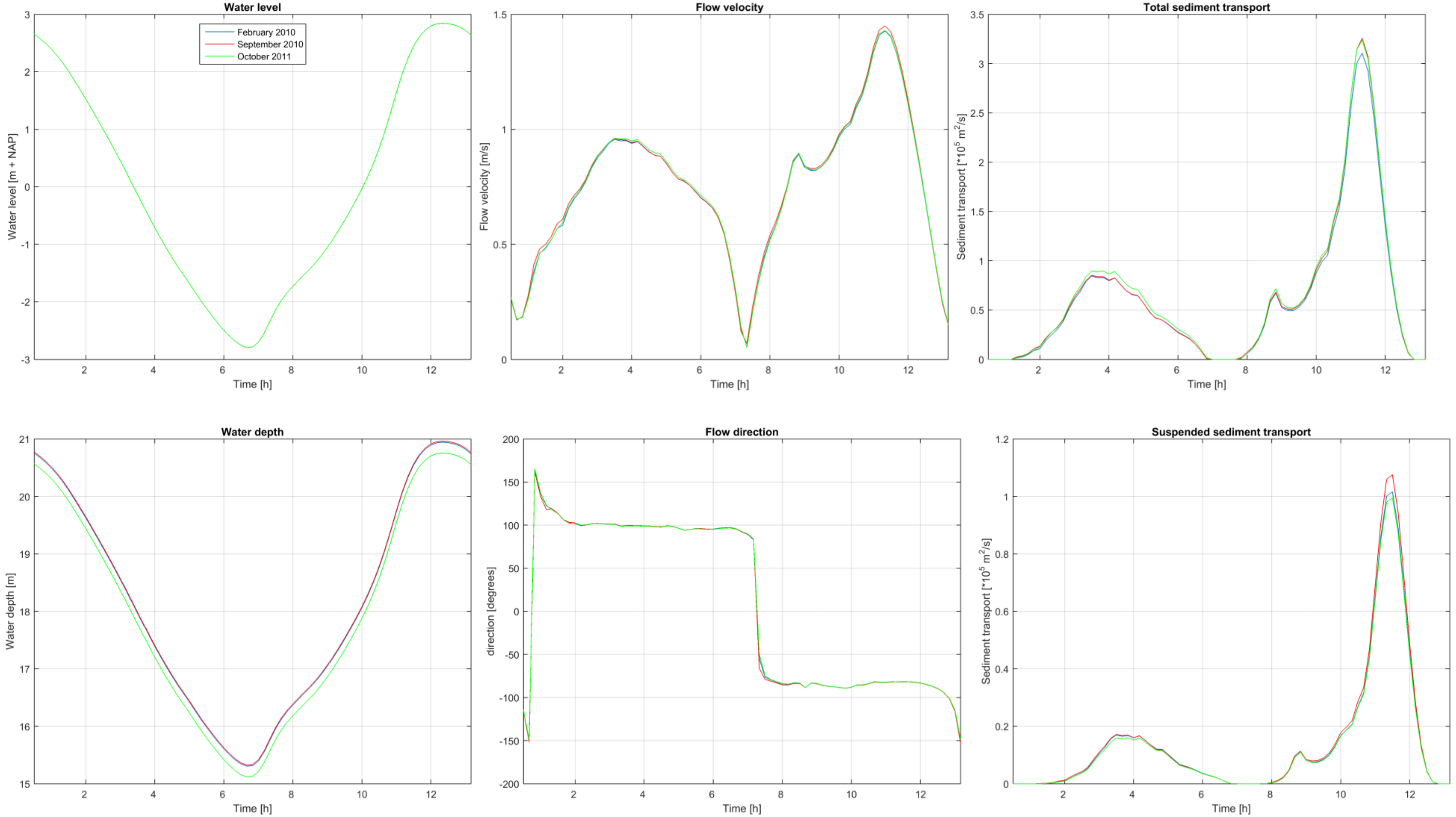

Figure D- 7 Water level (top left), water depth (bottom left), flow velocity (top middle), flow direction (bottom middle), total sediment transport (top right) and suspended sediment transport for control point 3 during spring tide

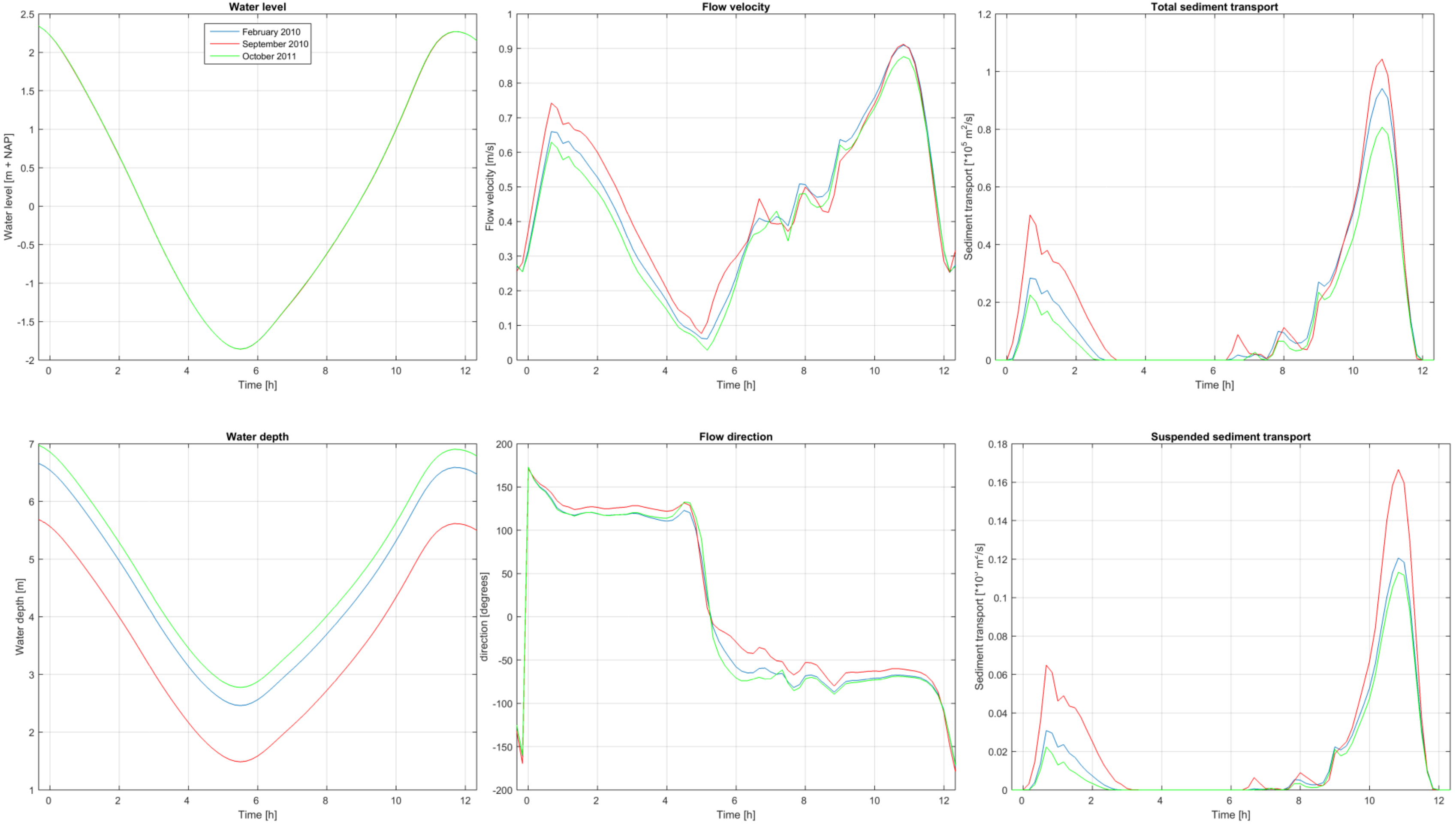

Figure D- 8 Water level (top left), water depth (bottom left), flow velocity (top middle), flow direction (bottom middle), total sediment transport (top right) and suspended sediment transport for control point 4 during neap tide

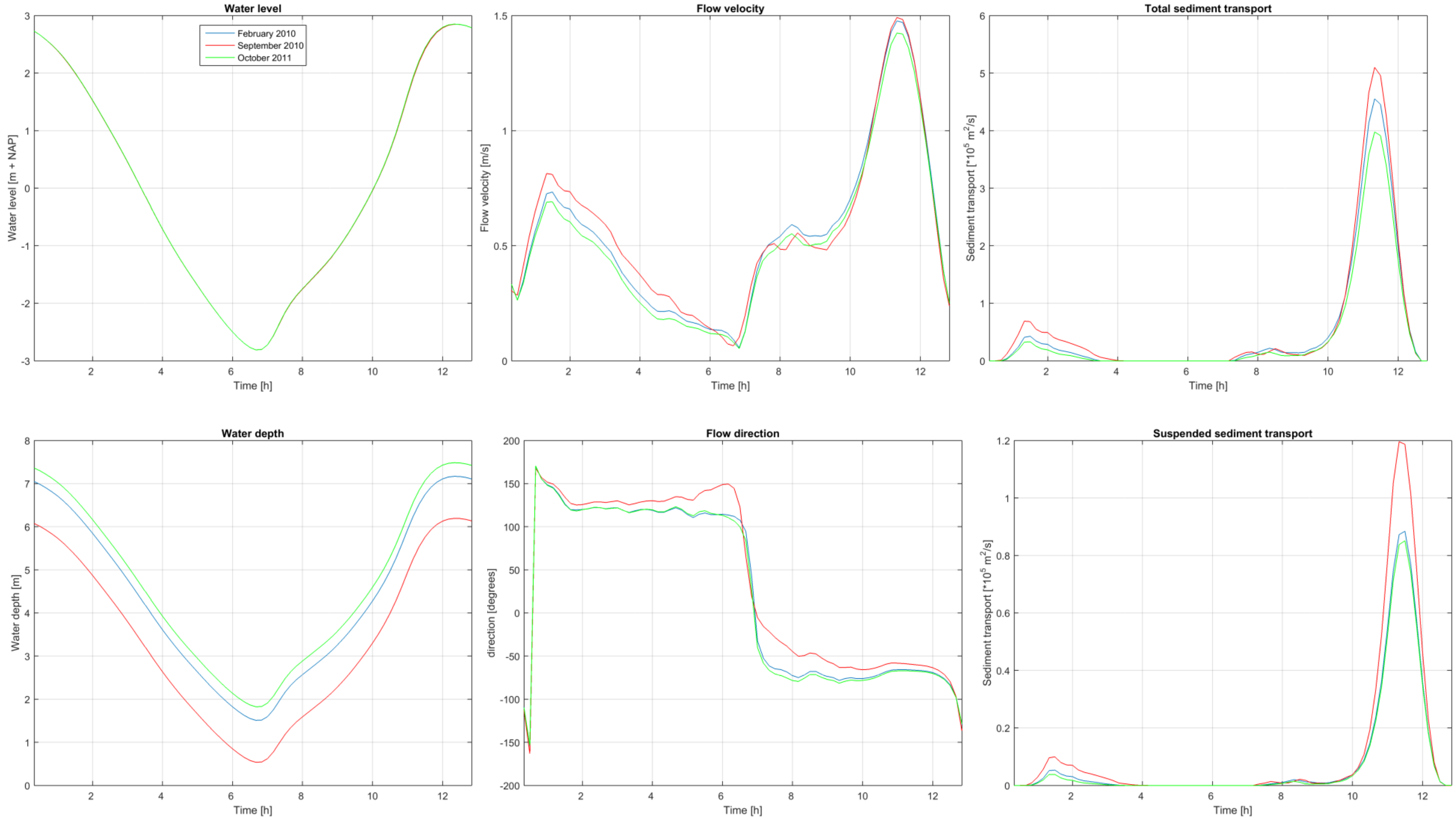

Figure D- 9 Water level (top left), water depth (bottom left), flow velocity (top middle), flow direction (bottom middle), total sediment transport (top right) and suspended sediment transport for control point 4 during spring tide

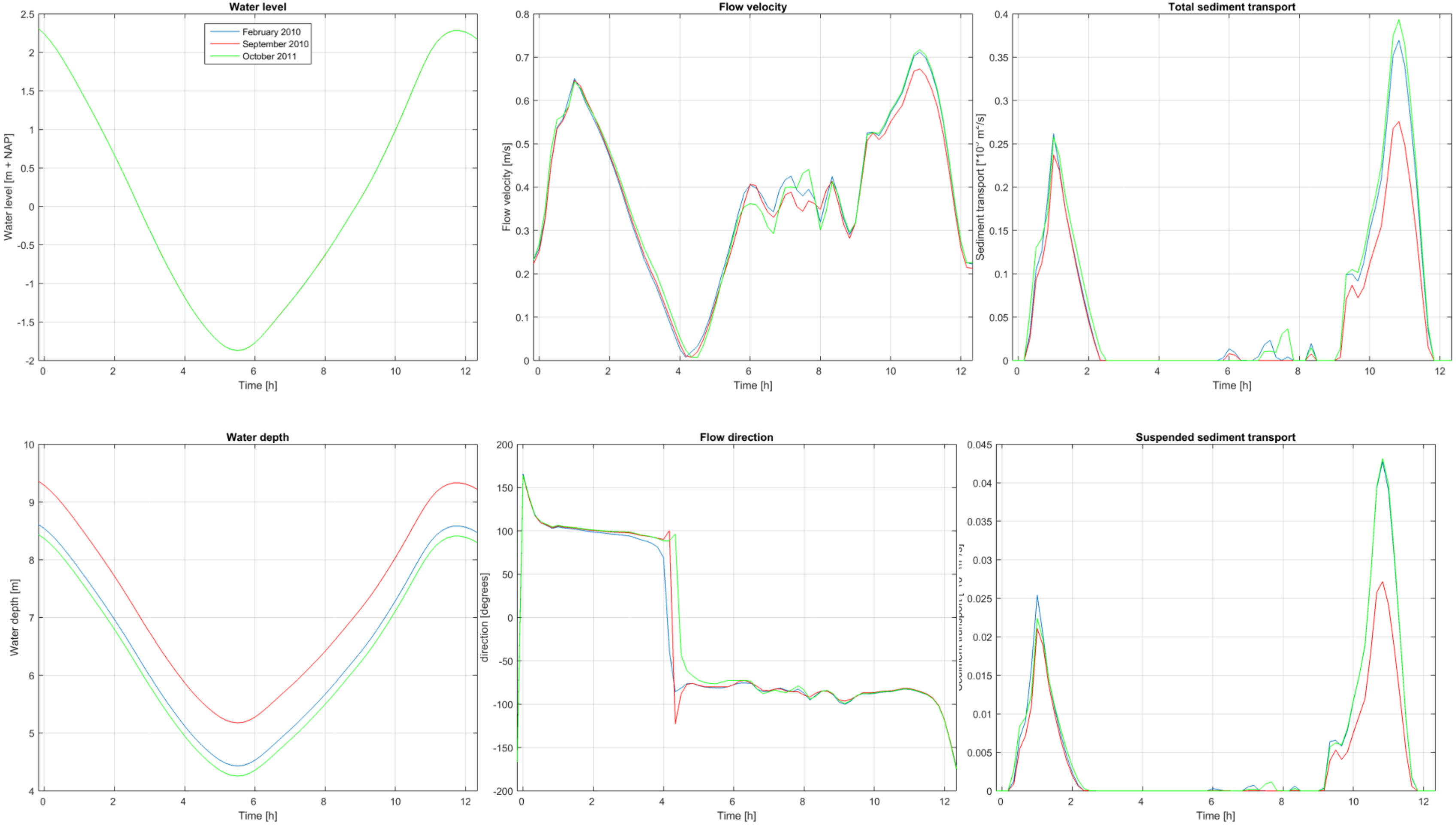

Figure D- 10 Water level (top left), water depth (bottom left), flow velocity (top middle), flow direction (bottom middle), total sediment transport (top right) and suspended sediment transport for control point 5 during neap tide

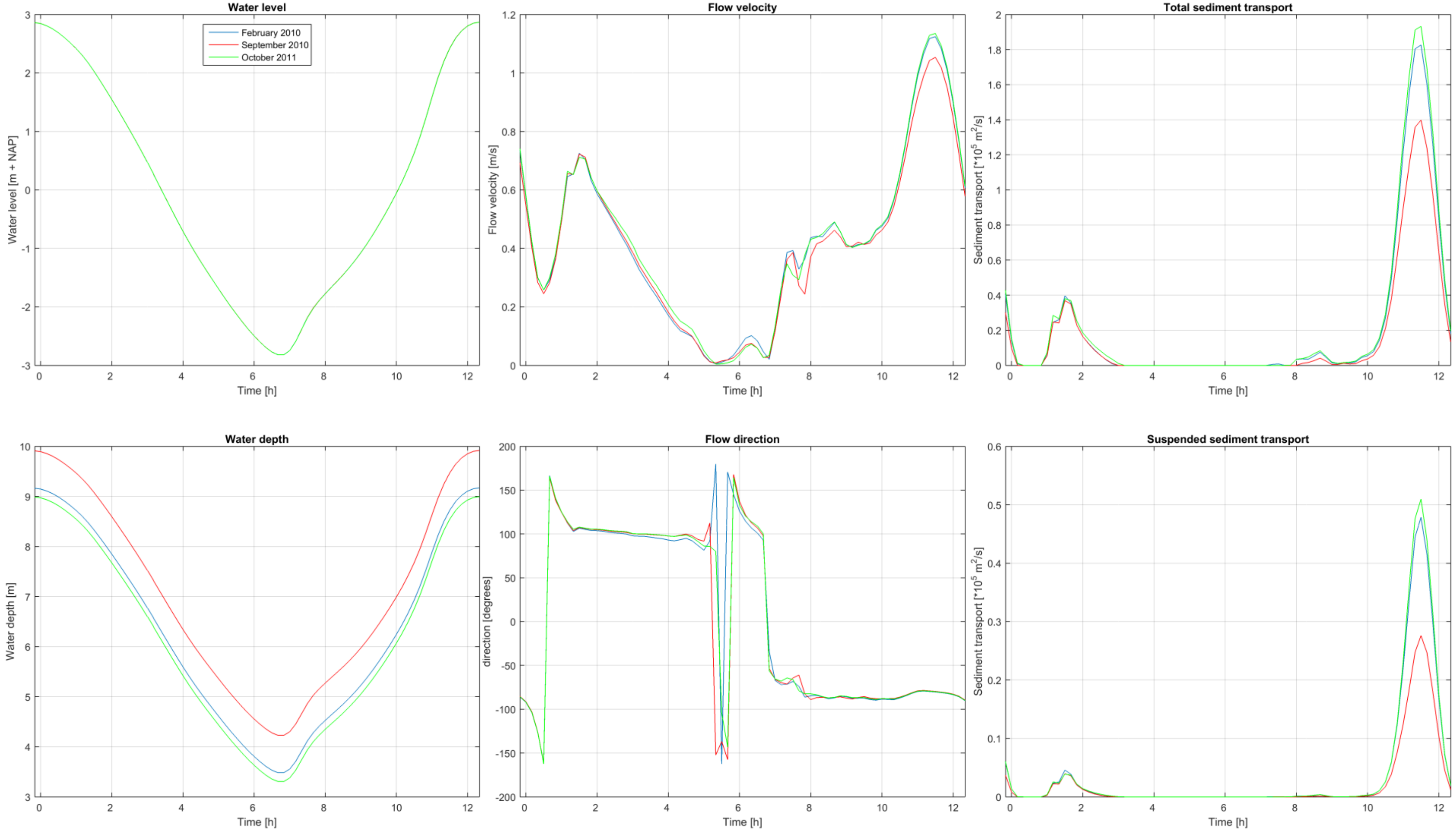

Figure D- 11 Water level (top left), water depth (bottom left), flow velocity (top middle), flow direction (bottom middle), total sediment transport (top right) and suspended sediment transport for control point 5 during spring tide

D. MEASUREMENT LOCATIONS

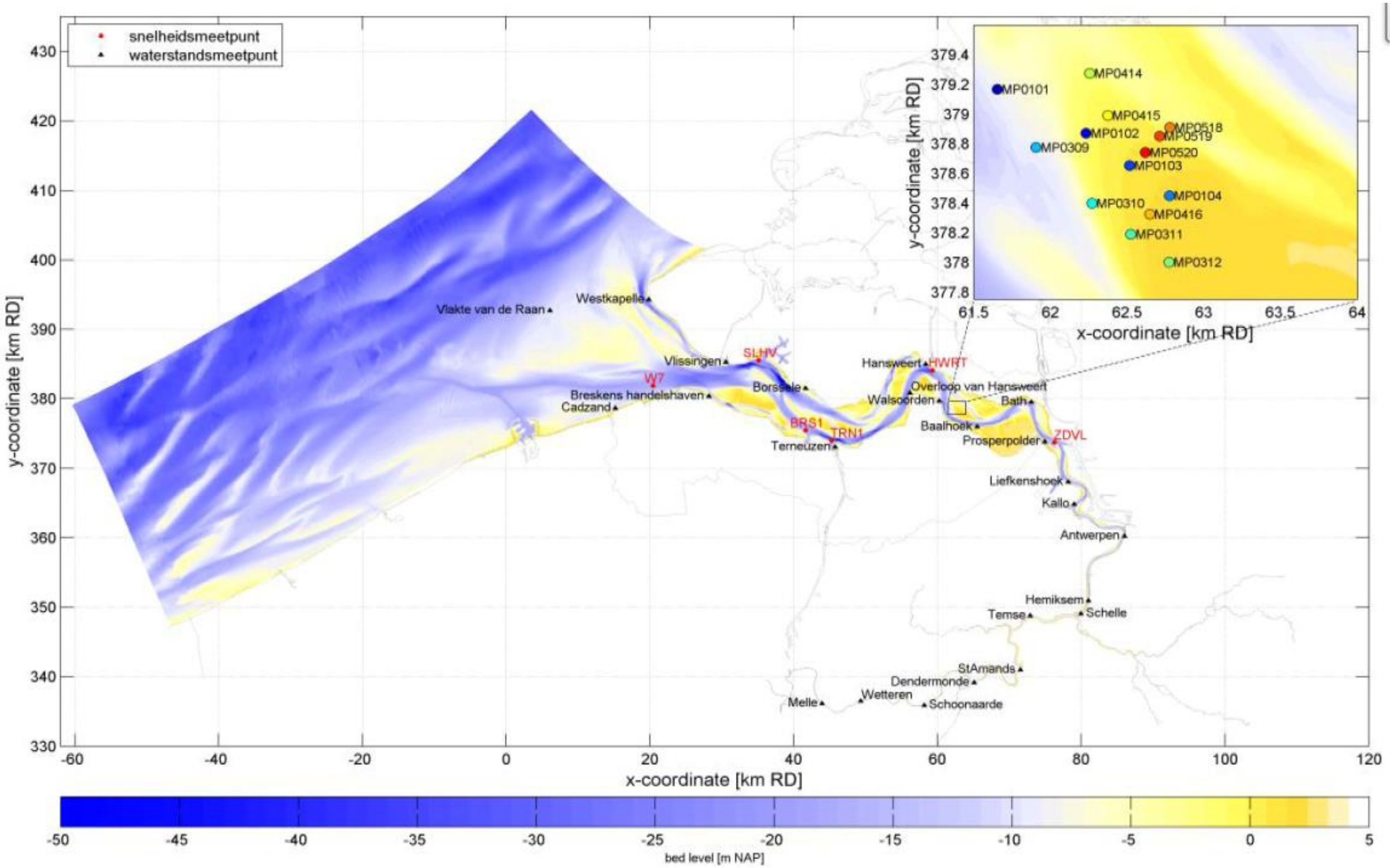

Figure D- 1 Measurement locations of the water level (black triangles) and flow velocities (red triangles) along the Scheldt estuary and MONEOS flow velocities observation points near intertidal shoal *Walsoorden* (top right)